Kansas Geological Survey
Open-file Report

Disclaimer

KANSAS GEOLOGICAL SURVEY
OPEN-FILE REPORT 1984-7

SEDIMENTOLOGY, DIAGENESIS, AND PETROPHYSICS OF SELECTED CHEROKEE GROUP (DESMOINESIAN) SANDSTONES IN SOUTHEASTERN KANSAS
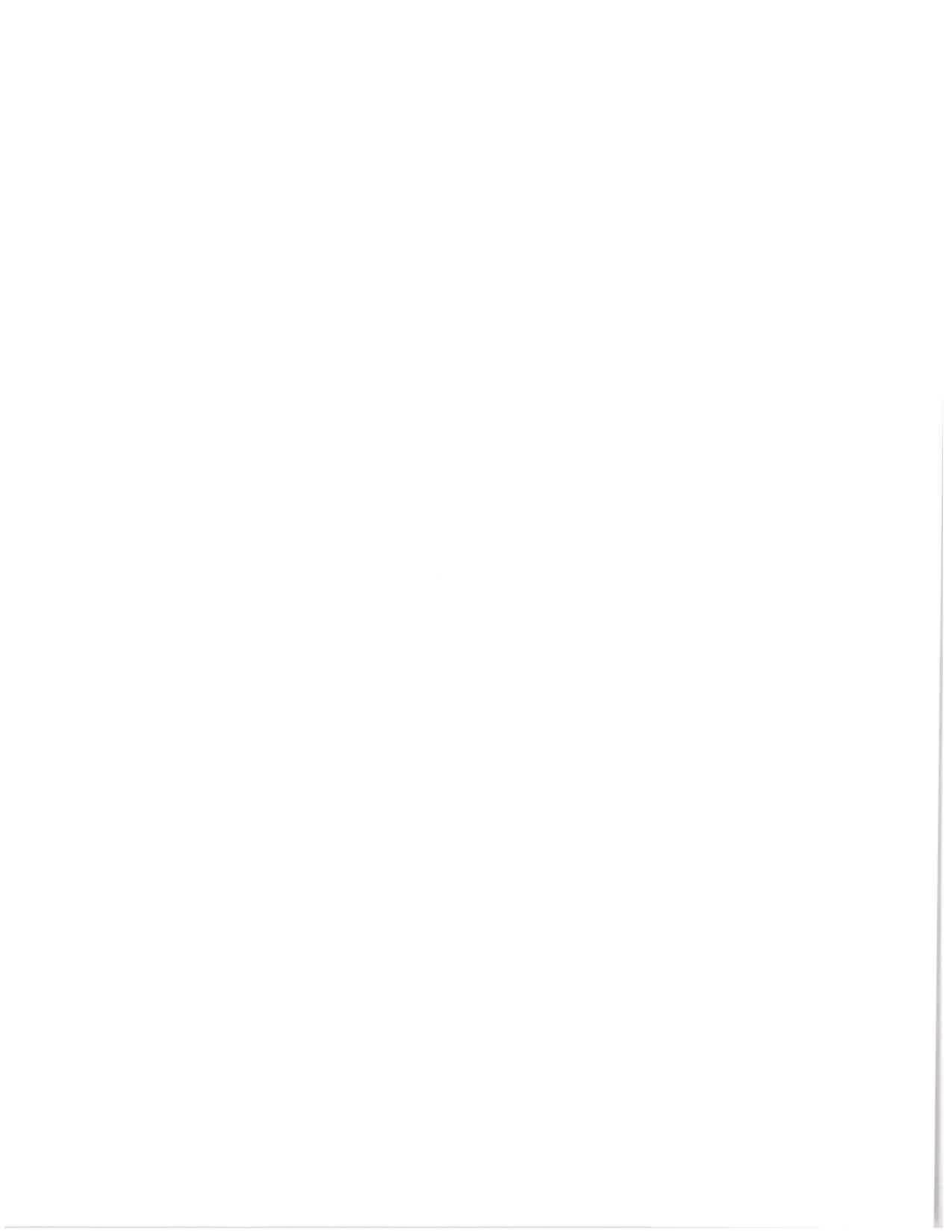
by

Marvin D. Woody

SEDIMENTOLOGY, DIAGENESIS, AND PETROPHYSICS OF

SELECTED CHEROKEE GROUP (DESMOINESIAN) SANDSTONES

IN SOUTHEASTERN KANSAS

by

Marvin D. Woody

B. S., University of Mississippi, 1979

Submitted to the Department of Geology and the
Faculty of the Graduate School of The University
of Kansas in partial fulfillment of the require-
ments for the degree of Master of Science.

Professor in Charge

Committee Members

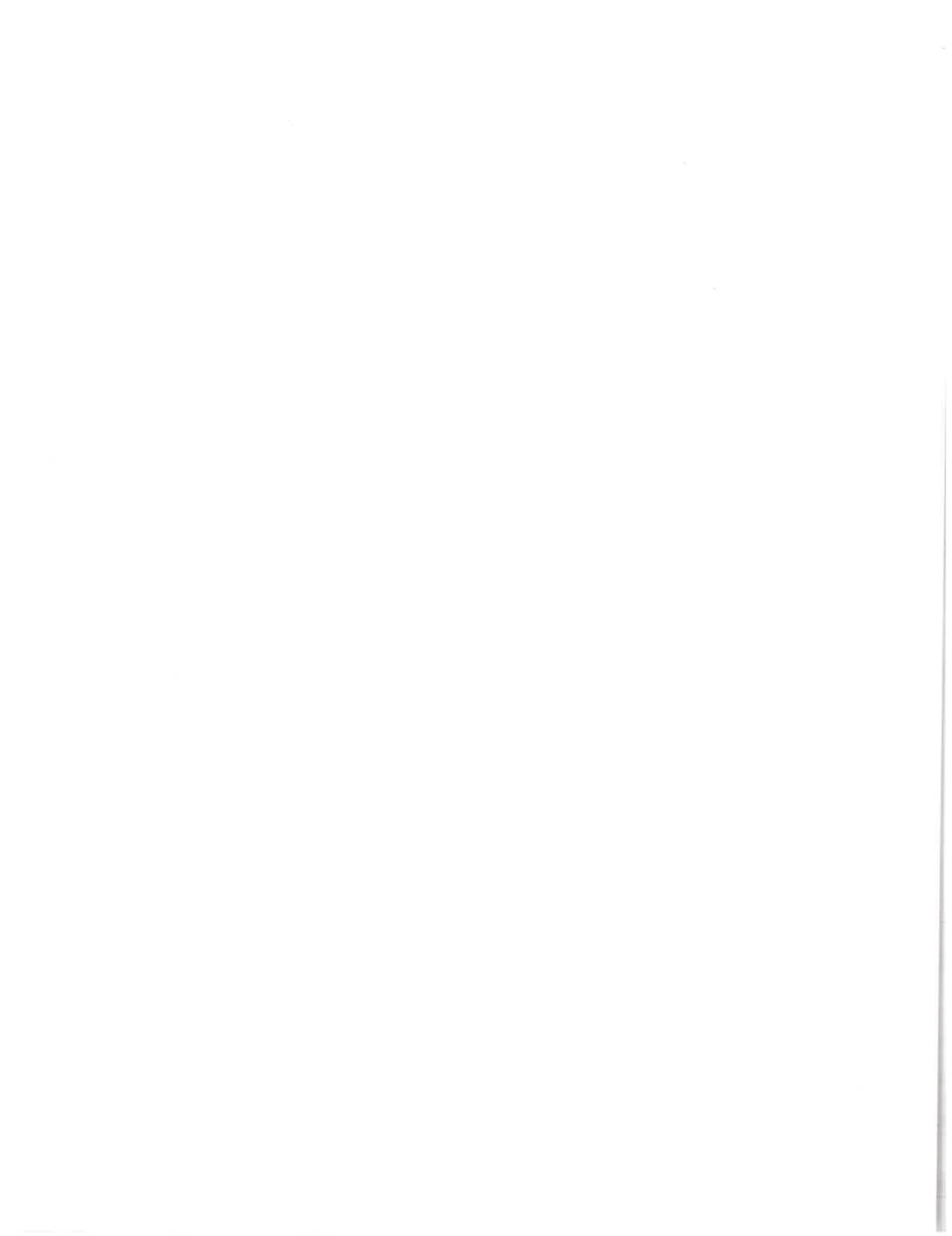For the Department

TABLE OF CONTENTS

TABLE OF CONTENTS (continued)

LIST OF ILLUSTRATIONS

LIST OF ILLUSTRATIONS (continued)

LIST OF ILLUSTRATIONS (continued)

LIST OF ILLUSTRATIONS (continued)

LIST OF ILLUSTRATIONS (continued)

LIST OF TABLES

ABSTRACT

Oil-producing sandstones of the Middle Pennsylvanian Cherokee Group in southeastern Kansas are potential enhanced recovery targets. Twenty-seven Cherokee Group sandstone bodies were studied to evaluate the influence of sedimentology and diagenesis on reservoir quality.

Sedimentologically, the sandstone bodies are fining-upward, medium- to very-fine-grained, continental channel-filling sequences up to 35 meters (116 feet) thick. From the base to the top of a channel sequence, five lithofacies that have been recognized are: 1) conglomeratic sandstones, 2) stacked sandstones, 3) crossbedded coarser sandstones, 4) rippled finer sandstones, and 5) interbedded sandstones, shales, and siltstones. Conglomeratic sandstones also capped some channel sequences. Sandstone mineralogy is generally the same throughout the area studied and is dominated by quartz with lesser amounts of feldspars, mica, and sedimentary and metamorphic rock fragments.

Diagenesis of the sandstones occurred in three stages. Stage 1 is syndepositional to early compactional precipitation of calcite concretions and spherulitic siderite resulting in nearly complete loss of porosity and permeability in scattered patches within the sandstones. Stage 2 consisted of precipitation of chlorite grain coatings and varying degrees of silica cementation inversely related to the presence of chlorite grain coatings. Chlorite grain

i

coatings commonly occur in the lower portions of channel
sequences, where it inhibited silica precipitation and
resulted in preservation of part of the primary porosity.
In the upper portions of channel sequences, the lack of
grain coatings permitted extensive silica cementation which,
in conjunction with compaction of soft rock fragments and
micas, reduce porosity and permeability. Stage 3 was the
precipitation of patchy kaolinite, siderite, and dolomite-
ankerite cements. Precipitation of kaolinite resulted in
the alteration of macropores to micropores. Carbonate
cements reduced porosity and permeability. Secondary
porosity was created by the dissolution of feldspars, micas,
and argillaceous rock fragments.

The diagenetic sequence of the Cherokee Group is
similar to sequences reported for other Carboniferous
sandstones of the same composition and for Tertiary sand-
stones in the Gulf Coast. Because the burial histories of
the sandstones studied here and those reported in the
literature are different but resulted in similar diagenetic
histories, the influence of time, fluid and rock
composition, and possibly geothermal gradient must have been
important to diagenesis of Cherokee Group sandstones. The
similarity of diagenetic histories for sandstones with
different ultimate burial histories emphasizes the lesser
importance of depth of burial in sandstone diagenesis.

In the Cherokee Group sandstones studied, liquid
porosities range from 5 to 28 percent; permeability to

simulated, oil field brine ranges from 0 to 427 milli-
darcies; and effective pore throat radii range from 0.88 to
17 micrometers. Variation in porosity, permeability, and
effective pore throat radius are related to grain size
variations, sedimentary structures, abundance of soft rock
fragments and micaceous partings, and assemblage and
abundance of diagenetic minerals.

A model of Cherokee Group sandstones predicts that
coarser grain size, less cementation, and fewer rock frag-
ments will be found in lower portions of channel sequences.
The lower portions of channel sequences will have higher
porosities and permeabilities and larger pore throats
relative to the upper portion of channel sequences. The
upper portion of channel sequences will have finer grain
size, more extensive cementation, and abundant rock
fragments, all of which result in lower porosities and
permeabilities and smaller pore throats.

ACKNOWLEDGEMENTS

INTRODUCTION

PURPOSE

Pennsylvanian deposits of the Cherokee Group in south-
eastern Kansas and northeastern Oklahoma contain petroleum
bearing sandstones that are presently being considered for
the application of enhanced oil recovery processes. Such
assessments of oil reservoirs require a multidisciplinary
approach including both geology and reservoir engineering.
The objectives of this research are to determine pertinent
geologic and petrophysical properties of Cherokee Group
sandstones and to establish relationships among these prop-
erties to aid in understanding fluid movement in reservoirs
during enhanced recovery operations. The geologic proper-
ties studied are sedimentary structures and their sequences,
detrital and diagenetic petrology, and grain size. Petro-
physical properties of the sandstones that are of interest
in this study are effective porosity, effective permeability
to liquids, and effective pore size distribution.

The area of study is the portion of the Cherokee Basin
in southeastern Kansas (Figure 1). Eighteen cores contain-
ing a total of 27 individual sandstone bodies from the
Cherokee Group were selected from the core library of the
Kansas Geological Survey (Figure 1, Table 1). Depths at
which cores were taken range from 9 meters (30 feet) on the
eastern side of the study area (K.G.S. Tar Sands "AA") to
over 1050 meters (3400 feet) on the western side of the

1

study area (Sinclair Weir No. 1). These sandstones were chosen to represent the variety of numerous narrow, elongate, lenticular, discontinuous sand bodies characteristic of the Pennsylvanian deposits of this area, several of which had been the subjects of earlier more general geologic studies, cited below. This is the first attempt to provide a detailed petrophysical characterization of Cherokee sandstone oil reservoirs in southeastern Kansas that would have more than local application.
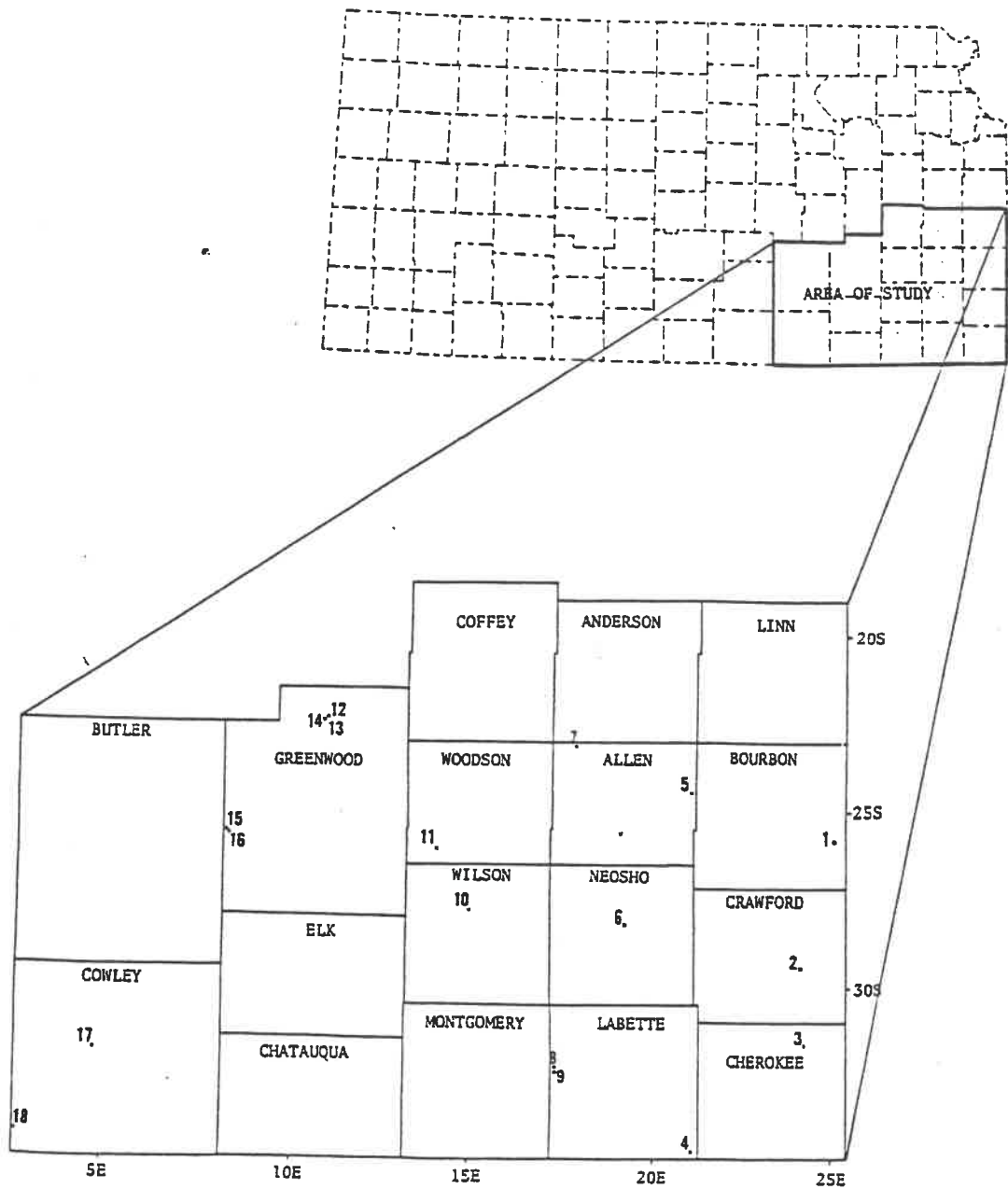
Figure 1. Index map showing the location of the cores used in this study. The numbers correspond to the numbers beside the well data listed in Table 1 of this text.

TABLE 1 - Cores used in this study

	WELL NAME	LOCATION	SANDSTONE DEPTHS feet (meters)
1.	K.G.S. Tar Sånds C	10-26S-25E	188 to 202 (57 to 62)
			240 to 271 (74 to 84)
2.	K.G.S. Tar Sands N	34-29S-24E	227 to 234 (69 to 71)
			300 to 322 (91 to 98)
3.	K.G.S. Tar Sands AA	2-32S-24E	30 to 36 (9 to 11)
4.	Tenneco Bradley 8	11-35S-21E	87 to 120 (27 to 37)
			151 to 173 (46 to 53)
5.	M. C. Colt 14AO Johnson	33-24S-21E	711 to 753 (217 to 230)
6.	Tesoro W-35 Baker	26-28S-19E	543 to 568 (166 to 173)
			571 to 580 (174 to 177)
7.	M. C. Colt 18AO Keown	22-23S-18E	836 to 846 (255 to 258)
			908 to 1022 (277 to 312)
			1123 to 1181 (342 to 360)
8.	Conoco J. Ord 34	26-32S-17E	669 to 720 (204 to 219)
9.	Conoco J. Ord 47	35-32S-17E	701 to 737 (214 to 225)

Table 1 (continued)

10.	Brazos 0-5 Pierpoint	9-28S-15E	1004 to 1049 (306 to 320)
11.	M. C. Colt 22AO Lauber	23-26S-14E	1034 to 1048 (315 to 319)
			1235 to 1260 (376 to 384)
12.	Phillips Demalorie 30AW	32-22S-11E	1913 to 1972 (583 to 601)
13.	Phillips Demalorie 33AW	32-22S-11E	1967 to 1993 (600 to 607)
14.	Phillips Demalorie 13AW	32-22S-11E	1951 to 1960 (595 to 597)
15.	Jackson Bros. Barrier 36	3-26S-8E	2465 to 2467 (751 to 752)
			2473 to 2508 (754 to 764)
16.	Jackson Bros. Crew 21	3-26S-8E	2486 to 2524 (758 to 769)
17.	Phillips Lena 1	17-32S-5E	3046 to 3069 (928 to 935)
18.	Sinclair Weir 1	30-34S-3E	3410 to 3421 (1039 to 1043)
			3428 to 3443 (1045 to 1049)

PETROLEUM GEOLOGY OF CHEROKEE GROUP SANDSTONES

The history of petroleum production from Cherokee Group sandstones began with a discovery in Paola, Kansas, in 1860 (within a year of the first commercial production of hydrocarbons in Pennsylvania) and continues to this date. Jewett (1954) and Chenoweth (1979) both discussed historical aspects of hydrocarbon production in southeastern Kansas and northeastern Oklahoma. The East Range counties of Kansas have yielded about 30 percent of the estimated 4.5 billion barrels of crude oil produced in Kansas to date (Oros, 1979). The Cherokee Group sandstones are a major contributor to this figure, which does not include natural gas.

The minimum estimated depth of burial in the basin is due to at least 1070 meters (3500 feet) of later Pennsylvanian and Permian deposits (McKee et al., 1967) and up to 150 meters (500 feet) of Cretaceous sediments (Ebanks and James, 1974). This resulted in an estimated total depth of burial for Cherokee Group sediments of 1200 meters (4000 feet) and temperatures of 60 to 70 degrees centigrade. These temperatures are sufficient to generate hydrocarbons (Gould, 1975).

Hydrocarbons in Cherokee Group sediments in Kansas are found primarily in sandstones. The petroleum must be locally derived, for no continuous migration route northward out of the Arkoma Basin exists (Weirich, 1953). Baker (1962) concurred that the hydrocarbons were indigenous and

6

believed that they were generated in the abundant, organic-rich shales associated with Cherokee Group sandstones. Compaction of surrounding shales and shaly siltstones provided a seal for the reservoirs (Hulse, 1978).

Production from Cherokee Group deposits is limited to sandstones bounded by impermeable shales and siltstones. Oil accumulation, generally limited to updip areas of sandstone bodies, is due to drape of the sandstones over pre-Pennsylvanian high areas in conjunction with a westward regional dip caused by later structural movement of the Ozark Uplift (Hulse, 1978). Such reservoirs in the Cherokee have been referred to as combination stratigraphic-structural traps (Busch, 1959).

Primary production in Cherokee Group sandstones is by solution gas drive, which has a quick loss in reservoir energy (Levorsen, 1973). Most Cherokee Group sandstone reservoirs are artificially provided reservoir energy by water injection when primary reservoir energy dwindles. Currently, many of these waterflooded oil fields are undergoing production declines or have been abandoned, although recent economic incentive has allowed continued production of such dwindling reservoirs. Such primary and secondary techniques recover from 30 to 60 per cent of the original oil in place (Ebanks, 1975). Studies are currently underway to evaluate the possibility of enhanced, or tertiary, recovery techniques to retrieve more petroleum from these sandstone reservoirs.

Gould (1975) reported three gradational ranges of crude oils in sandstone reservoirs of the Cherokee Group in southeastern Kansas: 1) light oils (36 to 42 degree API gravity) produced from depths of 427 to 792 meters (1400 to 2600 feet) in the western part of the basin, 2) medium oils (25 to 35 degree API gravity) produced from depths of less than 427 meters (1400 feet) in the central and eastern parts of the basin, and 3) heavy oils (less than 25 degree API gravity) produced from less than 427 meter (1400 foot) depths in the central and eastern part of the basin. Gould felt the differences are due to post-migration alterations of the oil within the reservoir, particularly thermal alteration in the medium oils and water washing and bacterial degradation in the heavy oils.

GEOLOGY OF THE CHEROKEE GROUP

NOMENCLATURE

Haworth and Kirk in 1894 first described the Cherokee Group from deposits in Cherokee County, Kansas (Jordan, 1957). The Cherokee Group is defined as the lower portion of the Desmoinesian Stage of the Middle Pennsylvanian Series and is equivalent to the European Upper Wesphalian of the Middle Carboniferous (van Eysinga, 1978; Figure 2). The base of the Cherokee Group lies unconformably above older rocks ranging in age from Atokan to Precambrian (Ham and Wilson, 1967). The top of the Cherokee Group is in conformable contact with the basal unit of the Marmaton Group, the Fort Scott Limestone.

In 1953, the name Cherokee was preempted because of prior use and replaced by the Krebs and Cabaniss Groups (Figure 3), their boundary being marked biostratigraph-ically by the change from the brachiopods Marginifera missouriensis, Spirifer rocky mountanus, S. occidentalis, and striated forms of Mesolobus to the presences of Marginifera muricatini and smooth forms of Mesolobus (Howe, 1956). In 1955, the name "Cherokee" was readopted due to widespread usage and the names Krebs and Cabaniss became subgroups (Howe, 1956). Jewett (1959) changed the rank of Krebs and Cabaniss to formation with the named sandstones, coals, and limestones as subdivisions.

9

EUROPEAN STRATIGRAPHY		
SYSTEM	SERIES	STAGE
CARBONIFEROUS	UPPER	STEPHANIAN
		WESTPHALIAN
		NAMURIAN
	LOWER	VISEAN
		TOURNAISIAN

NORTH AMERICAN STRATIGRAPHY			
SYSTEM	SERIES	STAGE	
PALEOZOIC ERATHEM	PENNSYLVANIAN	UPPER	VIRGILIAN
			MISSOURIAN
		MIDDLE	DESMOINESIAN
			ATOKAN
		LOWER	MORROWAN
	MISSISSIPPIAN	UPPER	SPRINGERIAN
			CHESTERIAN
			MERAMEC'AN
		LOWER	OSAGEAN
			KINDERHOOKIAN

Figure 2. Stratigraphic columns comparing European and North American stratigraphy (after van Eysinga, 1978).

	SERIES	STAGE	GROUP	FORMATION	STRATIGRAPHIC INTERVALS		
					HOWE (1956)	EBANKS et al. (1977)	HULSE (1978)

MIDDLE PENNSYLVANIAN — SERIES
DESMOINESIAN — STAGE
CHEROKEE — GROUP
KREBS | **CABANISS** — FORMATION

KREBS / CABANISS unit	HOWE (1956)	EBANKS et al. (1977)	HULSE (1978)
RIVERTON*	RIVERTON*	LOWER WARNER	BURGESS
WARNER*	WARNER*	WARNER	
ROWE*	ROWE*	UPPER WARNER	
DRYWOOD*	DRYWOOD*		
BLUEJACKET*	BLUEJACKET*	BLUEJACKET	BARTLESVILLE
SEVILLE	SEVILLE		
WEIR*	WEIR*	CABANISS	BURBANK
TEBO*	TEBO*	LOWER	SKINNER
SCAMMON*	SCAMMON*	CABANISS	CATTLEMAN
MINERAL*	MINERAL*		
FLEMING*	FLEMING*	MIDDLE	
CROWEBERG*	CROWEBERG*		VERDIGRIS
VERDIGRIS	VERDIGRIS		
BEVIER*	BEVIER*		
LAGONDA*	LAGONDA*	LAGONDA	SQUIRREL
EXCELLO	EXCELLO		
MULKY*	MULKY*		

Figure 3. Stratigraphy of the Cherokee Group in southeastern Kansas. Asterisks correspond to coal-bearing intervals in the Cherokee Group.

11

STRATIGRAPHY

Howe (1956) recognized 18 formations within the Cherokee Group at its outcrop (Figure 3). These formations are bounded by laterally continuous coals, carbonates, and shales. Unfortunately, many of these boundaries cannot be traced into the subsurface (Zeller, 1968). Ebanks et al. (1977) found 6 units and Hulse (1978) found 9 units traceable in the subsurface across the basin. These authors used them to define stratigraphic intervals (Figure 3). The difficulties of correlations of Cherokee Group sediments have only recently been emphasized (e.g., Ebanks, 1979). These problems arise because the discontinuous nature of the deposits was not recognized when the original stratigraphy was developed. Use of stratigraphic intervals provides a logical method to allow communication between workers while avoiding the plethora of names in use, many of which have been confused and misused over time. Howe (1956) and Zeller (1968) provide detailed discussions of the Cherokee Group stratigraphy.

STRUCTURAL SETTING AND REGIONAL TECTONICS

The Cherokee Basin is bounded by the Ozark uplift on the east, the Nemaha fault zone on the west, the Forest City basin to the north, and grades southward into the deeper Arkoma basin (Figure 4). Cherokee Group deposits are 110 to 125 meters (350 to 400 feet) thick in the study area (Jewett, 1954). The deposits thicken to over 2135 meters (7000 feet) in the deepest portion of the Arkoma Basin (Ham and Wilson, 1967). Cherokee Group deposits are exposed in the southeastern area of Kansas and the adjoining areas in Oklahoma and Missouri. These deposits presently dip west-northwest at a rate of 3 to 5 meters per kilometer from western Missouri to the Nemaha Fault Zone. Cherokee Group sediments were originally deposited with a southward dip, but recurring uplift since middle Permian time, coupled with westward tilting due to the Ozark Uplift, has resulted in their westward dip (Ebanks and James, 1974).

The structural setting for the Cherokee Basin was established in early to middle Desmoinesian time in conjunction with the major deformation of the Ouachita Mountains to the south (Ham and Wilson, 1967). The result was the development of a shallow platform downwarped to the south after movement of the Nemaha fault zone, a high-angle reverse-fault-complex parallel to and east of the Mid-Continent Rift System (Figure 4) (Green, 1977; Van Schmus and Bickford,
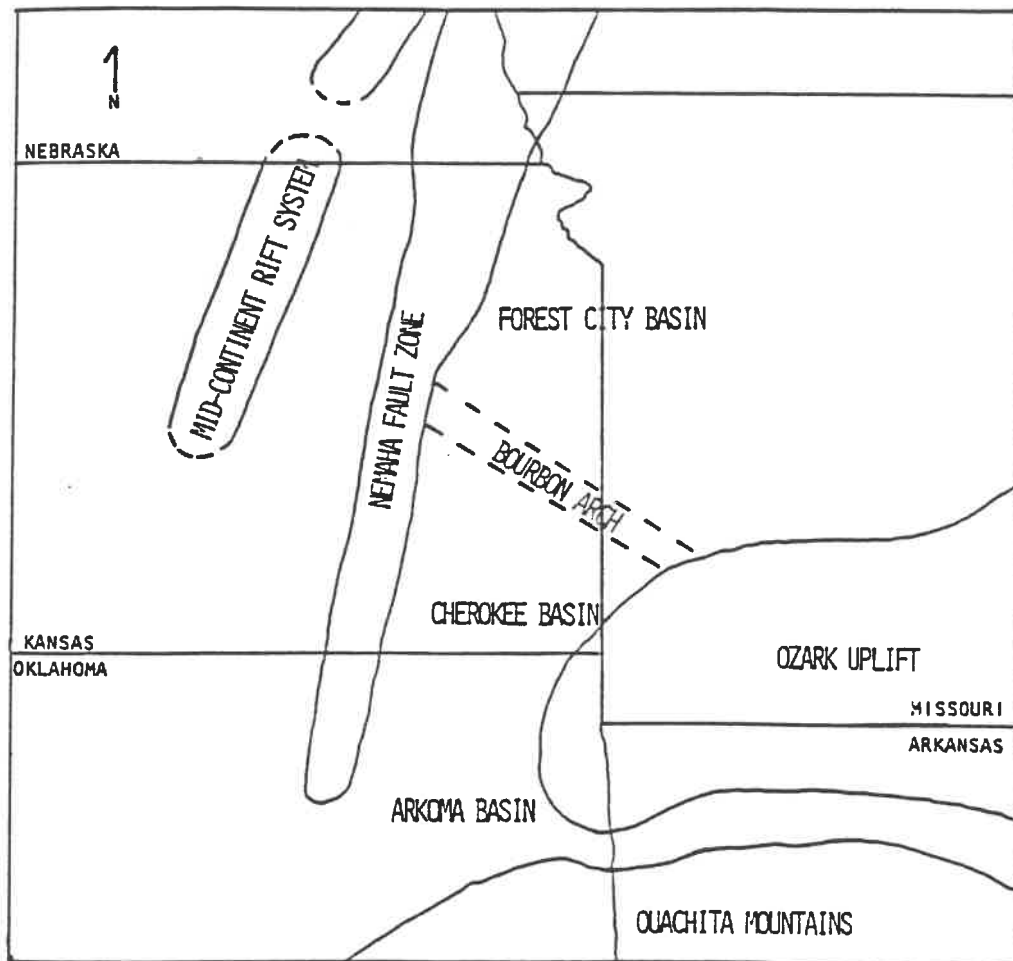
Figure 4. Regional structural elements discussed in the text (after Van Dyke, 1975).

1981). Although origin of the Nemaha fault zone is not clearly established, it is probably associated with the block faulting that produced the Ancestral Rockies and that was contemporaneous with formation of the Ouachita foldbelt (Kluth and Coney, 1981). This is all believed to be associated with the collision of Gondwana and Laurussia during the Late Carboniferous (Ziegler et al., 1979).

The Cherokee basin was separated from the deeper Forest City basin to the north by a high area on the pre-Pennsylvanian surface (Weirich, 1953) commonly referred to as the Bourbon arch. By late Desmoinesian time, the Bourbon arch was inundated and the Cherokee and Forest City basins were connected (Jewett, 1954).

Deposition of the Pennsylvanian sediments occurred during an overall northward transgression, which is indicated by onlap of progressively younger sediments on the eroded pre-Pennsylvanian surface along with a change from clastics to carbonates during the Desmoinesian Stage (Figure 5) (Weirich, 1953; Ham and Wilson, 1967; Visher et al., 1971; Ebanks and James, 1974; Bennison, 1979). The Cherokee Group represents the first of the cyclic deposits in the area. Cyclic deposition continued throughout the Virgilian Stage. Causes of the cyclicity are probably Gondwana glaciation (Crowell, 1978) and tectonic movement associated with the collision of Gondwana and Laurussia during the Late Carboniferous (Ziegler et al., 1979). Bennison (1979,

15
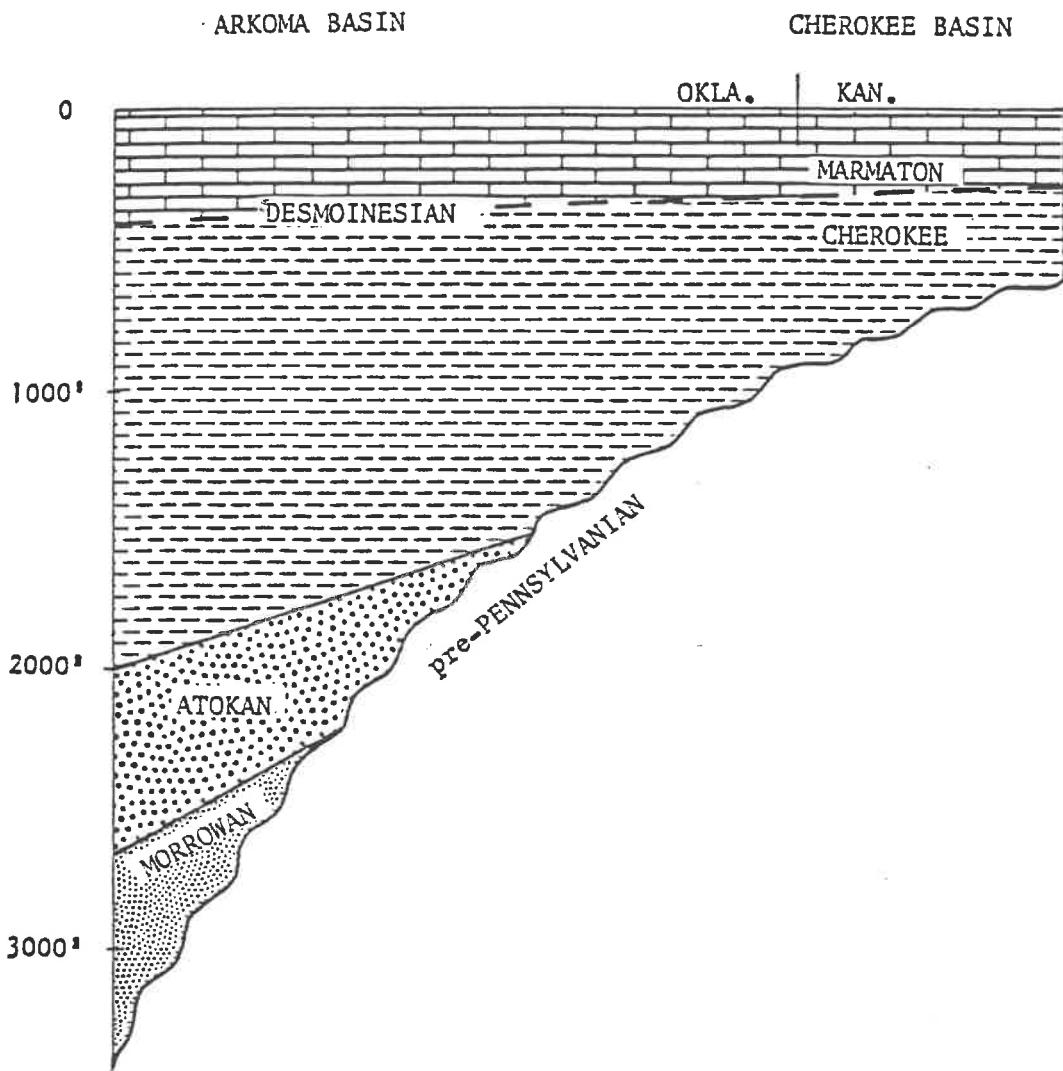
Figure 5. Generalized northward onlap of lower and middle Pennsylvanian rocks (after Ebanks and James, 1974).

p. 288-289) suggested the interplay of glaciation and tectonism as "a logical mechanism to explain some of the complexity of Pennsylvanian sedimentation" of the Midcontinent.

LITHOLOGY OF THE CHEROKEE GROUP

Core Description

Cores used in this study were selected to include sandstones in the Kansas portion of the Cherokee basin (Figure 1, Table 1). Outcrop samples were not used in order to avoid the effects of recent weathering associated with surface exposure. While not all of the sandstones were from producing areas, most had some hydrocarbon stain. Cores were carefully described, emphasizing sedimentary structures and the sequences in which they occurred. Descriptions also served as a basis for selection of samples to be used for thin sections and for core plugs used in petrophysical tests. Any available descriptions providing detail adequate for the purposes of this study were used. Graphical core descriptions are in Appendix B.

Shale

Shales make up more than 80 percent of the Cherokee Group rocks, but they have been little studied (Zeller, 1968). Baker (1962, p. 1628) recognized four main types of shales in the Cherokee Group: 1) Greenish-gray shales composed of quartz, chlorite, sericite, local concretions of siderite, and minor amounts of organic matter and associated pyrite. These shales are silty and have a small, sparse marine fuana. 2) Gray shales bearing quartz, chlorite, and sericite with significant amounts of organic matter and some

pyrite. This shale type is higher in clay content and plant and marine fossils than the greenish-gray shale. 3) Black, phosphatic shales composed of quartz, illite, chlorite, pyrite, and organic matter, with small phosphatic nodules and no silt; conodonts and orbiculoid brachiopods are common. 4) Olive-gray underclay containing quartz and clay minerals with common pyrite, ankerite veins, limestone nodules, and carbonized plant fragments. This type of underclay is commonly silty. Slickensided fractures notable in these underclays are helpful criteria for recognizing them in cores. Baker (1962) interpreted these underclays as soil profiles developed in shales and siltstones underlying organic deposits that became coals. Petroleum found in the sandstones in the Cherokee Group was derived from these four kinds of surrounding shales (Baker, 1962).

McMillan (1956) identified the underclays as gley, which is formed under peat beds in marshy conditions and develops by reactions between the underlying clay and organic compounds in the peat. These peat beds are sites of reducing and leaching conditions resulting in ferrous compounds.

Heckel (1977) interpreted the black, phosphatic, silt-free shales as representative of deep water conditions developed during times of highest sea level. A thermocline resulted in a cold, oxygen poor bottom layer where phosphate was concentrated and precipitated.

Coal

Coal is mined from shallow Cherokee Group rocks in Cherokee, Labette, and Crawford counties, Kansas, and adjacent areas in Oklahoma and Missouri. Although the coal is an economically important rock type in the Cherokee Group, the quality and lateral extent of the coals varies (Howe, 1956). Beds are commonly one foot (30 cm) thick but rarely more than five feet (150 cm) thick. The Weir-Pittsburg is the most economically important coal, (Zeller, 1968, p. 24) although numerous coal beds in the Cherokee Group section have been mined (Figure 3). In several of the cores used in this study, the coals have a caprock, a shaly fossil hash predominantly composed of brachiopod, echinoderm, and bryozoan fragments.

Limestone

Limestones of the Cherokee Group are light to medium gray and contain gastropods, brachiopods, echinoderms, bryozoans, foraminifera, ostracodes, and green algae (Zeller, 1968, Van Dyke, 1975, and Hulse, 1978). The Verdigris Limestone is the most widely identified marker bed in well logs of the Cherokee Group and is also referred to as the Ardmore Limestone (Figure 3) (Zeller, 1968). The limestones may be nodular and silty or sandy in places.

Sandstones

Sandstones of the Cherokee Group are the principal subject of this study. The following section is a discussion of the sedimentology of these sandstones. Petrographic and petrophysical aspects and the relationships among sedimentary, diagenetic, and petrophysical aspects are discussed later in this text. Graphical descriptions of the cores are in Appendix B.

Sandstones of the Cherokee Group that were studied range in thickness from 2 to 35 meters (6 to 116 feet). Mean thickness is 11 meters (36 feet). Many of the sandstones were not completely cored. Color of the sandstones ranges from tan to black; color variations are due primarily to the type and extent of oil staining. Most siltstones are dark gray. Oil staining hampers identification of sedimentary aspects by masking features in the cores, particularly where heavy oil stains are present. The sandstones are moderate- to moderately-well sorted, medium- to very-fine grained, and composed mostly of quartz with subordinate amounts of feldspar and rock fragments. Silica, carbonate, and authigenic clay cements are also present and can be identified in hand specimen, although thin section study is more conclusive.

Five lithofacies were recognized in the sandstones studied; A) conglomeratic sandstones subdivided into 1) thin basal and 2) thick sequence-capping subfacies; B) stacked sequences in one sandstone; C) crossbedded coarse

21

sandstones; D) rippled fine sandstones; and E) interbedded fine sandstones, shales and coarse siltstones (Figure 6). These lithofacies are based on the sandstones in cores studied in this research and may not include all of the types of sandstones present in the Cherokee Group. Figure 7 lists the characteristics of each lithofacies. These characteristics will be useful in developing the sophisticated sandstone models needed for enhanced recovery operations.

Rocks of lithofacies A, conglomeratic sandstone, are composed of granule-gravel to coarse-sand-sized clasts, derived from underlying strata, in a medium- to fine-grained sand matrix (Figure 8). Clasts include chert; angular, dark gray to black, silt and shale fragments; rounded clay ironstones; angular carbonaceous plant fragments; mixed siltstone, shale and sandstone clasts; coal clasts; and fragments of phosphatic concretions derived from black shales. No marine fossil debris was recognized in the basal lags. The basal contact of this lithofacies is sharp and erosional. The erosion cut down into light to dark gray siltstones, coals, greenish-gray to black shales, and sandstones. Bedding was not recognized in conglomerates. Two subfacies of lithofacies A are present: 1) thin basal conglomerates and 2) thick sequence-capping conglomerates.

Thin basal conglomerates were the first sediments deposited after an erosional event marked by the sharp base of some sandstones. Eleven of these deposits were found in

22
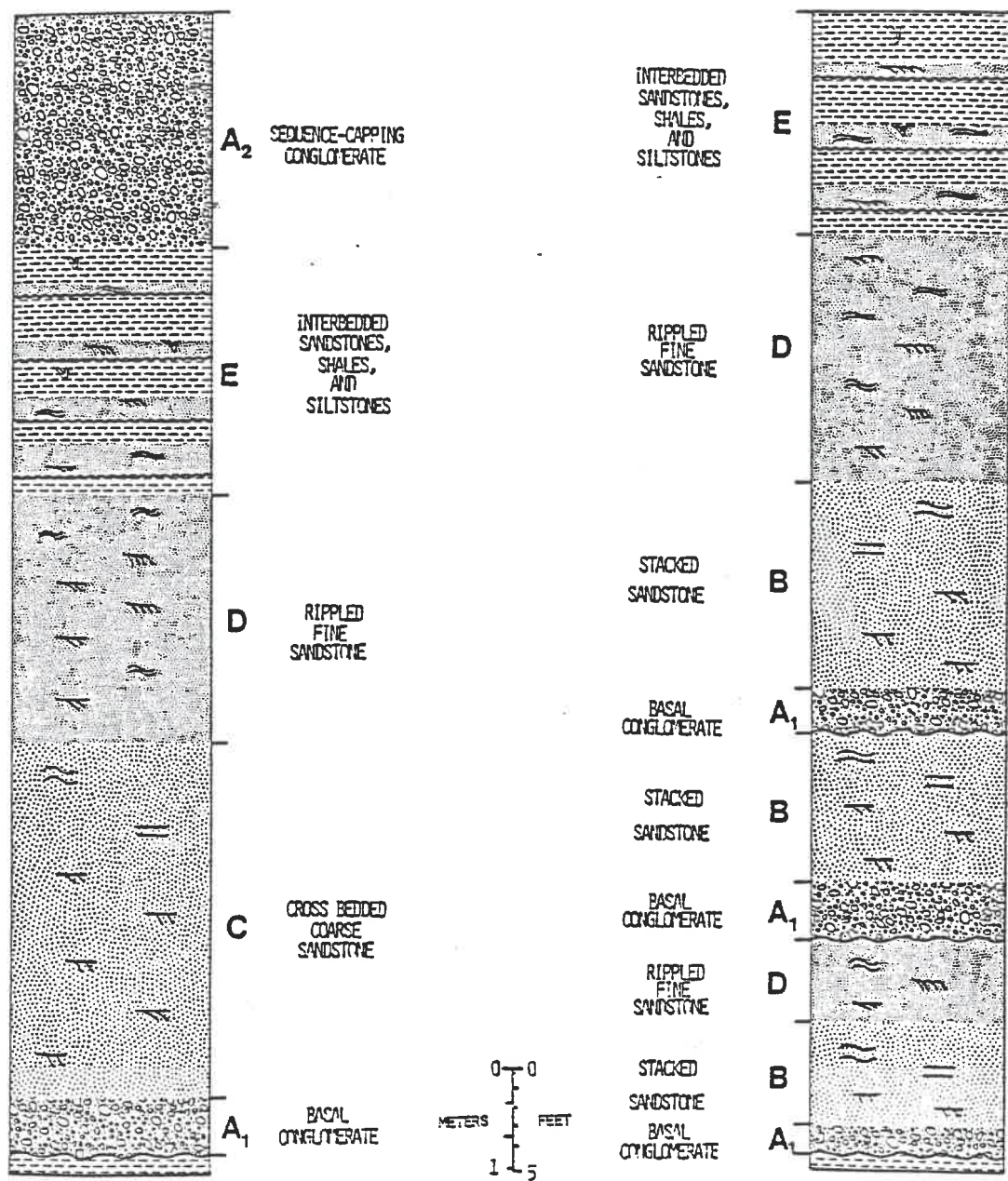
Figure 6. Idealized fining-upward sandstone sequences constructed from cores used in this study.

LITHOFACIES	THICKNESS, METERS		DISTINGUISHING CHARACTERISTICS
	RANGE	MEAN	
A₁ THIN BASAL CONGLOMERATE	0.15 TO 2.7	—	ABUNDANT GRANULE-GRAVEL TO COARSE-SAND CLASTS OF VARYING COMPOSITIONS, THINNESS OF DEPOSIT, POSITION AT BASE OF SEQUENCE.
A₂ THICK SEQUENCE-CAPPING CONGLOMERATE	1.5 TO 7.5	—	ABUNDANT GRANULE-GRAVEL TO, COARSE-SAND SILTSTONE-SANDSTONE -SHALE CLASTS, THICKNESS OF DEPOSIT, POSITION AT TOP OF SEQUENCE, OVERLAIN BY SHALES.
B STACKED SANDSTONES	0.15 TO 3.4	1.4	PART OF SEQUENCE CONSISTING OF AN EROSIONAL BASE FOLLOWED BY A BASAL CONGLOMERATE OVERLAIN BY A COARSE SANDSTONE, SEQUENCE IS REPEATED SEVERAL TIMES, LARGE-SCALE SEDIMENTARY STRUCTURES.
C CROSSBEDDED COARSER SANDSTONE	0.6 TO 12.8	5.3	ONE CONTINUOUS SANDSTONE SEQUENCE, LARGE-SCALE SEDIMENTARY STRUCTURES
D RIPPLED FINER SANDSTONE	0.8 TO 10.7	3.6	SMALL-SCALE SEDIMENTARY STRUCTURES.
E INTERBEDDED SANDSTONES, SHALES, AND SILTSTONES	0.8 TO 20.4	4.7	INTERBEDDED AND INTERLAMINATED SANDSTONES, SILTSTONES, AND SHALES, SMALL-SCALE SEDIMENTARY STRUCTURES.

Figure 7. Distinguishing characteristics and thickness of the sandstone lithofacies observed in this study.

the sandstones studied. Thickness ranges from 0.2 to 3 meters (0.5 to 9 feet). The lack of marine fossils, despite the proximity in vertical sections of marginal marine deposits, makes it seem likely that these conglomerates were deposited in channels in marginal marine or nearshore continental areas.

Thick sequence-capping conglomerates occur in two cores, Tenneco Bradley 8 (151 to 175.5 feet) and Colt Lauber 22AO (1235 to 1240 feet). These conglomerates are overlain by shales. The clasts in these thick conglomerates are all locally derived, mixed siltstone, shale, and sandstone fragments. Johnson (1973) interpreted this deposit in Tenneco Bradley 8 as a channel-cut-off fill. Thick sequence-capping conglomerates are distinguished from thin basal conglomerates by their thickness, position in the sandstone sequence, and composition of clasts.

Rocks of lithofacies B, stacked sandstone, and lithofacies C, crossbedded coarse sandstone, are each the result of traction and intermittent suspension transport. These two lithofacies are composed of medium- to fine-grained sand with some small carbonized plant fragments and micaceous partings. Both lithofacies have sharp lower and sharp or transitional upper contacts. The sandstones are dominated by large scale sedimentary structures, including high-angle cross beds (Figure 9), low-angle cross beds (Figure 10), horizontal, parallel to nonparallel bedding (Figure 11), and large-scale rippled bedding (Figure 12).

Figure 8. Slabbed core with a thin basal conglomerate (subfacies 1 of lithofacies A). Note the erosional base.

Figure 9. Large-scale, high-angle crossbeds.

Figure 8
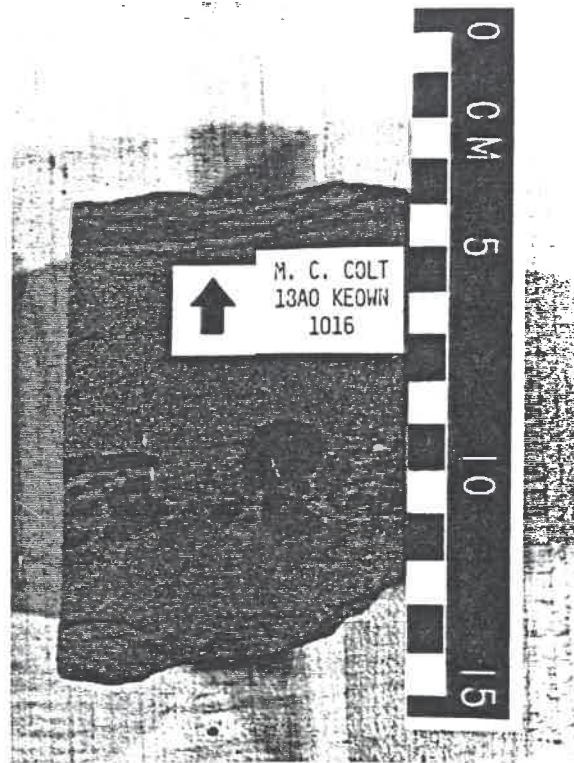
Figure 9
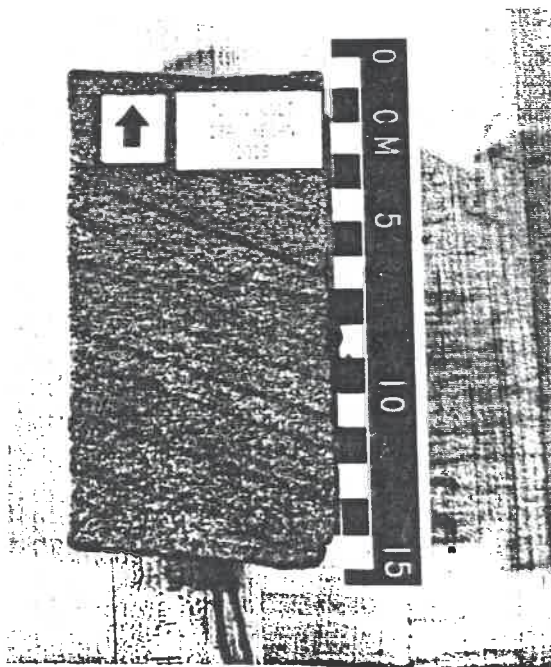
Figure 10. Large-scale, low-angle crossbeds.

Figure 11. Faint, large-scale, horizontal, parallel bedding.

Figure 10

BRAZOS
PIERPOINT 0-5
1958

Figure 11

M. C. COLT
14A0 JOHNSON
726
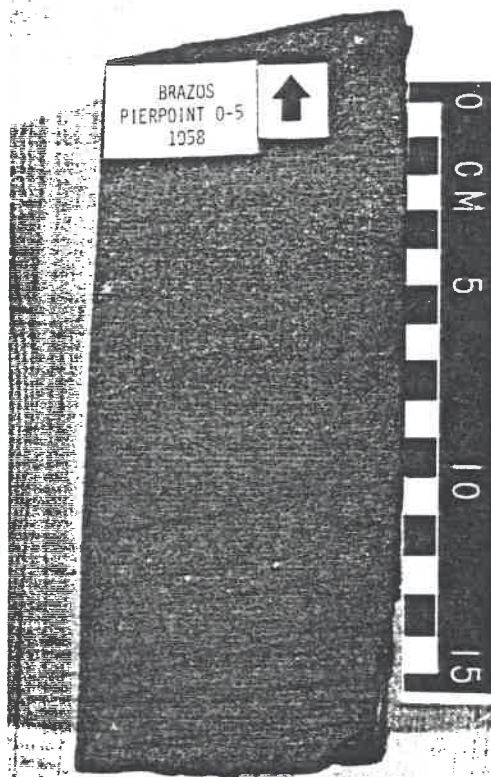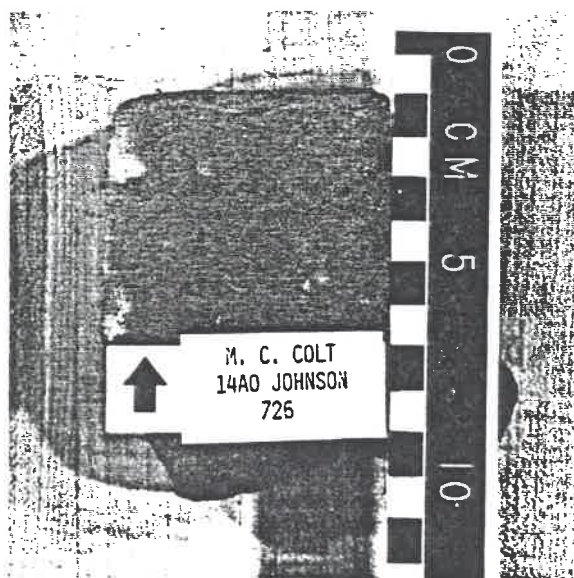
Figure 12.   Large-scale ripple bedding outlined by concentration of organic material.

Figure 13.   Small-scale, low-angle crossbedding with patchy, white, dolomite-ankerite cement.

Figure 12
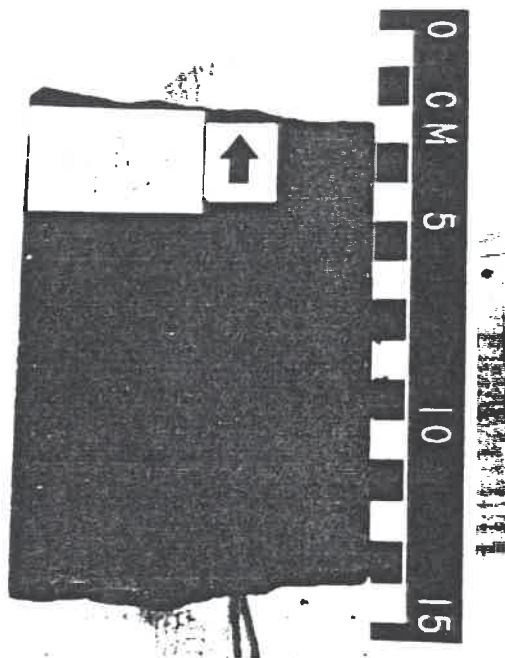
Figure 13
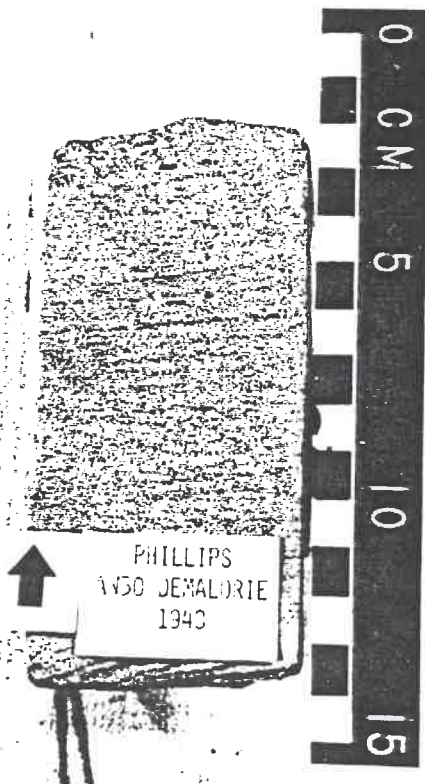
Individual crossbeds range from 1 to 5 centimeters thick and set thickness ranges from 10 centimeters to more than 1 meter. Bed and set thickness and grain size tend to decrease slightly upward through individual sand bodies. It is believed the large-scale sedimentary structures represent sand waves, dunes, and plane beds deposited by unidirectional currents (Harms et al., 1975).

The differentiation of lithofacies B and C is based on their association with the thin basal conglomerates, subfacies 1 of lithofacies A. Lithofacies B, stacked sandstone, is present in only two cores, Conoco Ord 34 and Phillips Demalorie AW33. This lithofacies ranges in thickness from 0.2 to 3.4 meters (0.5 to 11 feet) with a mean thickness of 1.4 meters (4.5 feet). It is a part of a set of several sequences. Each sequence consists of an erosional base overlain by a thin basal conglomerate (subfacies 1 of lithofacies A), which is overlain by a sandstone (lithofacies B). In Conoco Ord 34, this sequence is repeated three times and the set of sequences is 10 meters (33 feet) thick. The set of sequences is overlain by lithofacies D, which is described on pages 30 and 31. In Phillips Demalorie AW33, each sequence is capped by lithofacies D and the set of sequences is repeated three times. The deposit is 10 meters (32 feet) thick. The parts of sandstones including lithofacies B are believed to have been deposited by episodic currents that eroded into underlying strata,

deposited a basal conglomerate (subfacies 1 of lithofacies A), and then deposited a coarse sandstone (lithofacies B) with large-scale sedimentary structures.

Rocks of lithofacies C, crossbedded coarse sandstone, are present in 14 of the 27 sandstones studied and range in thickness from 0.6 to 13 meters (2 to 42 feet), with a mean thickness of 5 meters (17 feet). Although lithofacies B consists of a set of repeating sequences, lithofacies C does not. The parts of each sandstone body assigned to lithofacies C are believed each to have been deposited in one depositional episode by unidirectional currents.

Lithofacies C is in sharp contact at its base with either shales, coals, or thin basal conglomerates. Lithofacies C grades upward into rippled fine sandstones and interbedded sandstones, shales, and siltstones (lithofacies D and E, respectively) in most instances and is in sharp contact with the sequence-capping conglomerates of lithofacies A in Colt Lauber 22AO.

Lithofacies B was never found in the same sequence with lithofacies C. The two types of lithofacies, however, were found in the same sandstone. Conoco Ord 34 core contains lithofacies B, whereas the core from Conoco Ord 47, less than a mile away and in the same sandstone, contains lithofacies C. A similar situation also exists in Phillips Demalorie AW30 and AW33. Burggraf et al. (1981) reported a similar situation in outcrops of the Cherokee Group in Iowa.

The reasons for this association of lithofacies are discussed in a later section.

Rocks of lithofacies D, rippled fine sandstones, are composed of fine- to very-fine-grained sand with common micaceous and carbonaceous partings. These sandstones are dominated by small-scale sedimentary structures recognized as low-angle cross beds (Figure 13), ripples (Figure 14), and climbing ripples (Figure 15). The sedimentary structures are unidirectional and are interpreted to have been formed by small-scale ripples and sand waves (Harms et al., 1975). Bed and lamina thickness ranges up to 1 centimeter, and coset thickness is up to several meters. Thickness of this lithofacies ranges from 1 to 11 meters (2.5 to 35 feet). Mean thickness is 4 meters (12 feet). Lithofacies D overlies either lithofacies B, C, or E. The boundary between lithofacies is often difficult to place. Rippled fine sandstones are usually overlain by lithofacies E but also may be overlain by lithofacies A and C. The distinction between lithofacies B or C and D is the type and scale of sedimentary structures. The parts of sandstones assigned to lithofacies D are believed to have each been deposited in one episode by unidirectional currents.

Several other sedimentary features are found in lithofacies B, C, and D. Structureless or massive bedding may occur anywhere within a sequence (Figure 16). Using X-radiographs, Hulse (1978) found that apparently structureless intervals actually had sedimentary structures similar

31

Figure 14. Small-scale rippled bedding accentuated by the concentration of micaceous material along bedding planes.

Figure 15. Small-scale climbing ripples. Core sample is oriented so that the title is in an up-the-core position.

Figure 14
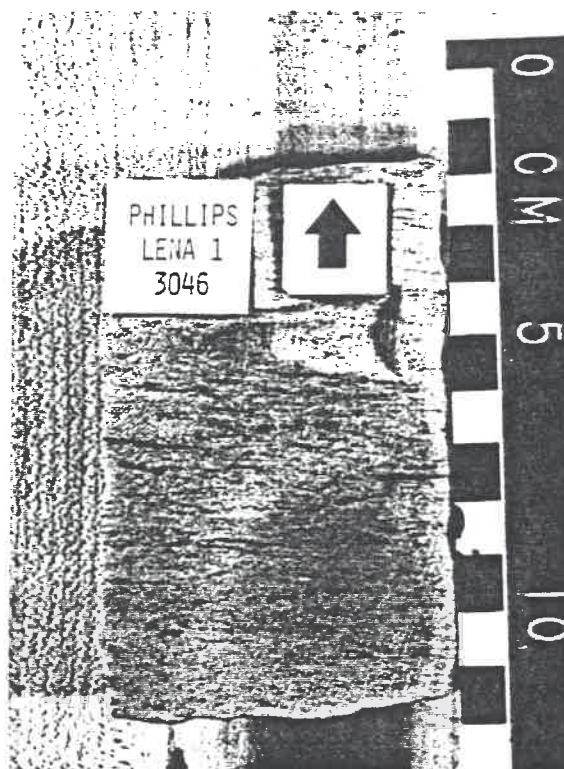
Figure 15

Figure 16.   Structureless bedding.

Figure 17.   Contorted bedding referred to as intraformation-
al recumbent folding (Reineck and Singh, 1975).   Note the
overlying and underlying beds have not been affected by the
folding.

Figure 16

M. C. COLT
14AO JOHNSON
742

0 CM 5 10 15

Figure 17

K.G.S.
TAR SANDS N
307

0 CM 5 10 15
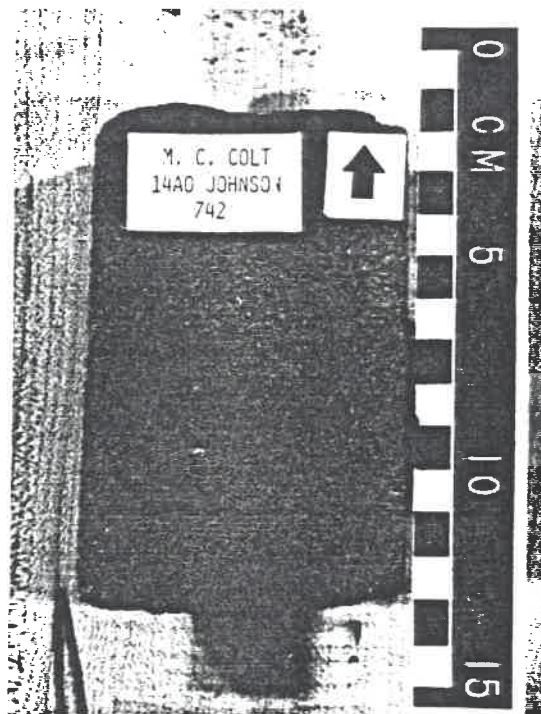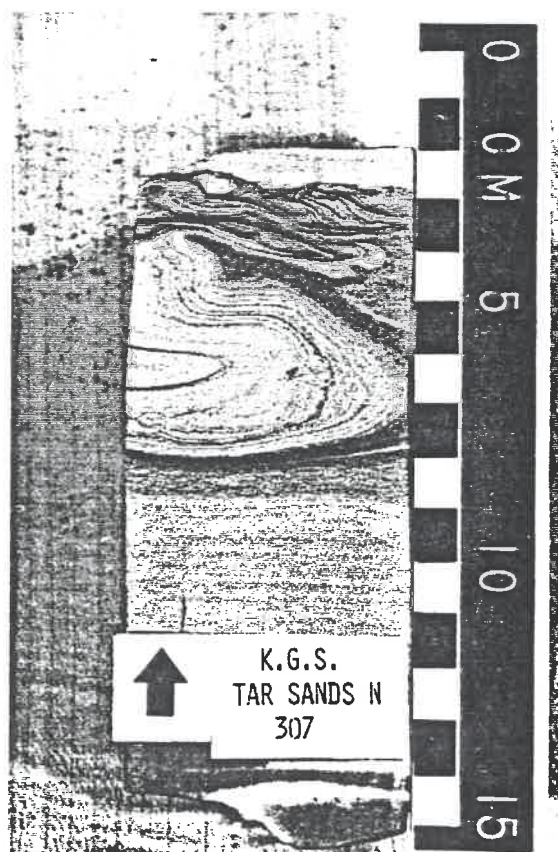
to subjacent and superjacent beds. In other words, seemingly structureless intervals in a large-scale crossbedded sequence were also made up of large-scale crossbeds. Contorted horizons, usually less than 15 centimeters (6 inches) thick, were noticed in some sandstone sequences (Figure 17). These contorted beds are recumbent folded, but the overlying and underlying beds are not affected. Burggraf et al. (1981) recognized similar features in outcrops of Cherokee Group sandstones in Iowa and noted that they occur in the upper portion of crossbeds. They cited Allen and Banks (1972), who developed a model for such intraformational recumbent folding (Reineck and Singh, 1975) that predicts that the formation of the folds requires liquefaction triggered by earthquake activity. Reineck and Singh, (1975, p. 78-79) attribute convolute bedding to differential liquefaction of a sedimentary layer. The liquefaction may be caused by compaction, overloading, seismic waves, or frictional shear of currents over sedimentary layers.

Rocks of lithofacies E, interbedded sandstones, shales, and siltstones, are composed of stacked laminae and beds of very-fine-grained sandstones, light- to dark-gray shales, and coarse siltstones. The lower contact of this lithofacies is often difficult to recognize because it is transitional with lithofacies C or D. Lithofacies E appears to have been deposited episodically. The deposits of each episode have a general upward increase in thickness and abundance of shale interbeds and interlaminae with an

34

accompanying decrease in thickness and abundance of sand-
stone interbeds and interlaminae. Sedimentary structures in
the very fine-grained sandstones and coarse siltstones are
climbing ripples (Figure 15) and planar laminae, whereas the
shales are horizontally laminated. Lamina thickness ranges
up to 1 centimeter, and set thickness ranges from 1 milli-
meter to 3 centimeters. Interbedded sandstones and shales
are often referred to as flaser (high sand, low shale)
(Figure 18), wavy (equal sand and shale) (Figure 19), and
lenticular bedded (low sand, high shale) (Figure 20)
(Reineck and Singh, 1975). All episodes do not include a
complete sequence from flaser to lenticular bedding.
Instead, they may grade abruptly into a burrowed light-to
dark-gray siltstone. Lithofacies E ranges from 1 to 20
meters (2.5 to 67 feet) thick. Mean thickness is 5 meters
(15 feet).

Burrowing was found in the siltstones and shales of
lithofacies E, particularly in the upper portion of a silt-
stone or shale. Burrows are not a common feature, however,
and only rarely are well-preserved burrows noted (Figure
21). Often the burrowing had disrupted bedding, which was
the primary means of identifying burrows (Figure 22). No
invertebrate fossils are found in hand samples or thin
sections of the sandstones. Plant fragments are common.
Root mottling is rarely observed and usually is associated
with coals.

Figure 18. Flaser bedding with high sand and low mud content.

Figure 19. Wavy or intermediate bedding with nearly equal amounts of sand and mud.

Figure 20. Lenticular bedding made up mostly of mud with minor amounts of sand.
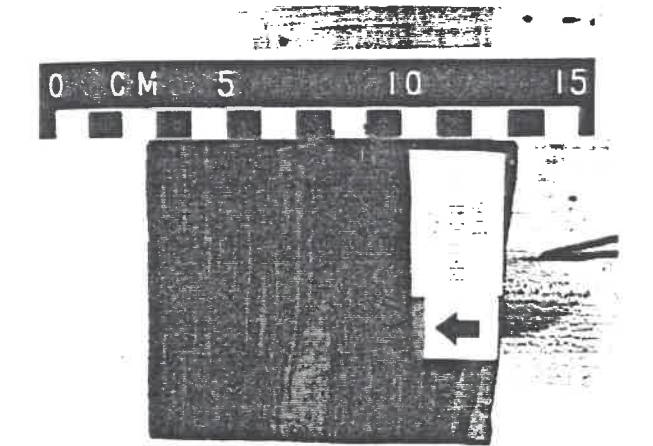
Figure 20
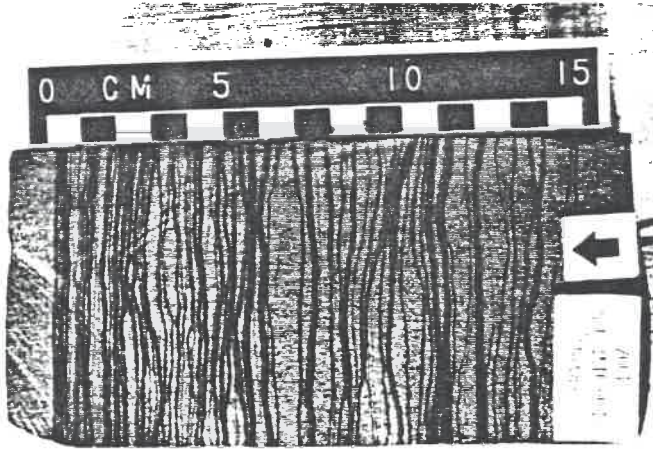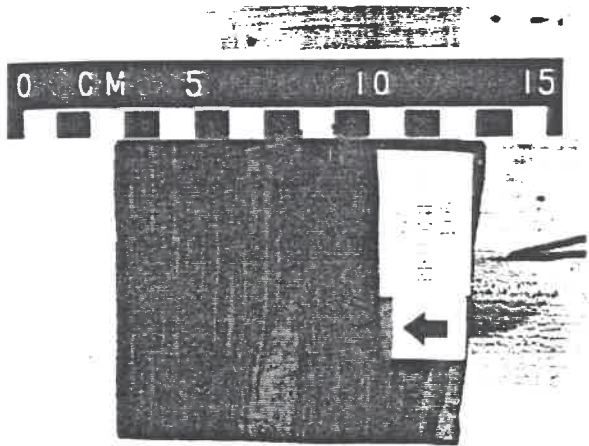
Figure 19

Figure 18

Figure 21. Well-preserved burrow.

Figure 22. Burrowed siltstone. Note the disrupted appearance of the bedding.

Figure 21
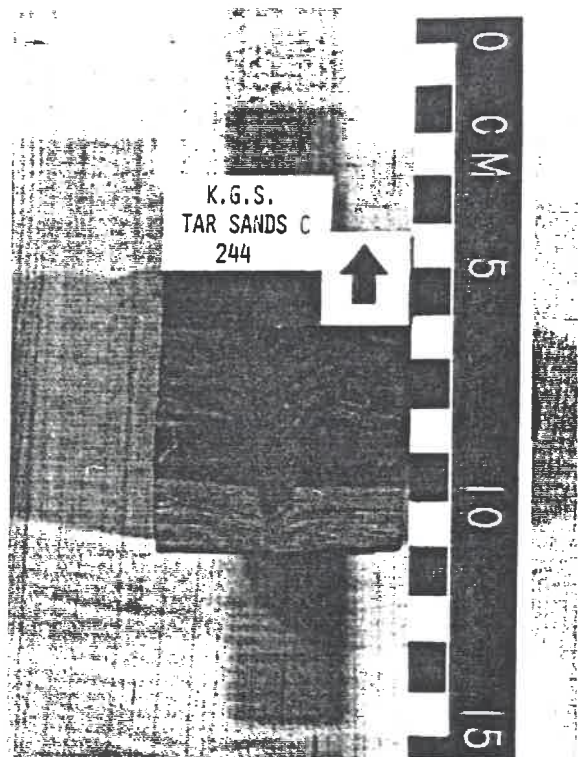
Figure 22
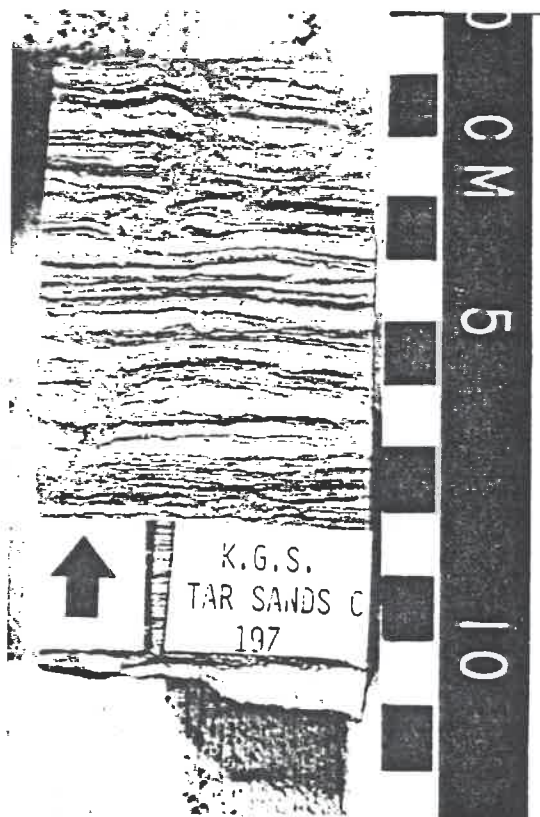
Figure 6 shows two idealized sequences showing the lithofacies relationships recognized in the sandstones studied. These sequences are marked by a general upward decrease in grain size and thickness and scale of sedimentary structures and an accompanying increase in frequency and thickness of micaceous partings, carbonaceous plant fragments, and argillaceous rock fragments. Such sequences are referred to as fining-upward sequences. Lithofacies A is not present at the base of every sandstone, but the basal contact of all sandstones but one is abrupt. Tesoro Baker W-35 had a basal contact that could be interpreted as transitional from an underlying dark siltstone that coarsened upward into a very fine-grained sandstone (core interval 571 to 583 feet). This sandstone is anomalous, as it has no hydrocarbon stain and is impermeable.

Numerous interpretations of the depositional environments of Cherokee Group sandstones have been presented. Ebanks and James, (1974, p. 23), summarized as follows:

> The Cherokee Basin has been depicted as the site of shifting and prograding alluvial and deltaic plains, estuaries, tidal delta complexes, beaches, and shallow shelf environments (Bass, 1936; Baker, 1962; Hayes, 1963; Visher, et al., 1971). Individual sandstone bodies in the Cherokee section have been variously described as ancient nearshore bars (Dillard, et al., 1941), barrier islands (Bass, 1936), tidal flat-tidal channel deposits (Hayes, 1963), and alluvial valley-fill sediments (Rich, 1923; Charles, 1941; McQuillan, 1968). Probably each of these interpretations is correct in some areas.

The currently accepted interpretation for the origin of many of the Cherokee Group sandstones is deposition in an

38

alluvial-deltaic setting where distributary channels were surrounded by peat bogs and various deltaic muds with occasional carbonate deposition in low-lying marine areas (Potter and Glass, 1958; Visher et al., 1971; Ebanks et al., 1977; Hulse, 1978; Brown, 1979). Burggraf et al. (1981) interpreted the Cherokee Group sandstones in Iowa as deposits of high-constructive deltas. It has been proposed that the sandstones could have been deposited in tidal channels, but the unidirectional bedding features and presence of complete fining upward sequences coupled with the lack of marine fauna make that interpretation unlikely (Hulse, 1978).

The Cherokee Group sandstones evaluated in this study were deposited by unidirectional currents in nearshore, continental channels as indicated by fining upward sequences of unidirectional bedding features coupled with a lack of marine fauna and sparse burrowing. Precise interpretation of depositional environments is speculative because of the lack of geometry and shape of the sandstone bodies and their lateral deposits. Throughout the rest of the text, differentiation of the sandstones will be based primarily on the scale of sedimentary structures which is directly related to grain size and composition. Two kinds of sandstones will be recognized: coarser-grained sandstone, which includes lithofacies A, B, and C; and finer-grained sandstone, which includes lithofacies D and E.

SANDSTONE PETROLOGY

METHODS

Mineralogy and petrology of the Cherokee Group were studied in 150 thin sections made from samples of the cores examined in this study. Some of the sections were cut for earlier studies (Ebanks et al., 1977; Hulse, 1978), and some samples were impregnated with blue or red epoxy during thin section preparation to aid in recognition of interconnected pore space. Thin sections were stained for carbonate cements using a mixed alizarin red-S and potassium ferricyanide staining technique (Dickson, 1966). Supplemental samples were studied using the scanning electron microscope (S.E.M.) and X-ray diffraction.

Table 2 is a compilation of data obtained from counts of 200 points on 15 thin sections. The point counts were made using a rectangular grid system designed to cover the entire slide. Using the same grid system, forty-seven thin sections, including the 15 used in the point counts, were also counted for grain size by using a calibrated ocular to measure the long axis of 100 monocrystalline quartz grains. Table 3 is a compilation of the average grain size and maximum grain size measured.

QUARTZ

Quartz is the most common mineral in the sandstones, making up from 50 to 70 percent. Monocrystalline quartz

TABLE 2 - Sandstone Mineralogy based on count of 200 points in each thin section.

Well Name	Tenneco Bradley		K.G.S. Tar Sands C		
feet	105.5	170	202	257	268
(meters)	32	52	62	78	82
DETRITAL					
Quartz					
Monocrystalline	106	104	97	101	126
Polycrystalline	6	4	6	3	2
Feldspar					
Potassium					
Unaltered	0	0	0	0	0
Altered	8	11	6	9	5
Plagioclase					
Unaltered	0	0	1	0	0
Altered	2	3	1	1	1
Rock Fragments					
Quartzite	7	3	0	5	2
Mica-Quartz	3	5	5	5	1
Chert	2	2	2	3	2
Silty-Shale	1	3	1	2	0
Argillaceous					
Nonfoliated					
Unaltered	4	1	3	1	2
Altered	4	5	1	2	0
Foliated					
Unaltered	1	0	3	0	4
Altered	1	0	1	2	0
Phosphatic	0	0	0	0	0
Carbonaceous	3	2	4	0	1
Micas					
Unaltered	0	1	5	5	0
Altered	2	10	11	1	0
Heavy Minerals	1	1	1	1	1
AUTHIGENIC					
Silica					
Euhedral	33	34	6	22	51
Interlocking	33	47	72	60	73
Siderite					
Spherulitic	0	0	0	0	0
Rhombic	1	4	1	2	1
Dolomite-Ankerite	1	6	6	2	5
Kaolinite	20	7	1	8	8
Pyrite	0	0	0	0	0
Chlorite	1	0	0	1	0
Illite-Smectite	0	0	0	2	0
PORE SPACE	26	28	44	44	39

41

TABLE 2 (continued)

Well Name	Tesoro Baker W-35		Conoco Ord 34	Colt 18AO Keown	
feet	556	565	685	840	1014.5
(meters)	170	172	209	256	309
DETRITAL					
Quartz					
Monocrystalline	90	110	85	59	85
Polycrystalline	0	3	1	5	2
Feldspar					
Potassium					
Unaltered	0	0	0	2	0
Altered	8	9	9	20	8
Plagioclase					
Unaltered	0	0	0	0	0
Altered	1	1	5	2	2
Rock Fragments					
Quartzite	6	4	3	1	9
Mica-Quartz	7	6	2	5	2
Chert	2	5	6	8	2
Silty-Shale	0	0	0	3	3
Argillaceous					
Nonfoliated					
Unaltered	6	2	6	5	10
Altered	9	1	0	13	0
Foliated					
Unaltered	1	3	7	2	7
Altered	3	0	0	8	0
Phosphatic	0	1	0	0	6
Carbonaceous	0	0	0	0	1
Micas					
Unaltered	9	0	2	4	0
Altered	14	4	5	16	6
Heavy Minerals	0	0	0	1	0
AUTHIGENIC					
Silica					
Euhedral	28	29	23	18	13
Interlocking	49	69	47	37	47
Siderite					
Spherulitic	0	0	0	0	14
Rhombic	4	5	10	9	0
Dolomite-Ankerite	3	5	11	4	8
Kaolinite	8	16	0	3	13
Pyrite	3	0	2	3	0
Chlorite	1	0	1	2	3
Illite-Smectite	0	0	0	0	0
PORE SPACE	25	25	45	25	19

TABLE 2 (continued)

Well Name	Colt 22AO Lauber		Jackson Bros Crew 21	Sinclair Weir 1	
feet	1039	1248	2515	3418	3437
(meters)	317	380	767	1042	1048
DETRITAL					
Quartz					
Monocrystalline	86	94	75	95	109
Polycrystalline	2	1	2	3	3
Feldspar					
Potassium					
Unaltered	0	0	0	3	0
Altered	7	15	11	17	9
Plagioclase					
Unaltered	0	0	0	1	0
Altered	1	1	4	5	2
Rock Fragments					
Quartzite	1	5	5	2	17
Mica-Quartz	6	6	1	4	6
Chert	1	3	6	2	6
Silty-Shale	12	1	0	0	1
Argillaceous					
Nonfoliated					
Unaltered	1	0	12	11	9
Altered	0	6	0	6	0
Foliated					
Unaltered	2	5	14	5	8
Altered	0	0	0	4	0
Phosphatic	2	0	0	0	0
Carbonaceous	5	7	0	0	0
Micas					
Unaltered	7	3	5	1	0
Altered	6	4	11	7	0
Heavy Minerals	1	0	0	0	0
AUTHIGENIC					
Silica					
Euhedral	21	30	33	20	38
Interlocking	54	58	26	58	60
Siderite					
Spherulitic	30	7	0	0	0
Rhombic	5	0	2	6	1
Dolomite-Ankerite	3	0	15	0	4
Kaolinite	3	7	6	1	11
Pyrite	0	1	0	0	0
Chlorite	3	1	1	2	1
Illite-Smectite	0	0	0	2	0
PORE SPACE	16	33	30	23	13

43

TABLE 3 - Grain sizes based on count of 100 monocrystalline quartz grains in each thin section.

Well Name	Sample Depth (feet)	Grain Sizes Average	Maximum phi units	Standard Deviation S
K.G.S. Tar Sands C	202	2.81	1.87	0.58
	250	3.07	1.98	0.59
	257	2.90	1.82	0.54
	268	2.81	1.98	0.41
K.G.S. Tar Sands N	230	3.40	2.02	0.63
	304.5	3.38	1.93	0.62
	320.2	3.37	2.38	0.44
K.G.S. Tar Sands AA	30	2.92	1.73	0.50
	35	2.85	1.68	0.60
Tenneco Bradley 8	95	2.35	1.13	0.55
	105.5	2.27	1.09	0.43
	112	2.01	0.82	0.54
	155	2.65	1.76	0.45
	170	2.53	0.70	0.66
Colt 14AO Johnson	714	1.95	0.77	0.58
	725	2.28	1.13	0.73
	742	1.71	1.04	0.44
Tesoro W-35 Baker	556	3.00	1.82	0.50
	565	2.43	1.29	0.53
Colt 18AO Keown	840	3.13	2.11	0.47
	948	2.30	1.19	0.48
	982	2.52	0.73	0.64
	1014.5	1.75	0.71	0.66
	1019	2.98	1.82	0.48
	1160	2.10	1.07	0.41
	1169.7	1.98	1.04	0.51

TABLE 3 (continued)

Well Name	Sample Depth (feet)	Grain Sizes Average	Maximum	Standard Deviation S
		phi units		
Conoco Ord 34	685	3.28	2.04	0.48
	726	3.01	1.73	0.47
Conoco Ord 47	712	3.52	1.87	0.46
	729	3.52	2.43	0.39
Brazos 0-5 Pierpoint	1016.8	3.28	1.97	0.57
	1043	2.32	1.25	0.51
	1050	2.72	1.68	0.51
Colt 22AO Lauber	1039	2.95	1.63	0.49
	1242	2.34	1.59	0.50
	1248	2.52	1.04	0.50
	1259.5	2.76	1.68	0.47
Phillips 30AW Demalorie	1930.5	2.83	1.63	0.59
	1970.8	3.00	1.93	0.51
Jackson Bros. Barrier 36	2502	3.52	2.10	0.59
	2505.5	2.54	1.19	0.48
Jackson Bros. Crew 21	2507	2.68	1.32	0.54
	2515	2.40	1.13	0.51
	2523.8	2.65	1.43	0.57
Phillips Lena 1	3061.3	2.56	1.47	0.60
Sinclair Weir 1	3418	3.48	2.74	0.43
	3437	1.94	0.98	0.50

makes up 40 to 55 percent of the sandstones and is sub-
rounded to subangular, subequant to rarely elongate, very
fine to medium sand sized, and slightly undulose. Vacuoles
were often noted in detrital grains and occur both as
randomly oriented features and as bubble trains (Boehm
Lamellae) (Figure 23). In addition, various microlite
inclusions were observed including apatite and zircon and
less commonly acicular needles (Figure 24). A rare phenome-
non in quartz grains was the presence of locally abundant,
vermicular chlorite (Figure 25). Many grains have a subhed-
ral to euhedral shape due to optically continuous quartz
overgrowths (Figures 23, 26, and 36). Clay coatings were
observed between individual detrital grain cores and over-
growths (Figure 26). In addition to the subhedral to
euhedral quartz overgrowths, patchy, subhedral to anhedral,
interlocking silica cement occurs, which gives groups of
grains a mosaic or quartzite appearance (Figures 27 and 28).
This is particularly common in the finer grained sandstones
at the top of sequences. Subhedral to euhedral overgrowths
are more typical of the coarser grained portion of sequen-
ces. Some quartz grains have undergone replacement by very
fine carbonate inclusions or extensive corrosion of grain
boundaries by rhombic dolomite-ankerite and siderite cement
(Figure 29). Rarely, doubly terminated, authigenic quartz
crystals have developed within dolomite cement.

Other types of quartz also occur. Some monocrystalline
quartz grains display highly undulose extinction (greater

46

Figure 23. Euhedral quartz overgrowth on a quartz grain (Q). Arrow points to thin, discontinuous clay coating on the detrital grain. The nearby pore is filled with patchy dolomite-ankerite cement (C). Note the vacuoles in the detrital quartz grains. Scale is 0.10 mm. (Jackson Bros. Crew 21 at 2515 feet).

Figure 24. Photomicrograph of a lone rhomb of dolomite-ankerite (C) in extensively vacuolized, or partially dissolved, feldspar (F). Arrow points to a microlite inclusion in a quartz grain. Scale is 0.10 mm. (Tenneco Bradley 8 at 93.5 feet).
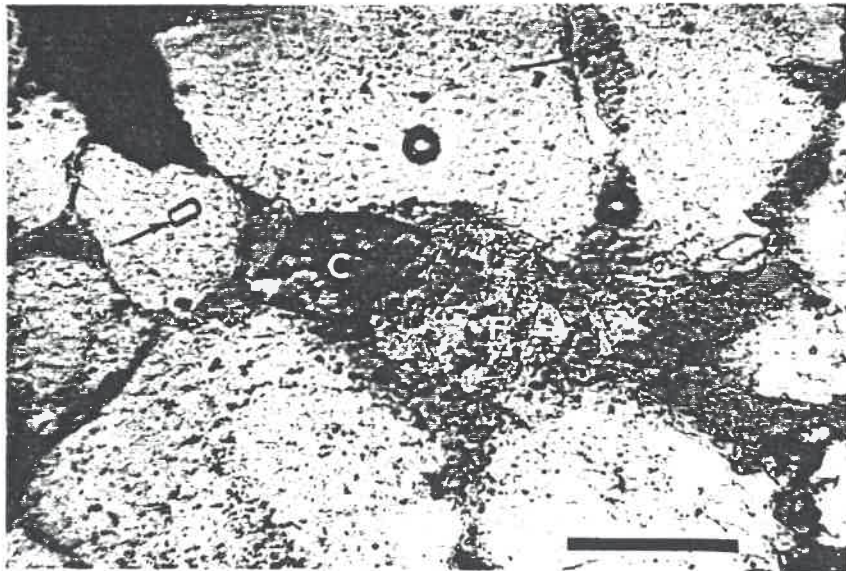
Figure 23

Figure 24

Figure 25. Photomicrograph of a quartz grain with abundant inclusions of vermicular chlorite (arrow). Scale is 0.10 mm. (Tenneco Bradley 9 at 116 feet).

Figure 26. Photomicrograph showing well developed clay coating on a detrital grain (arrow). Note the pore with angular boundaries which is probably secondary (P). Scale is 0.10 mm. (Conoco Ord 47 at 712 feet).
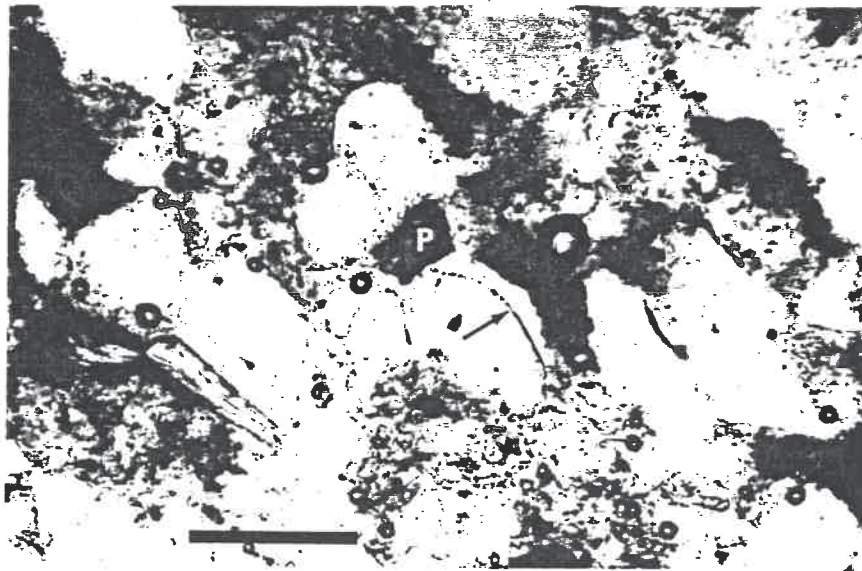
Figure 25

Figure 26

Figure 27. Photomicrograph showing quartz grains with patchy, welded, mosaic or interlocking silica overgrowths (MQ). Also note the siderite cement (C). Scale is 0.10 mm. (Conoco Ord 47 at 714 feet).

Figure 28. Photomicrograph with crossed nicols showing same area in Figure 27 above. Scale is 0.10 mm. (Conoco Ord 47 at 712 feet).
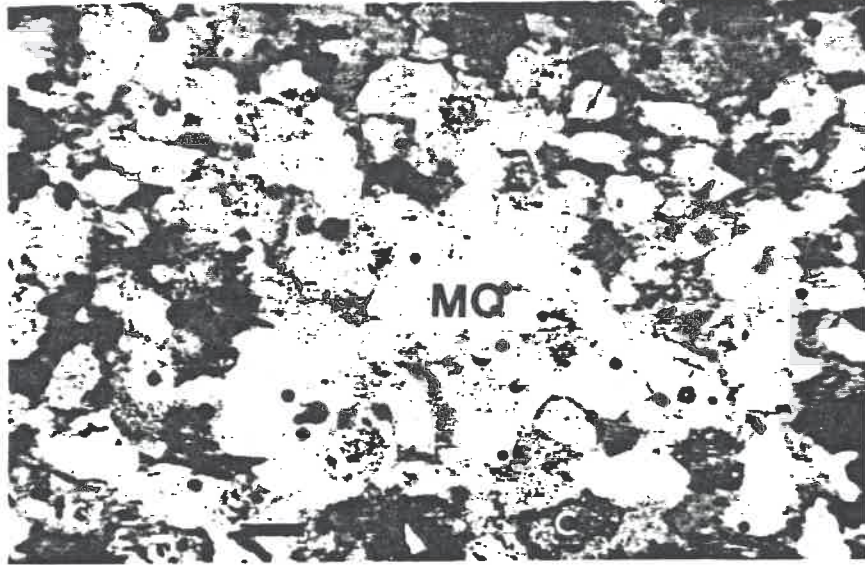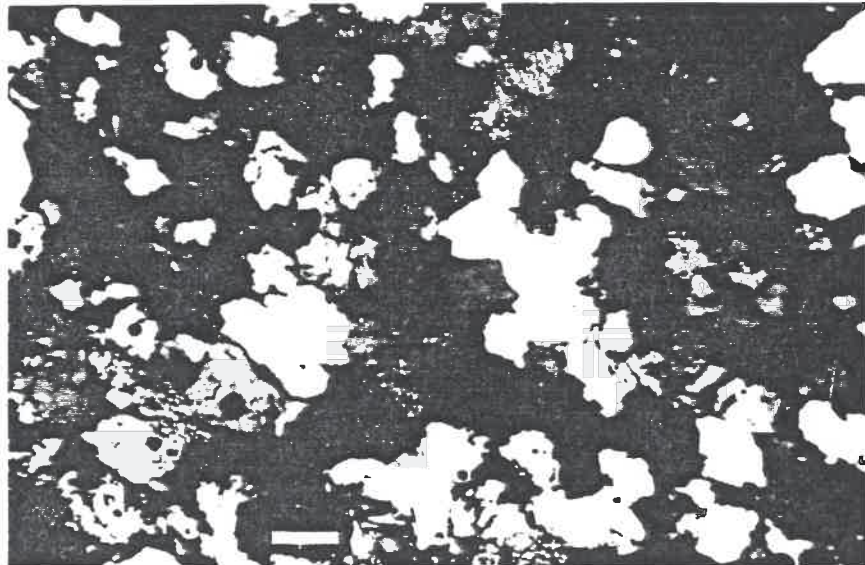
Figure 27

Figure 28

Figure 29. Photomicrograph with arrow pointing to quartz grain boundaries corroded by dolomite-ankerite cement (C). Scale is 0.10 mm. (Tenneco Bradley 8 at 155 feet).

Figure 30. Crossed nicols photomicrograph displaying poikilotopic, pore-filling, concretionary calcite cement (C) with an unaltered fractured plagioclase feldspar (F) and abundant spherulitic siderite (arrow points to one spherule). Scale is 0.10 mm. (Colt Keown 18A0 at 1015 feet).
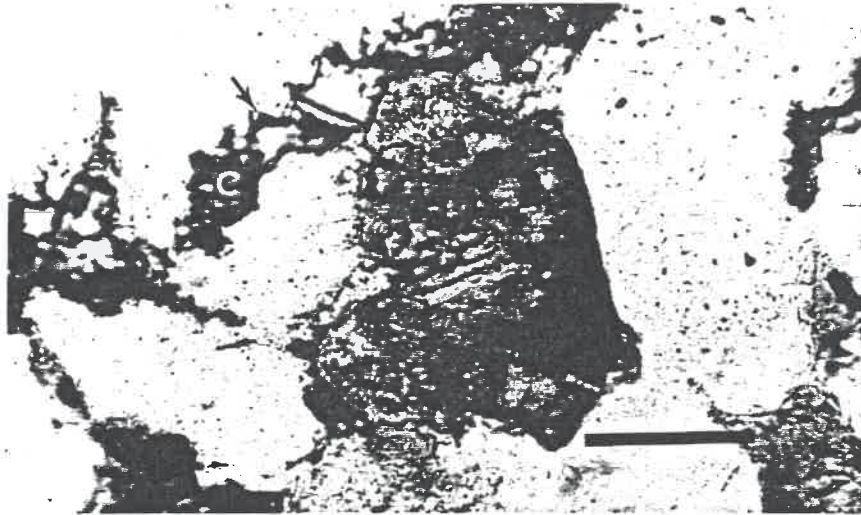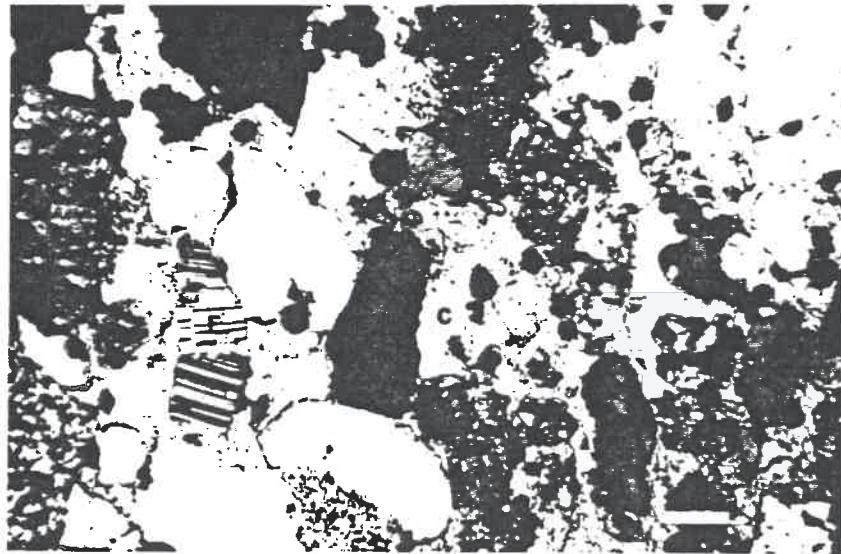
Figure 29

Figure 30

than 10 degrees). Others show a semi-composite to composite nature. Polycrystalline grains composed of two or more quartz grains were noted. Sutured metamorphic quartz grains are also present, but these usually constitute less than one percent of the rock. Other quartz-bearing rock fragments will be discussed as rock fragments. These include chert, foliated mica-quartz gneiss fragments, and quartzite fragments.

FELDSPARS

Twinned and untwinned feldspars constitute up to 15 percent of the sandstones. The ratio of untwinned to twinned feldspars ranges from 1:1 to 5:1 and is generally about 3:1. Most of the twinned feldspars are plagioclase with albite twinning (Figures 30 and 33). It is assumed that most of the untwinned feldspars are potassium feldspars (Figure 24), although Hulse (1978) found untwinned plagioclase feldspar. Microcline with cross hatch twinning was rarely observed (Figure 31). Some grains with uneven twinning lamellae were seen and tentatively identified as microcline (Figure 32) (Pittman, 1971). Feldspar grains are coarse silt to very fine sand sized, angular to subangular, and subequant.

Both altered and unaltered feldspars were observed. Chemical alteration and dissolution of feldspars are common. Products of chemical alteration include kaolinite as small patches with low birefringence, sericite and illite as small

Figure 31. Photomicrograph with crossed nicols of a micro-
cline grain with cross-hatch twinning. The grain has been
corroded by siderite cement along its boundary (arrow).
Scale is 0.10 mm. (Colt Keown 18AO at 1015 feet).

Figure 32. Photomicrograph with crossed nicols of an
extensively vacuolized, or partially dissolved, feldspar
(arrow) with uneven twinning lamellae which are believed to
be an indicator of microcline (Pittman, 1971). Scale is
0.10 mm. (Colt Keown 18AO at 1015 feet).
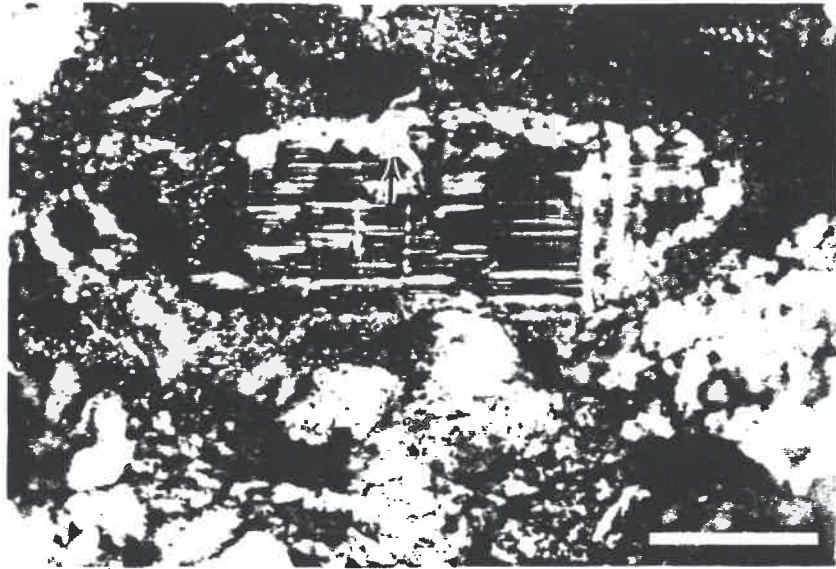
Figure 31
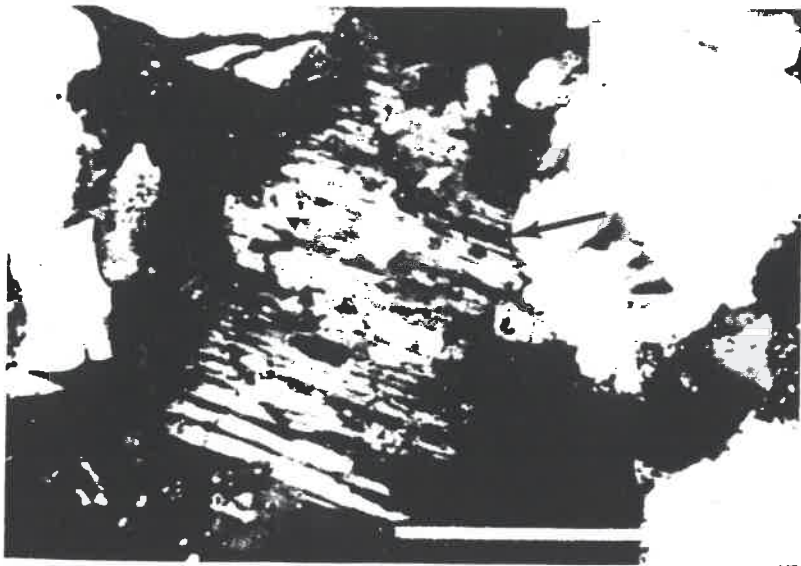
Figure 32

Figure 33. Photomicrograph with crossed nicols showing a fractured and partially hydromica replaced (bright areas) plagioclase feldspar (arrow). Scale is 0.10 mm. (Tenneco Bradley 8 at 95 feet).

Figure 34. Photomicrograph showing angular, secondary pore, probably a dissolved feldspar filled with vermicular booklets of kaolinite (K); (Tenneco Bradley 8 at 105.5 feet).
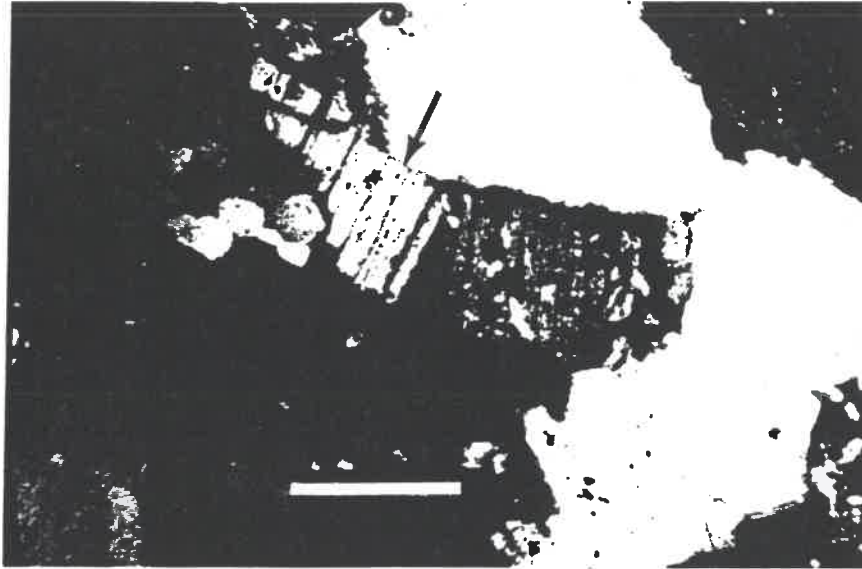
Figure 33
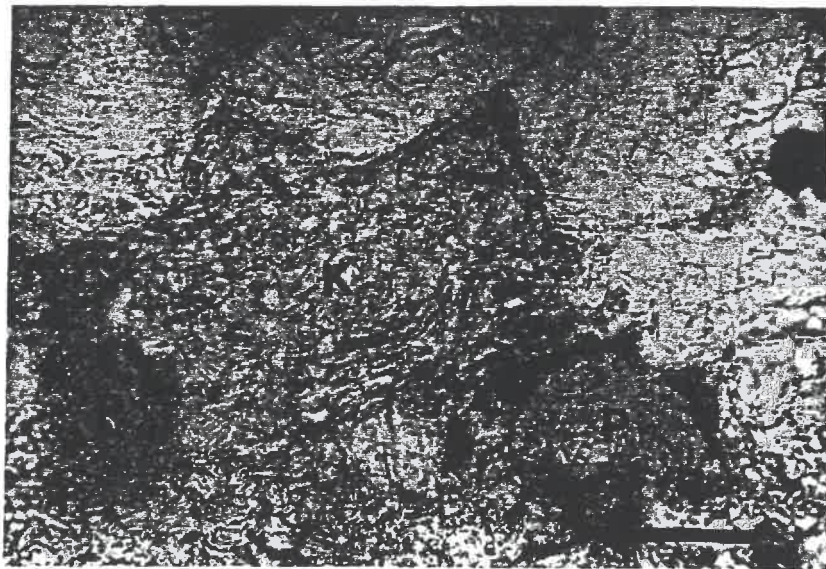
Figure 34

elongate hydromica grains along cleavage planes (Figure 33), and rare chlorite. Identification of altered feldspar grains is difficult if a large portion of the grain has been altered. The most useful criteria are the recognition of cleavage traces, parallel sericite grains, remnant grain shapes, and remnant twinning. Dissolution of feldspars is more common than alteration and ranges from extensive vacuolization to essentially complete dissolution or honey-combed grains (Figure 33) (Schmidt and MacDonald, 1979). The evidence for completely dissolved feldspars is molds of dissolved grains that retain the original angular shape of the grain (Figures 34 and 37). In general, coarse sandstones have had more extensive partial dissolution of feldspar grains than fine sandstones. This is probably related to greater volumes of water flowing through the coarse sandstones, which generally have higher permeabilities. In addition to chemical alteration and dissolution of feldspars, replacement by carbonate minerals has occurred (Figures 24 and 31).

Heald and Larese (1973) and Land and Milliken (1981) have reported feldspar dissolution as a possible contributor to secondary porosity in sandstone reservoirs. The presence of blue epoxy in partially dissolved feldspars of Cherokee Group sandstones indicates that such secondary porosity contributes to effective (interconnected) pore space.

Figure 35. Photomicrograph of patchy kaolinite cement (K), organic fragments (O), and primary pores (P). Scale is 0.10 mm. (Tenneco Bradley 8 is 105.5 feet).

Figure 36. Photomicrograph of an oversized pore filled with kaolinite (K). Arrow points to subhedral quartz overgrowth on a quartz grain. Scale is 0.10 mm. (Tenneco Bradley 8 at 105.5 feet).
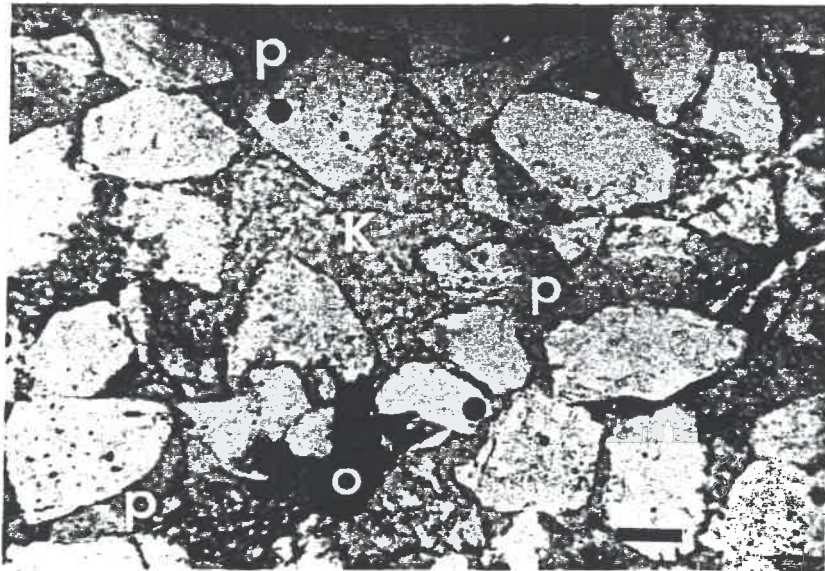
Figure 35
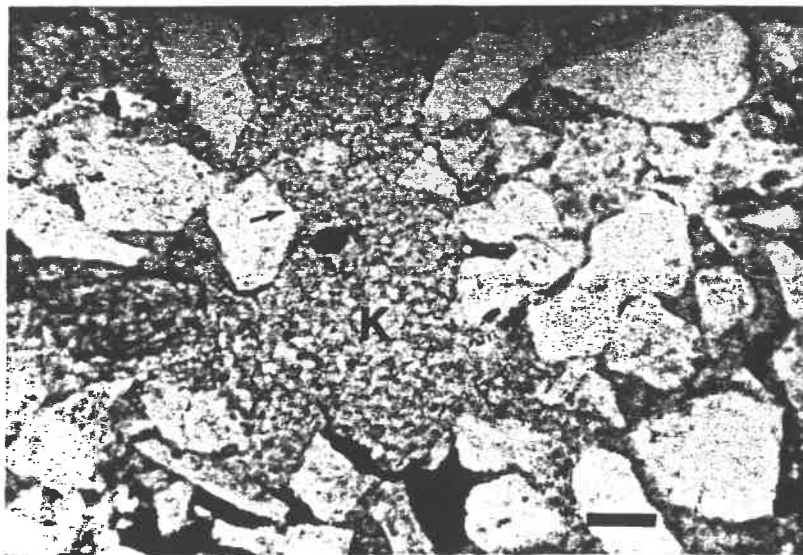
Figure 36

Figure 37. Photomicrograph of a secondary pore filled with kaolinite (K). Note the biotite presumably bent during compaction around the subsequently dissolved detrital grain. Primary pores (P) have not been filled with kaolinite. Scale is 0.10 mm. (Tenneco Bradley 8 at 105.5 feet).

Figure 38. Photomicrograph with crossed nicols of a metamorphic quartz-mica gneiss fragment (G). Scale is 0.10 mm. (Conoco Ord 47 at 712 feet).

Figure 37

Figure 38

Dissolution of feldspar occurs by two major mechanisms: 1) rapid exchange from grain surfaces of mono- and divalent cations for H+ in the aqueous solution (e.g., Garrels and Howard, 1957; Wollast, 1967; Helgeson, 1971; Berner and Holdren, 1979) and 2) long-term incongruent (nonlinear kinetics), diffusion controlled surface reactions (e.g., Paces, 1973; Busenberg and Clemency, 1976) and long term congruent (linear kinetics) surface reactions (e.g., Lagache, 1976; Petrovic, 1976; Berner and Holdren, 1979).

Fractures in feldspars were occasionally observed (Figures 30 and 33). These fractures are more commonly noted in twinned plagioclase grains where it occurs parallel to and between twinned lamellae.

Feldspar overgrowths are a rare but consistent cement in all of the sandstones except where concretions have occurred. It is uncertain whether these cements occurred before or after feldspar dissolution because unaffected overgrowths can be found around partially dissolved detrital feldspars. Compositional differences, due to lower crystallization temperatures of the overgrowths, can permit preservation of overgrowths while the detrital core dissolves.

ROCK FRAGMENTS

Metamorphic Rock Fragments

Metamorphic rock fragments make up no more than two percent of the detrital fraction of Cherokee sandstones.

They consist of foliated quartz-mica gneiss fragments and quartzite fragments.

Foliated quartz-mica gneiss fragments are typically composed of parallel interlayed quartz and muscovite, chlorite, or biotite (Figure 38). These grains have an average grain size much like monocrystalline quartz grains and are usually subrounded to rounded. They behaved as hard, detrital grains during compaction, a criterion used to differentiate them from soft argillaceous rock fragments. Alteration of quartz-mica gneiss fragments is rare and consists of etching and replacing by carbonate cements and sericite, and chlorite replacement of micas. Partial sericite replacement of quartzite fragments may have caused them to look like gneiss fragments.

Quartzite fragments made up of numerous silt sized quartz grains are another common metamorphic rock fragment (Figure 39). The distinction between quartzite fragments, coarse-grained chert fragments, and polycrystalline quartz is not sharp. All of these grains behave rigidly and therefore show no compactional effects. Grains are subrounded to well rounded, subequant to equant, and fine to very fine sand size.

Sedimentary Rock Fragments

Sedimentary rock fragments make up from one to more than 20 percent of individual samples. The types recognized are argillaceous rock fragments and chert.

58

Several types of argillaceous rock fragments were recognized. Pure argillaceous rock fragments can be subdivided into two types: foliated and nonfoliated. Mixed siltstone, shale, and sandstone fragments are included as argillaceous rock fragments.

Nonfoliated argillaceous rock fragments are typically composed of clays with low birefringence and rare, randomly oriented sericite and illite (Figure 40). The color of these grains in plane-polarized light ranges from light gray to brownish-red. Grain shape is the most useful characteristic for differentiating them from foliated argillaceous rock fragments. Nonfoliated argillaceous rock fragments almost always show compactional effects because they have been forced into pore spaces and around harder detrital grains resulting in concavo-convex contacts (Figure 40) (Taylor, 1950). These soft rock fragments are common in the micaceous fine sandstones, which usually have little cement. The only commonly associated cement is subhedral to anhedral quartz overgrowths that form the mosaic or interlocking texture. These rock fragments are more typically found in sandstones with relatively lower porosities and permeabilities due to the blocking of pores by compacted rock fragments, silica cements, and the smaller pore throats due to finer grain size.

Some of the argillaceous rock fragments have been replaced by fine-grained siderite. This resulted in clasts that could be misidentified as carbonate rock fragments, but

Figure 39. Photomicrograph with crossed nicols of a quartzite fragment (arrow). Scale is 0.10 mm. (Colt Keown 18AO at 1015 feet).

Figure 40. Photomicrograph of a nonfoliated argillaceous rock fragment (arrow) that has been forced around other detrital grains and into surrounding pores. Note the partially dissolved feldspar grain (F). Scale is 0.10 mm. (Tenneco Bradley 8 at 116 feet).
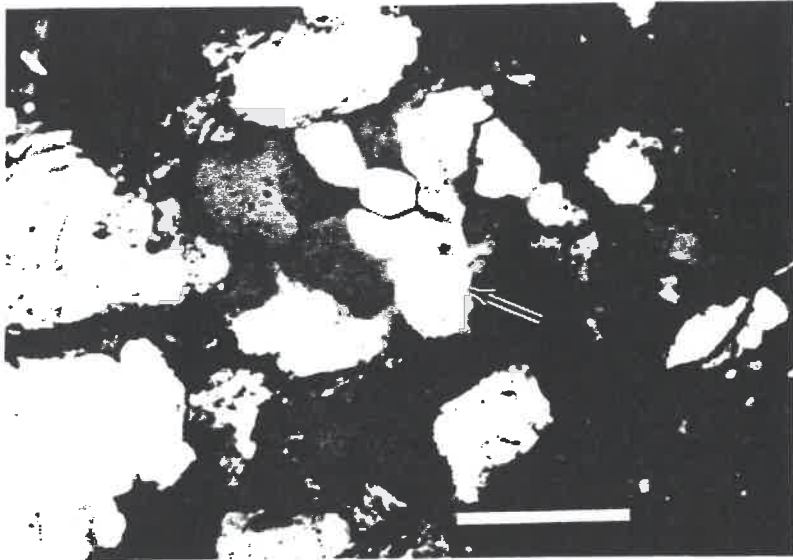
Figure 39
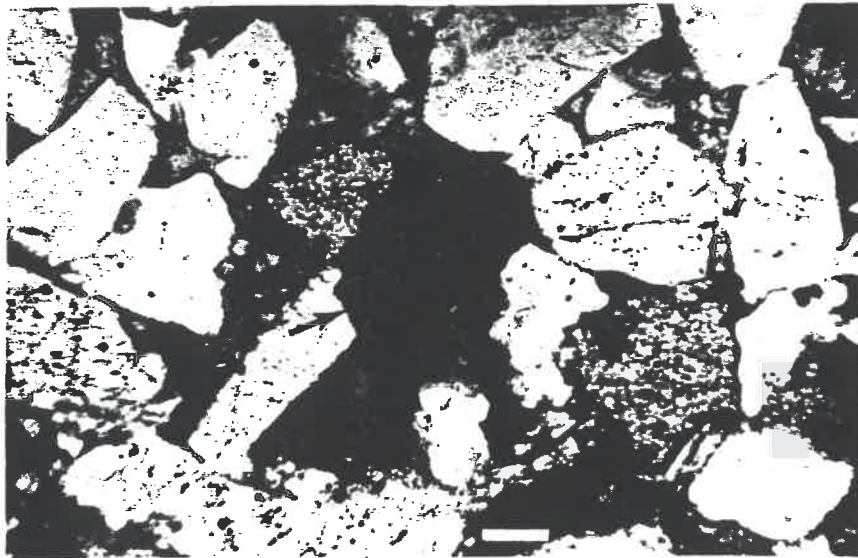
Figure 40

Figure 41. Photomicrograph of an elongate siltstone-shale fragment (S). Note the concavo-convex grain boundaries (Taylor, 1950). Scale is 0.10 mm. (Conoco Ord 34 at 726 feet).

Figure 42. Photomicrograph with crossed nicols of a chert grain (C) outlined in white. Scale is 0.10 mm. (Colt Keown 18AO at 1015 feet).
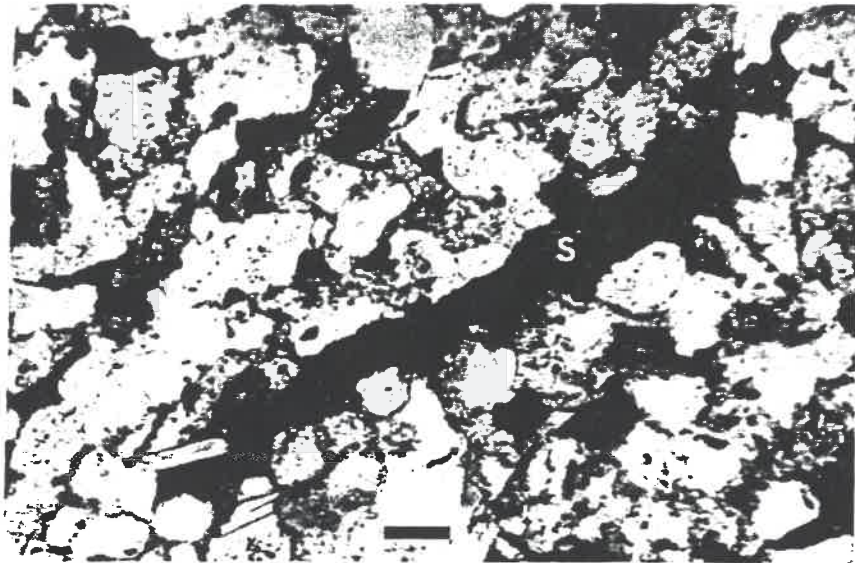
Figure 41
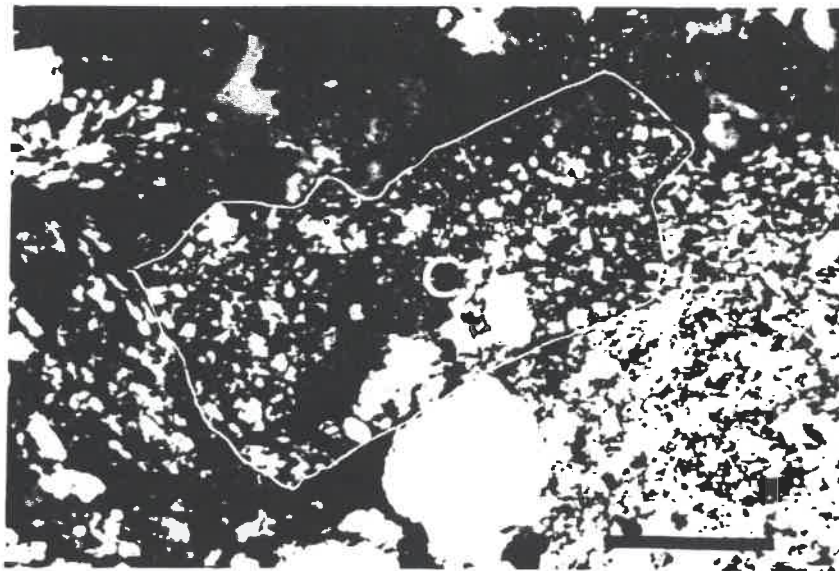
Figure 42

they show compactional effects leading to their interpretation as argillaceous rock fragments.

Foliated argillaceous rock fragments differ from nonfoliated rock fragments in the following ways. 1) The foliated rock fragments contain oriented grains of sericite. Other phyllosilicates also appear to be oriented in parallel planes. 2) The foliated types do not appear to have been affected by compaction and instead behaved as rigid grains. Occasionally, grains were noted whose boundaries had not been affected although the grain itself had been broken or bent. 3) It is possible that some of these grains were originally feldspars that have been altered to kaolinite and mica but still contain remnants of the detrital grain. This would explain the retention of shape and the parallel orientation of their micas.

A third type of argillaceous sedimentary rock fragment is mixed siltstone, shale, and sandstone clasts composed of silt-sized grains of quartz, feldspar, mica, and rock fragments in a clay matrix (Figure 41). These clasts are at least medium to coarse sand sized and are always elongate. Their edges are typically rounded, and their contacts with surrounding grains are almost always concavo-convex. This kind of rock fragment was rarely found in lithofacies B, C, and D, except in concentrated layers, but is common in the interbedded sandstone-shale lithofacies, E, at the top of sequences. It was probably eroded from nearby sediments during rapid-flow conditions and quickly redeposited.

62

In general, abundance of rock fragments does not vary from sandstone to sandstone as much as within an individual sequence, where, excluding conglomerates, the rock fragments are more common at the top of the sequence than at the base. The biggest contributors to this difference are the nonfoliated argillaceous and mixed siltstone, shale, and sandstone fragments which were probably derived close to the point of deposition (Pettijohn, et al., 1972). More abundant argillaceous rock fragments lead to decreased porosity and permeability. Where they are common, these fragments have inhibited the amount of cementation that occurred by reducing both porosity and pore throat size. The most common diagenetic effect in sections with abundant soft rock fragments is compaction and silica cementation, although ferroan dolomite, siderite, and kaolinite cements do occur.

Chert is another type of sedimentary rock fragment recognized. It commonly comprised one to two percent of the sandstone. Three varieties were recognized: fine-grained chert, coarse-grained chert, and green chert.

Fine-grained and coarse-grained chert are typically clear in plain light and inclusion free (Figure 42). Coarse-grained chert is difficult to differentiate from quartzite and polycrystalline quartz grains because transitional varieties occur.

Green chert was rarely recognized as a constituent. It is light green, nonpleochroic in plane polarized light, and has interference colors characteristic of chert under

crossed nicols. Folk (1974) referred to such chert as green jasper and attributed the color to chlorite inclusions.

Chert grains are subrounded to rounded, equant, and fine to very fine sand to coarse silt sized. The only notable alteration is etching of grains related to carbonate cements. This chert is of detrital origin and represents reworking of an older sediment (Folk, 1974, p. 81).

ACCESSORY MINERALS

Micas and Chlorite

Muscovite, biotite, and chlorite together make up at least one percent of the sandstones studied. Grains occur as elongate grains larger than 0.04 millimeters and may be as long as 1 millimeter (Figures 43 and 44). Muscovite is typically more common than the others.

Muscovite is clear in plane-polarized light and shows typical interference colors in crossed nicols. Chlorite is generally light green in plane-polarized light with anomalous interference colors in crossed nicols. Biotite ranges from light green to brown and is distinguished from chlorite by its strong pleochroism. Most phyllosilicate grains are not one mineral species, but instead are combinations of the three. This makes precise identification difficult, although one variety usually dominates.

Mica and chlorite grains increase in abundance and size upwards in sandstone sections. They are particularly common in the interbedded sandstone and shale lithofacies. This type of pattern is related to the decreasing energy of the depositional environment, which allows deposition of the platy, slowly settling phyllosilicate grains. Micas and chlorite at the top of sections show fewer compactional effects because of their larger size, greater abundance, and association with shaly material that spreads the effects of

compaction over more grains than in the lower portion of sequences where soft grains are less abundant.

Biotite is most highly altered, occasionally being extensively oxidized, as indicated by a brown color, in which case identification is based strictly on grain shape (Figure 44). Oxidation yields iron oxides which mask the interference colors.

Muscovite is partially altered to kaolinite in places and disrupted by cements. Millot (1970) recognized similar alteration effects on micas. Mica grains are commonly bent and occasionally broken due to compaction (Figure 43).

Organic Material

A consistent trace component of the sandstones is fragments of organic matter (Figure 45). These are typically black to red and very fine sand sized. Associated with these fragments are pyrite, leucoxene, and fine-grained siderite. These fragments are a possible source of carbon dioxide and also helped maintain the reducing conditions that characterize the burial history of these rocks. In some sections, it was noted that carbonate cementation was more active around zones of concentration of these fragments. The organics appear to have been concentrated in layers, probably due to a slight decrease in the current strength during deposition. According to Folk (1974, p. 101) "organic matter is most abundant where formation is

66

Figure 43. Photomicrograph of muscovite (M) splayed during compaction. Note the moldic porosity (P) due to dissolution of the detrital grain. Scale is 0.10 mm. (Tenneco Bradley 8 at 112 feet).

Figure 44. Photomicrograph of oxidized biotite (B) identified by its shape. Arrows point to quartz grains cemented by interlocking silica. Scale is 0.10 mm. (Tenneco Bradley 8 at 105.5 feet).

Figure 43
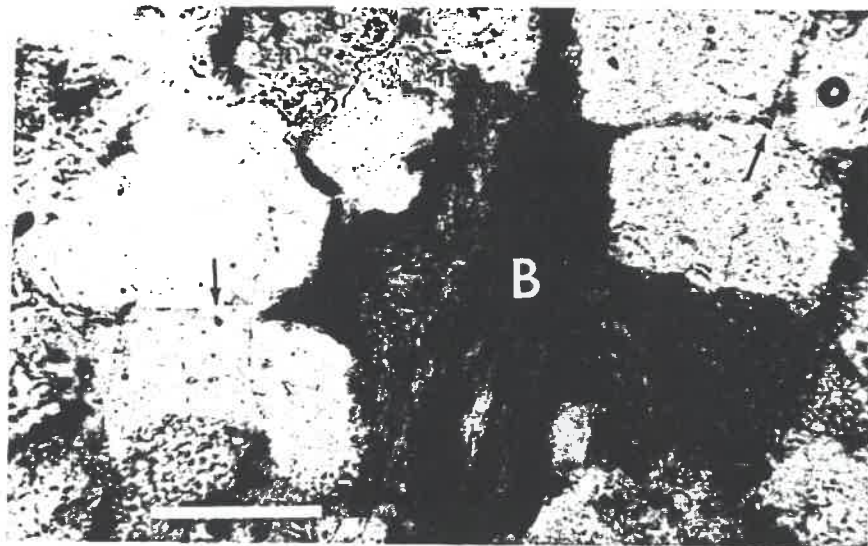
Figure 44

Figure 45. Photomicrograph with crossed nicols of a black, organic fragment (O) and siderite cement (S). Note the corrosion of the detrital grain boundaries. Scale is 0.10 mm. (Tenneco Bradley 8 at 93.5 feet).

Figure 46. Scanning electron micrograph of platelike, chlorite grain coatings (C) (Wilson and Pittman, 1977) and small, noncoalescing, authigenic quartz (Q). (2500x; Phillips Lena 1 at 3061 feet).
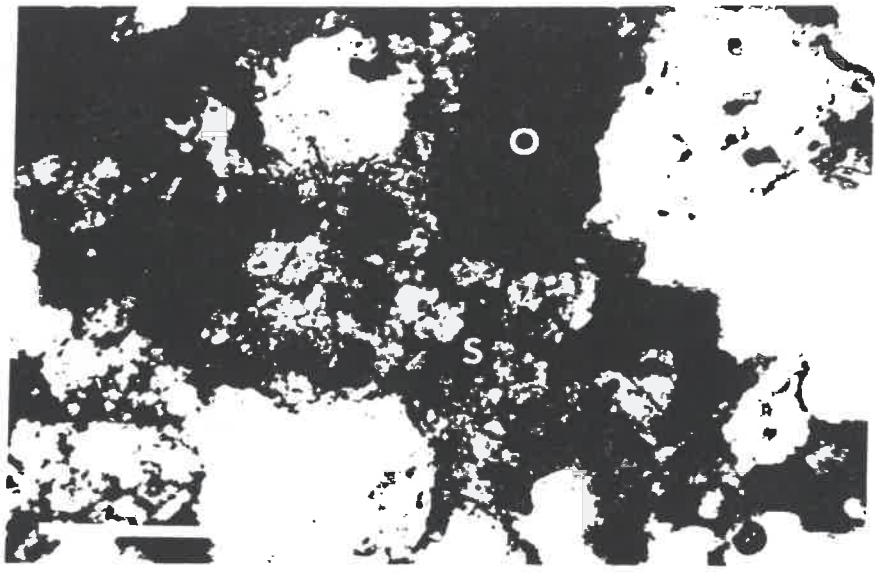
Figure 45

Figure 46

rapid, burial is fast, and bacteria are not active ... stagnant, reducing waters are most favorable".

Heavy Minerals

Trace amounts of heavy minerals were regularly encountered in thin sections. Included in the assemblage are zircon, tourmaline, rutile, and, rarely, garnet. Burggraf et al. (1981) report the following assemblage of heavy minerals in sandstones of the Cherokee Group in Iowa: magnetite, ilmenite, zircon, garnet, tourmaline, chloritoid, rutile, sphene, leucoxene, and iron oxides. Grains are mostly very fine sand to coarse silt sized. Grains are subangular to rounded.

CEMENTS

Cements constitute up to 15 percent of a sample in thin sections studied. Eleven different kinds of cement with at least 14 different habits were recognized. The cements have been subdivided into the following groups for discussion: 1) clay coatings on grains; 2) silica cements and feldspar overgrowths; 3) carbonate cements including siderite, dolomite-ferroan dolomite (ankerite), and calcite; 4) primary and secondary pore filling clays including kaolinite, illite, and chlorite; and 5) pyrite and leucoxene. The sequence of cementation will be discussed later in the text.

Clay Coatings

Clay coatings on detrital grains were observed in most samples (Figure 26). They range from thick and continuous to thin and discontinuous. Scanning electron microscopy revealed that individual platelets oriented perpendicular to grain surfaces closely resembled the chlorite described by Wilson and Pittman (1977) (Figure 46). In thin sections the coatings range from green to reddish brown. Reddish-brown clay coatings are believed to be oxidized chlorite. Identification with a polarizing microscope is difficult because the coatings are thin. Clay coatings have had a particularly important role in preserving porosity and permeability because they inhibited the growth of other cements by reducing the number of points of nucleation on grain surfaces

(Pittman and Lumsden, 1968). Clay coatings are more common in the coarse sandstones (lithofacies B and C) than in the fine sandstones (lithofacies D and E).

Silica Cements and Feldspar Overgrowths

Silica cements occur as overgrowths on quartz grains. Two types were recognized. In the coarse sandstones (lithofacies B and C), well-developed subhedral to euhedral quartz overgrowths occur (Figures 23, 26, and 36). In the fine sandstones (lithofacies D and E), silica cements occur primarily as patchy, interlocking, anhedral to subhedral quartz overgrowths with sutured boundaries (Taylor, 1950) that give groups of grains a mosaic or quartzite texture (Figures 27, 28, and 44). The silica cement of the fine sandstones tends to eliminate the porosity and permeability, whereas the coarse sandstones have moderately well-preserved pore space, even where silica cement is present.

Feldspar overgrowths on untwinned detrital feldspars are a rare cement. These are particularly conspicuous in thin section because they are low-temperature overgrowths that are clear and unaltered while the less stable, detrital feldspar grains are commonly extensively vacuolized to partially dissolved or sericitized and kaolinized.

Carbonate Cements

Three distinct carbonate cements were recognized: 1) calcite as an early, concretionary, poikilotopic cement;

71

2) dolomite-ankerite as a patchy, pore-filling cement; and
3) siderite as a pore-filling cement replacing framework
grains. Carbonate cements were differentiated using petro-
graphic criteria and carbonate staining techniques (see
Appendix B).

Calcite cement was recognized in only two thin sections
(Cherokee Keown 18AO at 1004 feet and Tesoro Baker W-35 at
579 feet). The cement in both of these samples is a local-
ized concretionary feature adjacent to a thin bed of carbo-
naceous shale. The cement occurs as a poikilotopic cement
that completely fills all of the pore space, leaving essen-
tially no permeability (Figure 30). These concretions occur
in both sandstones and shales. Curtis (1978) discussed the
link between mudstone diagenesis and carbonate cementation.

The second type of carbonate cement recognized was a
ferroan dolomite that occurs both as discrete rhombs (Figure
24) and as a patchy, poikilotopic cement encompassing sever-
al detrital grains (Figures 23 and 47). Folk (1974, p. 100)
referred to sandstones with this latter type of cement as
luster-mottled. Dolomite-ankerite cement can be recognized
macroscopically in cores because it gives the rock a white,
speckled appearance (Figure 13).

The third type of carbonate cement, siderite, occurs in
three distinct habits. 1) Siderite occurs as very early
spherules that are locally concentrated in both sandstones
and surrounding shales (Figures 30 and 48). This cement is
often referred to as buckshot siderite (Ebanks, pers. comm.,

72

1981). 2) Siderite also occurs as a microcrystalline replacement mineral, particularly in the nonfoliated argillaceous rock fragments. These were originally identified as carbonate rock fragments, but subsequent investigation led to the conclusion that they are replaced grains because they almost always show the effects of compaction associated with soft rock fragments, including loss of form due to bending around harder detrital grains and squeezing into pores. Grain character is obscured by iron-oxide staining that is caused by oxidation of original rock fragments. 3) The final form of siderite is discrete, rhombic crystals and patches of crystals encompassing several framework grains (Figure 31, 45, and 49). The discrete rhombs are particularly common in the fine sandstones. Core samples containing siderite have a reddish-brown, spotty appearance.

Authigenic Clays

Three types of authigenic pore-filling and replacement clays were recognized: kaolinite, illite, and chlorite. Only kaolinite is volumetrically important.

Kaolinite is irregularly distributed and fills primary intergranular pores, secondary oversized pores, and secondary pores created by dissolution of feldspar. Kaolinite is particularly abundant in the coarse sandstones (lithofacies B and C), where it occurs as a replacement mineral in feldspars, micas, and argillaceous rock fragments and as patches of vermicular booklets (Figures 34, 35, 36, and 37). It is

Figure 47. Photomicrograph of patchy dolomite-ankerite cement (C) encompassing several detrital grains. Scale is 0.10 mm. (Tenneco Bradley 8 at 93.5 feet).

Figure 48. Photomicrograph of spherulitic siderite (arrow). Scale is 0.10 mm. (Tesoro Baker W-35 at 573 feet).
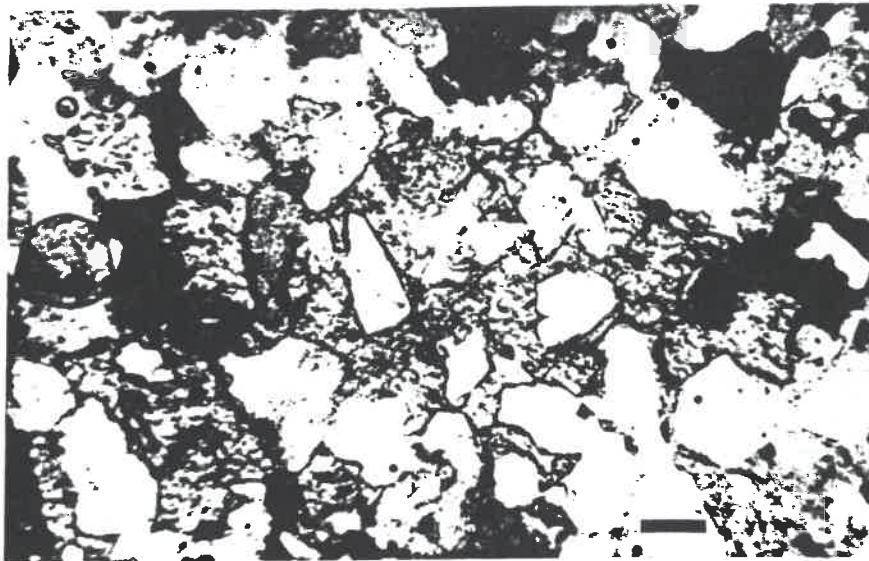
Figure 47
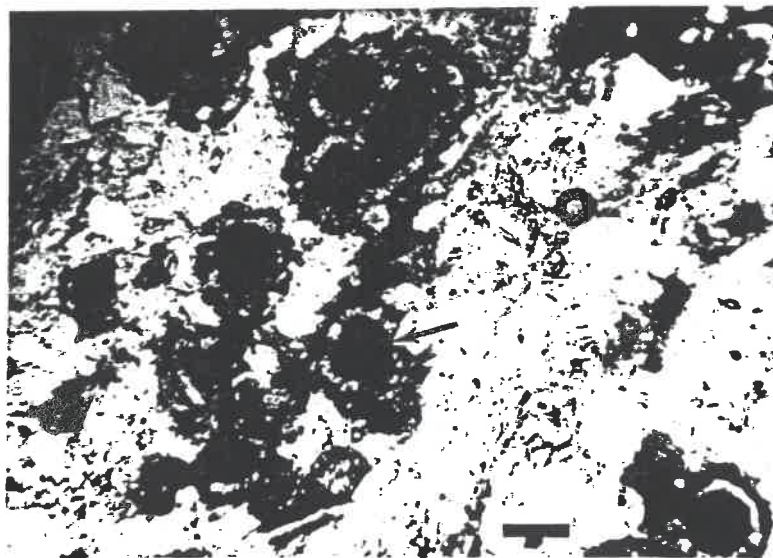
Figure 48

Figure 49. Photomicrograph of siderite cement (S). Note the characteristic dark rim (arrow). Scale is 0.10 mm. (Conoco Ord 47 at 712 feet).

Figure 50. Scanning electron micrograph of coarse, stringy, lathlike illite (Wilson and Pittman, 1977). (640x; Phillips Lena 1 at 3061 feet).

ote
mm.
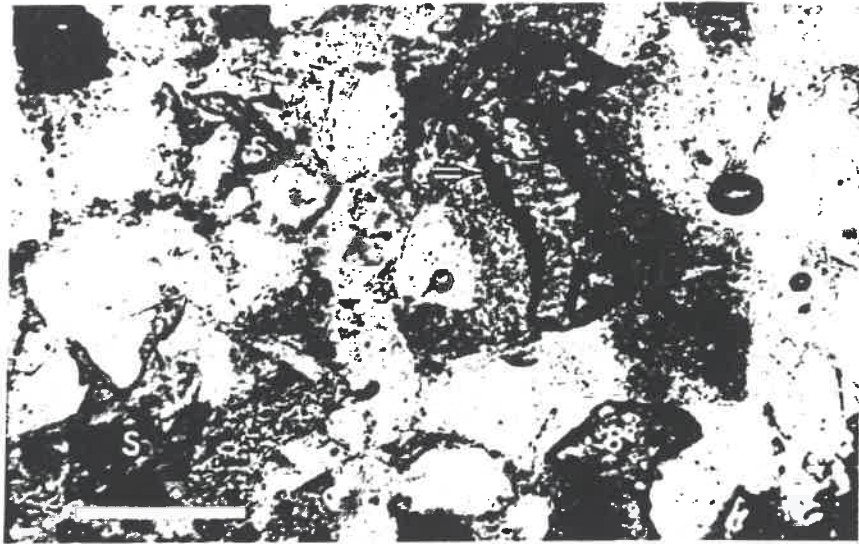
Figure 49
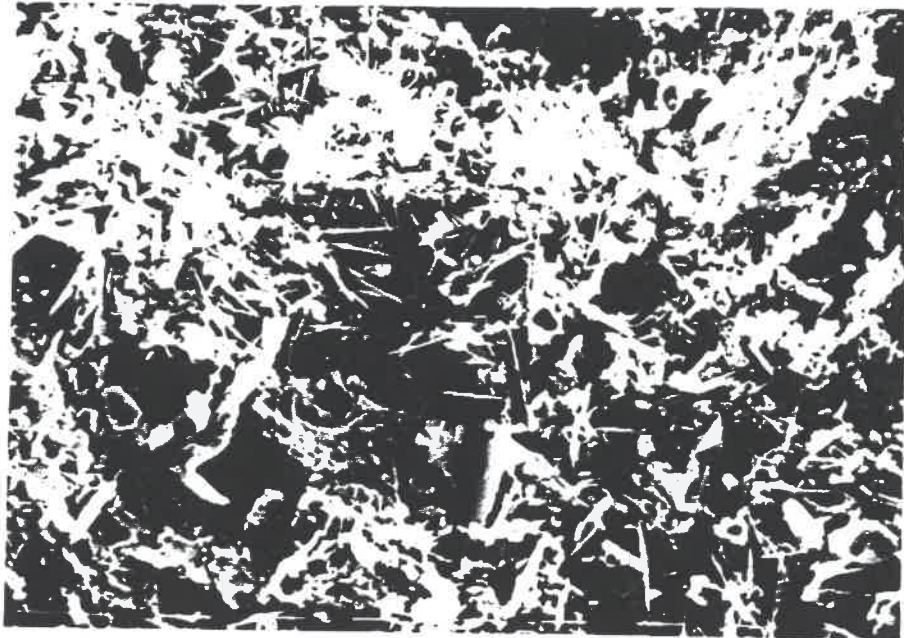
Figure 50

less abundant as a cement in the interbedded sandstone and shale deposits at the top of the sandstone sequences. Two distinct phases of kaolinite cementation were recognized. The first is kaolinite that occurs as large groups of crystals (booklets) and the second is finer-grained kaolinite in close association with fine-grained hydromicas (sericite and illite). Rex (1966) also recognized two distinct phases of kaolinite cementation, which resulted in kaolinite of distinct sizes. Kaolinite replacement of feldspars, micas, and argillaceous rock fragments is a rare but consistent phenomenon in the sandstones and was discussed by Millot (1970). Shelton (1964), Boles (1978), and Milliken et al. (1981) noted that decomposition of feldspar may provide a source for authigenic kaolinite and quartz.

Small amounts of authigenic illite and chlorite were seen in the sandstones. Scanning electron microscopy allowed identification of the stringy, lathlike texture of illite (Figure 50) (Wilson and Pittman, 1977). This clay occurs only in trace amounts, partially filling pore spaces. Microscopic identification is difficult due to fine grain sizes, although occasionally the chlorite and illite were recognized by their interference colors and indices of refraction as pore-filling cements. Because authigenic pore-filling chlorite and illite are minor constituents in the sandstones studied, they represent an insignificant reservoir problem for the Cherokee Group sandstones studied.

Authigenic chlorite occurs as a clear, light-green, weak to nonpleochroic mineral partially replacing muscovite, biotite, and feldspars and is distinguished from detrital chlorite, which shows effects of transportation and has well-developed basal cleavage. Dapples (1979) interpreted the presence of authigenic chlorite as evidence of a reducing environment. This is further confirmed by the presence of pyrite, carbonaceous matter, and siderite. Some evidence, however, suggests periods of less reducing conditions or high pH, particularly the oxidation of iron-bearing minerals and rock fragments. Oxidation is confined to samples from wells on the shallower, eastern side of the basin (to depths of several hundred feet) and is believed to be a Cenozoic phenomenon associated with the continued uplift of the bounding structural elements to the east and exposure of the minerals to oxygenated meteoric waters.

Pyrite and Leucoxene

Pyrite and leucoxene are ubiquitous trace constituents in the sandstones and are closely associated with organic fragments and burrows (Figure 51). The pyrite typically occurs as small groups of crystals, often circular in cross section. These may be framboidal-pyrite burrow fillings, although pyrite was not recognized in S.E.M. studies.

Pyrite is an important mineral because its presence indicates reducing conditions, probably due to organic matter that was metabolized by sulfate-reducing bacteria.

Figure 51. Reflecting light photomicrograph of pyrite (arrow). Scale is 1 mm. (Colt Keown 18AO at 1015 feet).

Figure 52. Slab photograph of concretionary siderite. Note the disruption of the associated bedding (K.G.S. Tar Sands at 183 feet).

Figure 51

K.G.S.
TAR SANDS C
183
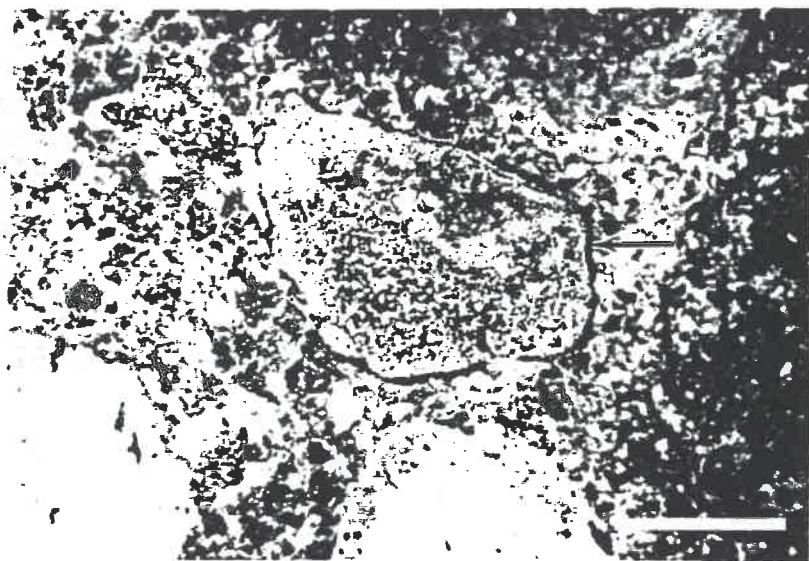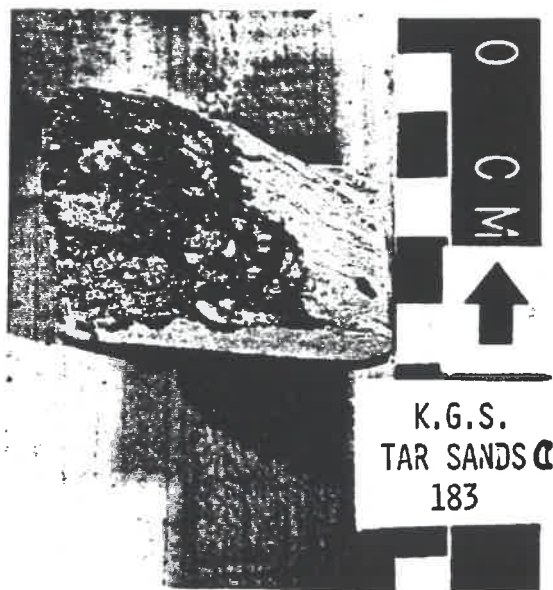
Figure 52

It also presents a paradox in unraveling the cementation history because of the presence of siderite, which does not form in the presence of high concentrations of dissolved sulfur necessary for iron sulfides (such as pyrite) to precipitate (Garrels and Christ, 1965). Siderite can precipitate if the sulfur is removed from solution during early diagenesis by precipitating primitive iron sulfides (Berner, 1980).

DIAGENESIS of CHEROKEE GROUP SANDSTONES

The diagenetic sequence is summarized as follows. 1) The formation of localized, possibly concretionary, poikilotopic calcite and spherulitic siderite cements in both sandstones and shales reduced porosity and permeability to zero and effectively stopped diagenesis in these local areas. 2) Pyrite was precipitated in close association with organic fragments due to the bacterial decomposition of the organics and the associated liberation of sulfur. 3) The precipitation of clay coatings on grains, mostly plate-like chlorite, inhibited the subsequent precipitation of quartz and feldspar overgrowths. 4) In areas of sparse, thin, discontinuous clay coatings, the precipitation of quartz and feldspar overgrowths occurred. 5) The diagenetic sequence following the precipitation of quartz overgrowths becomes complex and involves the precipitation of patchy, vermicular booklets of kaolinite; discrete, rhombic crystals and patches of siderite and dolomite or ferroan dolomite (ankerite); and the dissolution and replacement of feldspars, micas, and rock fragments (Figure 53). The complexity of the sequence may be attributed to local supersaturation or small nucleation densities (Keller, 1970). Hydrocarbon emplacement postdates all of the diagenetic activity reported.

Figure 53. Diagenetic sequence in selected Cherokee Group sandstones in southeastern Kansas. Solid line indicates the dominant diagenetic reactions during a particular diagenetic stage. Dashed lines indicate less active diagenesis.

81

DISCUSSION

Calcite is present as a pore-filling, poikilotopic cement in only a few thin sections. It is in close association with shale interbeds in Colt Keown 18AO and Tesoro Baker W-35, which may have been the source of the necessary ions. The cement filled all pore space and halted diagenesis in the samples where it developed. Associated with this cement are spherules of siderite, which are also concretionary and were documented macroscopically in both sandstones and shales (Figure 52). Calcite and spherulitic siderite are believed to be the first cements to occur because detrital grains are floating (Taylor, 1950) in these cements; and these detrital grains show no effects of alteration, rare overgrowths, and no other cementation, implying they have been shielded from any subsequent diagenesis (Figure 30). Loucks et al. (1977) reported similar effects due to localized, concretionary cementation in Tertiary sandstones of the Gulf Coast. Because the grains are floating in the cement and the cements distort shale laminae, it is believed that the cementation occurred before compaction was completed. Although concretionary cement is rare, it may locally compartmentalize the reservoir.

In the sandstones that are not affected by such pore infilling, the first stage of diagenesis was probably the formation of pyrite in association with bacterial decomposition of organic debris. Berner (1970) discussed the stages of formation of pyrite. For this study it is important to

82

recognize pyrite because it results from reducing conditions, low pH, and high dissolved-sulfur concentrations (Garrels and Christ, 1965). Bucke and Mankin (1971) placed pyrite as the final stage of authigenesis of Desmoinesian strata. The major problem with such an interpretation is the presence of siderite, which requires a low dissolved sulfur concentration, an unlikely condition if pyrite was the last authigenic mineral to form, since this implies sulfur was still in the aqueous phase (Garrels and Christ, 1965). If the dissolved sulfur were incorporated into pyrite early, however, it would allow siderite precipitation. Pyrite is always in close association with organic rock fragments which supports the belief that it incorporated sulfur derived from decomposition of organic fragments. Pyrite formation or the formation of less ordered iron sulfides is commonly an early diagenetic process. This would explain survival of the bacteria necessary to generate the sulfur (Berner, 1980). Berner (1981) classified mineral suites containing both pyrite and siderite as indicators of highly reducing, methanic, anoxic, nonsulfidic chemical environments, particularly freshwater and in which the sulfur is tied up early by precipitation of primitive iron sulfides. This allows for later precipitation of siderite under low concentrations of dissolved-sulfur.

The first widespread stage of cementation in the sandstones was the precipitation of chlorite coatings on grains.

The timing of chlorite coatings in the sequence of diagene-
sis is indicated by limited development of subsequent
cements (especially quartz overgrowths) on grains with such
coatings. Land and Dutton (1978) recognized chlorite grain
coatings as the first authigenic mineral in the sequence for
Desmoinesian sandstones of north central Texas. Hawkins
(1978) found a similar sequence in Upper Carboniferous sand-
stones of England.

The next stage was the formation of quartz and feldspar
overgrowths. Scanning electron microscopy showed that
quartz overgrowths were poorly developed as small, nonco-
alescing nuclei on grain surfaces with well-preserved clay
coatings (Figures 54 and 55), while quartz overgrowths on
grains with little or no clay coatings were large, well
developed, monocrystalline overgrowths (Figure 56). Heald
(1965); Pittman and Lumsden (1968); Heald and Larese (1974);
and Hawkins (1978) reported similar findings. Pittman and
Lumsden (1968) reported on the Spiro Sand of Oklahoma where
porosity was poorly preserved when chlorite grain coatings
were sparse, thin, and discontinuous, whereas in sandstones
where the chlorite coatings were thick and continuous,
porosity was well preserved due to the lack of quartz over-
growths. Cecil and Heald (1967) found, in an experimental
study, that clay coatings on quartz grains inhibited the
formation of quartz overgrowths. In places, quartz over-
growths in the sandstones studied have completely filled the
available pore space, particularly in the sandstones of the

84

Figure 54. Scanning electron micrograph of chlorite coatings (C) on detrital grains, with protruding noncoalescing quartz overgrowths (Q). (2500x; Jackson Bros. Barrier 36 at 2496 feet).

Figure 55. Scanning electron micrograph showing chlorite grain coatings (C), quartz overgrowths (Q), and large vermicular booklet of kaolinite (K), which were precipitated in that sequence. (2500x; Jackson Bros. 36 at 2496 feet).
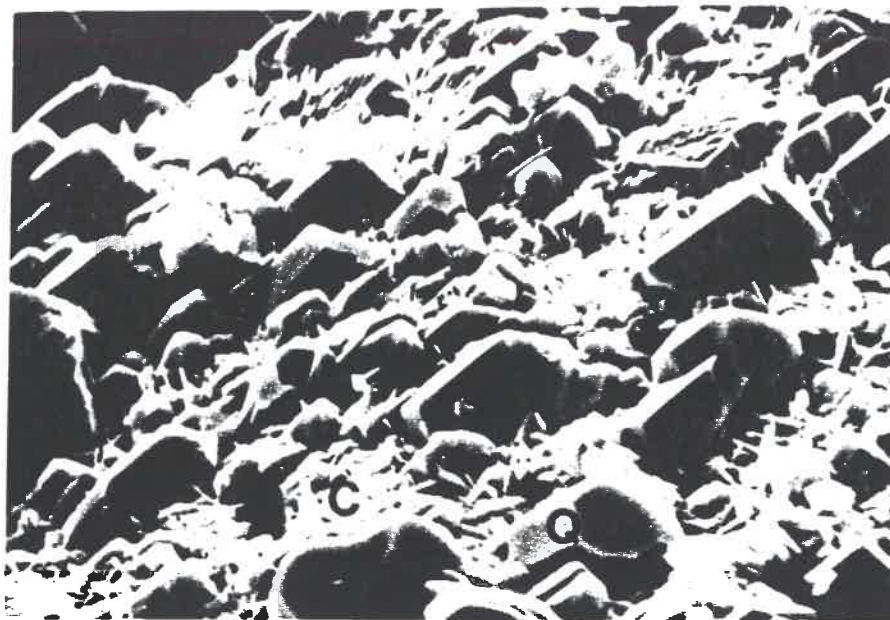
Figure 54

Figure 55

Figure 56. Scanning electron micrograph of a large quartz overgrowth (Q) followed by kaolinite (K) in diagenetic sequence. Note the absence of chlorite grain coatings. (1250x; K.G.S. Tar Sands C at 257 feet).

Figure 57. Photomicrograph of intergranular porosity (p). Scale is 0.10 mm. (Conoco Ord 34 at 726 feet).
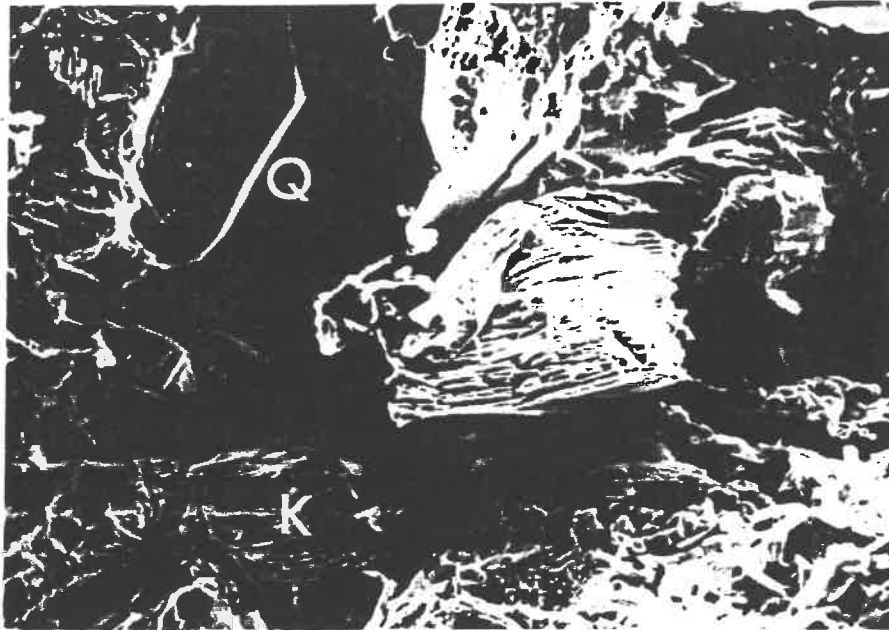
Figure 56

Figure 57

interbedded sandstones, siltstones, and shales. This is due to the lack of chlorite coatings.

Following the widespread development of overgrowths, the diagenetic sequence becomes complex, including the dissolution and leaching of feldspars, argillaceous rock fragments, and micas; and the precipitation of kaolinite, dolomite-ankerite, and siderite. Again this interpretation agrees with the interpretation of Land and Dutton (1978) for Desmoinesian sandstones in north-central Texas.

Dissolution and leaching of feldspars, micas, and argillaceous rock fragments resulted in kaolinite precipitation by releasing the necessary cations (Si and Al). Kaolinite filled original pores and angular molds of dissolved grains. Bucke and Mankin (1971) recognized four factors which allowed precipitation of kaolinite: 1) abundance of organic matter, which maintains a low pH; 2) feldspars as a source of aluminum and silicon; 3) partially degraded illite as an efficient acceptor for the cations released during feldspar decomposition; and 4) water-filled pores as media and spaces for kaolinite growth. Hower et al. (1976) and Boles and Franks (1979) further suggested that the process of alteration of smectitic clays to illitic clays during compaction requires the addition of cations, a likely sink for the cations released during feldspar decomposition. Fothergill (1955) reported that kaolinite content is higher in sands with secondary quartz than in those

without quartz cement. This relationship was not recognized in this study.

Siderite and dolomite-ankerite cements locally etch detrital grains (Figures 29 and 31). The carbonate cements postdate quartz overgrowths as shown by their position in pores around quartz overgrowths and detrital grains (Figure 23).

INTERPRETATION

The diagenesis of the sandstones can be subdivided into three major stages: 1) syndepositional, localized, formation of concretionary calcite and spherulitic ("buckshot") siderite plus iron sulfides in association with organic fragments; 2) precipitation of extensive chlorite grain coatings followed by overgrowths of silica and feldspar; and 3) dissolution of feldspars, micas, and argillaceous rock fragments; replacement of grains by carbonate cements; and precipitation of kaolinite, siderite, and dolomite-ankerite cements (Figure 53). Keller (1970) introduced the idea of microenvironments of cementation. This explains the patchy distribution of stage 3 cements and may provide a solution to the enigma surrounding the precipitation of both siderite and pyrite. Pyrite formation could have occurred within a microenvironment characterized by reducing conditions, low pH, and high sulfur concentrations while siderite, which requires low concentrations of dissolved sulfur, could have formed in a separate, but nearby, microenvironment. Other

evidence that could be used to substantiate the microenvironments theory is the proximity of vermicular booklets of authigenic kaolinite to feldspars which could be interpreted as a microenvironment where dissolution of feldspars provided the ions necessary for the precipitation of kaolinite (Figure 34, 35, 36, and 37).

All three stages of diagenesis are better developed in the coarser (generally fine-grained) sandstones of lithofacies B and C and the finer (very-fine-grained) sandstones of lithofacies D than in the interbedded sandstones and shales of lithofacies E. The sandstones of lithofacies B, C, and D generally have higher porosities and permeabilities because: 1) the micas and soft rock fragments are uncommon and therefore fill little pore space, 2) chloritic clay coatings on grains, which inhibit quartz overgrowths, are common, and 3) feldspar dissolution appears to have been active. Coarser grain size results in large pore throats allowing active flow of pore waters through the rocks and active diagenesis.

In contrast are the interbedded sandstone-shale sequences (lithofacies E) which have more extensive loss of pore space during the second stage. This is explained by: 1) the silica cements which form the mosaic or interlocking texture that results in little remaining pore space for flow of pore waters and subsequently less precipitation of stage 3 cements; and 2) abundant, malleable rock fragments (nonfoliated argillaceous), siltstone-shale clasts, and

micaceous partings which, when compacted, are forced into surrounding pores and around nearby grains. Explanation 1 is supported by the theory that shale compaction releases silica, which is reprecipitated locally (Hower, et al., 1976; Boles and Franks, 1979). There are several other feasible explanations for the interlocking silica cements of interbedded sandstone-shale sequences. One is that, due to the generally finer grain size of these deposits, relative to coarser sandstones, pore throats are smaller and similar volumes of silica cement in both types of sandstone would result in more extensive occlusion of pore space in the finer sandstones. Another possible explanation is the lack of extensive clay coatings on grains in the interbedded sandstones and shales. As mentioned previously in the text, these clay coatings inhibit subsequent silica cementation and, therefore, affect porosity reduction.

Unfortunately, the diagenetic sequence may be more complex than the three stages just discussed. Dewatering of shales involves the alteration of smectite to more rigid illite clays. This alteration requires availability of exchangeable cations, predominantly potassium, which are easily obtained from alteration of feldspars, micas, and rock fragments, implying that stage 3 diagenesis was occurring during at least part of stage 2 diagenesis. Rex (1966) noted the tendency for quartz-kaolinite associations to be common. Scanning electron microscopy confirms this

relationship for Cherokee Group sandstones, although kaolinite is a microenvironment cement.

Stage 2 and 3 diagenesis are consistent with previously published observations. Burst (1969), in a study of Gulf Coast sediments, recognized three major stages of shale diagenesis. The first stage is the dewatering of shales, their water content being reduced from an original 70 per cent to 30 per cent. This dewatering involved the expulsion of large volumes of pore fluids, presumably enriched in ions, into associated more porous and permeable sandstones. This agrees very well with the extensive stage 2 cementation, formation of clay coatings and silica cementation, of the Cherokee Group sandstones in this study. Burst's second stage of dehydration of shales follows the expulsion of water from the shales and is primarily driven by temperature. Burst's second stage of diagenesis includes the illitization of the shales during alteration from smectite and requires the intake of cations. Three important sources of these cations are feldspars, micas, and argillaceous rock fragments. This stage also involves the generation of hydrocarbons and is correlative to microenvironment diagenesis of stage 3 recognized in this study. Stage 3 of Burst's diagenesis reactions is the slow, complete loss of interlayer water in clays and requires a long time period.

The literature on diagenetic sequences in shallow shelf, Upper Carboniferous fluvial-deltaic sandstones is

sparse. Figure 58 is a summary and comparison of the diagenetic sequences reported by this research and previous workers (Bucke and Mankin, 1971; Teisseyre, 1973; Hawkins, 1978; Land and Dutton, 1978). Note the general similarity of all of these sequences.

Loucks et al. (1977) reported a diagenetic sequence, which is very similar to the one recognized in this research, in Lower Tertiary Frio Formation sandstones in the Gulf Coast (Figure 59). This is particularly interesting, because the Cherokee Group sandstones in southeastern Kansas have had a relatively shallow burial and low temperature history. In contrast, the Frio sandstones of the Gulf Coast were eventually buried in a deep basin and experienced temperatures exceeding 150 degrees centigrade (Milliken et al., 1981).

In studies of Tertiary sediments of the Gulf Coast, Perry and Hower (1970), Hower et al. (1976), Boles (1978), and Boles and Franks (1979), and Milliken et al. (1981) reported minimum temperatures for illitization reactions and hydrocarbon maturation of at least 50 degrees centigrade. These authors suggested that temperatures approaching 100 degrees centigrade are necessary for cementation and hydrocarbon generation reactions to proceed at a reasonable rate. Gulf Coast Tertiary sandstones and shales have been deposited in a rapidly subsiding continental margin basin which has resulted in relatively rapid burial to depths greater than 3500 meters (11,000+ feet) with temperatures exceeding

DIAGENETIC SEQUENCE	PACAE AND HAWKIN (1971)	TEISSEYRE (1973)	HAWKINS (1978)	LAND AND DUTTON (1978)	THIS RESEARCH
	1) Quartz overgrowths	1) Quartz cement I	1) Clay coatings siderite replacement	1) Chlorite rims around grains	1) Calcite and siderite concretions pyrite
	2) Kaolinite	2) Feldspar dissolution kaolinite	2) Quartz overgrowths	2) Quartz overgrowths	2) Chloritic clay coatings on grains quartz and feldspar overgrowths
	3) Calcite	3) Siderite, calcite, and ankerite cement	3) Kaolinite and illite	3) Calcite	3) Feldspar dissolution kaolinite, siderite, and dolomite- ferroan dolomite cements
	4) Dolomite	4) Quartz cement II	4) Chalcedonic quartz ferroan dolomite and ferroan calcite other clays	4) Dissolution of calcite, feldspars, and rock fragments	
	5) Pyrite and siderite	5) Authigenic chlorite and sericite		5) Ferroan calcite, ankerite, and kaolinite cements	
				Sequential position of pyrite uncertain	
MAXIMUM DEPTH OF BURIAL	2900 meters (9500 feet)	4000 meters (13,000 feet)	1097 meters (3600 feet)	2320 meters (7600 feet)	1200 meters (4000 feet)
STUDY AREA	Oklahoma	Central Sudetes southwestern Poland	Bothamsall Oilfield Central Pennine Basin East Midlands, England	West Tuscola Field Concho Platform Taylor County, Texas	Cherokee Basin southeastern Kansas

Figure 58. Generalized diagenetic sequences reported in Upper Carboniferous sandstones. Note the similarity of the sequences.

150 degrees centigrade. Cherokee Group sandstones and shales in Kansas were deposited on a stable, cratonic shelf with burial depths of 1200 meters, yet they have a pattern of cementation similar to those reported for the Gulf Coast (Figure 59). The maximum estimated temperature to which the Cherokee Group was subjected is no more than 60 to 70 degrees centigrade (Gould, 1975; Land and Dutton, 1978). This suggests that temperatures reached in the basin barely exceeded the predicted minimum for illitization, cementation, and hydrocarbon generation (Perry and Hower, 1970). Optimum temperatures for cementation, dissolution, and alteration probably never were reached.

Boles and Franks (1979) report that at temperatures greater than 70 degrees centigrade, discrete smectite disappears in Wilcox Group sandstones and shales of southern Texas (Gulf Coast). Brenner (pers. comm., 1981) reports the presence of both partially illitized and discrete smectite in Cherokee Group shales of Kansas, indicating that temperatures in the basin approached 70 degrees. Milliken et al. (1981) reported precipitation of extensive quartz cements at around 75 to 80 degrees centigrade and kaolinite at around 100 degrees centigrade. Boles (1978), Boles and Franks (1979), and Milliken et al. (1981) further reported the precipitation of iron carbonate cements at temperatures above 120 degrees centigrade. The sequence of cementation in Upper Carboniferous sandstones is almost identical with that of the Gulf Coast, but the temperatures at which the

	This Research	Loucks, Bebout, and Galloway (1977)
DIAGENETIC SEQUENCE	1) POIKILOTOPIC PORE-FILLING CALCITE SPHERULITIC SIDERITE PYRITE 2) CHLORITIC CLAY COATINGS ON GRAINS FELDSPAR OVERGROWTHS WELL DEVELOPED EUHEDRAL TO INTERLOCKING (WELDED) QUARTZ OVERGROWTHS 3) ALTERATION AND DISSOLUTION OF FELDSPARS, MICAS, AND ARGILLACEOUS ROCK FRAGMENTS PORE-FILLING KAOLINITE REPLACIVE AND PORE-FILLING SIDERITE AND ANKERITE (IRON-RICH CARBONATE) CEMENTS	1) FELDSPAR LEACHING 2) POIKILOTOPIC PORE-FILLING CALCITE CLAY COATINGS AND RIMS FELDSPAR OVERGROWTHS QUARTZ OVERGROWTHS 3) MASSIVE (WELDED) AND EUHEDRAL QUARTZ OVERGROWTHS PORE-FILLING CALCITE CEMENT 4) LEACHING OF FELDSPARS, VOLCANIC AND CARBONATE ROCK FRAGMENTS, AND CALCITE CEMENTS 5) PORE-FILLING KAOLINITE AND IRON-RICH CARBONATE CEMENTS
MAXIMUM DEPTH OF BURIAL	1200 METERS 4000 FEET	3600 METERS 12,000 FEET
MAXIMUM TEMPERATURE	70° C	180° C

Figure 59. Generalized diagenetic sequences reported in this research on the Cherokee Group sandstones of southeastern Kansas and in the Lower Tertiary Frio Formation sandstones of the Gulf Coast. Although the sequences are very similar, the depths of burial and temperatures of burial in the Frio Formation are at least twice that of the Cherokee Group.

cements were precipitated appears to have been much lower (Figure 59). Future research, aimed at resolving the apparent discrepancies in temperature and depth required for diagenesis of the sandstones discussed here, is needed. It is suggested that the influence of time, temperature, and fluid concentrations during diagenesis of shallow shelf sandstones needs to be carefully evaluated. The abundance of Cherokee Group sandstone cores available from southeastern Kansas provides an excellent opportunity for such studies.

It is predicted from theoretical considerations that at lower temperatures, diagenetic reactions proceeded at a slower rate (Petrovic, 1976). Lahann (1980) suggests that if the temperature is maintained near the minimum temperature for illitization (50 degrees centigrade), extensive migration of hydrocarbons and cementation will occur. The presence of extensive cementation and abundant hydrocarbons in Cherokee Group sandstones may support this suggestion. It is also possible that the geothermal gradient in the cratonic interior (including southeastern Kansas) was higher during the late Paleozoic and early Mesozoic than the present gradient. This could also explain the diagenesis and hydrocarbon generation which occurred in the Cherokee Basin.

PETROPHYSICAL PROPERTIES

Three petrophysical properties of selected samples of Cherokee Group sandstones were determined: effective porosity by liquid re-saturation, permeability to brine or gas, and pore size distribution by mercury injection porosimetry. Hulse (1978) and Marafa (1980) report a strong relationship between scale of sedimentary structures and petrophysical properties. The results described here are based on testing of samples of Cherokee sandstones with different sedimentary structures, grain sizes, and mineralogies. All core plugs tested were cut horizontally. No samples were tested for vertical permeability. Marafa (1980) showed that permeability for vertically cut samples is slightly lower than that of horizontally cut samples. This is explained by the tendency for grains that decrease the connectivity of pores, such as micas, platy organic fragments, and shale fragments, to be concentrated along bedding planes. By linking the petrophysical data to geologic aspects, variations in the petrophysical properties are explained later in this text.

Core plugs 1.85 centimeters in diameter and 1.50 to 3.80 centimeters long were taken for petrophysical tests. Variations in length were due to variations in the diameter of the original cores. The upper limit on length is based on physical constraints of the apparatus used for permeability determinations. Appendix A summarizes the methods and calculations for determinations of petrophysical properties used in this study. Table 4 lists all of the measurements

TABLE 4 - Petrophysical data.

Well Name	Sample Depth feet	Porosity percent	Permeability millidarcies	Effective Radius micrometers	Lithofacies
K.G.S. Tar Sands "C"	199	8.52	0.0		D
	201.5	11.06	0.76	3.54	D
g*202	202	10.79	1.02	1.44	D
	242	13.66	1.08		D
	243.5	21.91	178.99		C
	246	17.59	29.73		C
g	250	21.10	317.55		C
	253	19.11	110.19		C
	255	22.39	264.78		C
g	257	21.48	143.00	7.83	C
	259.5	23.10	395.35		C
	264	22.18	54.65		C
g	268	23.08	76.22	10.15	C
K.G.S. Tar Sands "N"	g 230	5.35	0.12		D
	233	12.25	0.30		D
	301.2	19.10	5.86		D
g	304.5	19.40	15.36		D
	312	19.15	1.08		C
	313.5	18.61	26.17		C
g	320.2	20.35	22.65		C

"g" indicates samples on which grain size measurements were conducted on the corresponding thin sections.

* indicates data reported by Marafa (1980).

TABLE 4 (continued)

Well Name		Sample Depth feet	Porosity percent	Permeability millidarcies	Effective Radius micrometers	Lithofacies
K.G.S. Tar Sands, "AA"	g	30	15.28	1.28		D
		30.7	17.95	6.04		D
		31	16.78	16.13		D
		31.5	16.65	7.71		D
		33.5	15.32	27.64		D
		34.0	8.84	1.58		D
	g	35.0	8.84	1.10		D
		35.8	7.46	0.14		D
		36.3	8.72	1.50		D
Tenneco Bradley 8		92	11.63	0.00		E
	g	93.5	21.80	158.82		C
		95	22.41	193.35		C
		97	23.42	173.11		C
		98.5	24.00	294.60		C
		100	20.76	412.32		C
		103.5	24.47	332.86		C
	g	105.5	24.21	387.77	16.86	C
		109	24.24	92.48		C
	g	112	23.47	233.45		C
		116	20.92	2.06		A
		119	17.91	0.24		A
		121	11.63	5.46		E
	g	155	21.59	72.11		A

"g" indicates samples on which grain size measurements were conducted on the corresponding thin sections.

99

TABLE 4 (continued)

Well Name	Sample Depth feet	Porosity percent	Permeability millidarcies	Effective Radius micrometers	Lithofacies
Tenneco Bradley 8	158	20.47	41.15		A
	159	20.32	233.24		A
	161	18.86	4.29		A
g	170	19.64	34.67	5.89	A
M.C. Colt 14AO Johnson	710	21.98	7.64		C
g	714a	27.18	93.55		C
	714b	26.51	39.13		C
	719	28.84	93.02		C
g	725	24.28	10.07		C
	730F	25.92	157.78		C
	730S	24.08	6.86		C
	737	25.62	9.60		C
g	742	23.86	124.80		C
	749a	24.10	117.79		C
	749b	23.99	166.58		C
Tesoro W-35 Baker	547	15.30	1.96		D
g	556	17.52	13.57	4.89	C
	561	17.63	9.21		C
g	565	21.04	61.90	10.15	C
	573	9.50	0.03		D
	579	5.58	0.00		D

"g" indicates samples on which grain size measurements were conducted on the corresponding thin sections.

TABLE 4 (continued)

Well Name	Sample Depth feet	Porosity percent	Permeability millidarcies	Effective Radius micrometers	Lithofacies
M. C. Colt 18AO Keown	836	17.54	31.64		E
	g 840	15.94	38.28	5.77	E
	g 948	21.49	427.04		E
	961	17.14	90.86		E
	976	21.56	129.04		C
	g 982	23.38	305.63		C
	999	18.11	84.31		C
	1004	6.46	0.04		C
	g1014.5	20.61	50.06	17.13	A
	g1019	14.50	33.86		A
	1150	7.14	0.00		C
	1156	18.31	1.25		A
	g1160	25.43	16.93		C
	g1169.7	24.03	220.35		C
	1173	20.09	57.81		C
	1179	22.52	114.82		C
Conoco Ord 34	676	15.94	3.12		D
	681a	13.18	0.93		D
	681b	14.22	2.17		D
	g 685	17.81	3.07	2.28	B
	691	17.51	10.62		B
	698	15.37	8.71		B
	g 726	15.83	32.97		B

"g" indicates samples on which grain size measurements were conducted on the corresponding thin sections.

TABLE 4 (continued)

Well Name	Sample Depth feet	Porosity percent	Permeability millidarcies	Effective Radius micrometers	Lithofacies
Conoco Ord 47	704	18.20	3.29		D
	709	14.61	1.86		D
	g 712	16.78	7.66		D
	719	16.71	3.68		D
	g 729	15.29	1.25		D
Brazos 0-5 Pierpoint	1010	17.24	58.78		E
	g1016.8	12.51	0.56		D
	1019.8	17.79	21.31		D
	1025.8	16.81	35.04		D
	1029.3	19.20	127.89		D
	1031.8	20.10	91.89		D
	1036	15.87	34.27		C
	1039.8	19.47	63.99		C
	1043	19.23	75.98		C
	g1045.8	16.17	44.63		C
	1050	16.37	38.53		C
	g1057	10.60	2.59		C
M.C. Colt 22AO Lauber	g1039	16.19	12.28	5.03	E
	1043	13.40	3.59		E
	1047	13.55	1.93		E
	1238	13.43	2.84		A
	1239	18.55	18.13		A

"g" indicates samples on which grain size measurements were conducted on the corresponding thin sections.

TABLE 4 (continued)

Well Name	Sample Depth feet	Porosity percent	Permeability millidarcies	Effective Radius micrometers	Lithofacies
M.C. Colt 22AO Lauber	g1242	23.89	93.42		C
	1245	22.27	111.92		C
	g1248	22.44	122.60	10.34	C
	1253	23.25	152.85		C
	1257	21.55	64.97		C
	g1259.5	20.99	122.24		C
Phillips Demalorie AW30	g1930.5	17.06	18.62		D
	1947.7	12.72	1.37		C
	1950.8I	15.08	6.49		C
	1950.8M	18.06	19.84		C
	1959.1	16.85	9.81		C
	1964.2	16.05	3.84		C
	1965.4	14.37	0.98		C
	g1970.8	16.92	9.37		C
Phillips Demalorie AW33	1978.6	16.44	26.04		D
	1982.1	12.31	0.31		D
	1987.9	16.63	5.39		D
Jackson Bros. Barrier 36	2463	14.48	0.00		E
	2485	10.34	0.00		E

"g" indicates samples on which grain size measurements were conducted on the corresponding thin sections.

103

TABLE 4 (continued)

Well Name	Sample Depth feet	Porosity percent	Permeability millidarcies	Effective Radius micrometers	Lithofacies
Jackson Bros. Barrier 36	*2489	24.70	1.14		E
	*2490.5	17.86	16.35		D
	*2490.5	18.05	7.73		D
	2495.5	15.96	9.64		C
	2496	16.70	22.31		C
	*2497.8	20.35	7.41		C
	*2497.8	22.00	7.73		C
	*2498	27.52	3.22		D
	g*2501	28.41	1.68		D
	*2505	21.84	41.16		C
	*2505	22.31	46.01		C
	g*2505.5	23.47	12.47		C
	*2507	22.81	29.42		C
Jackson Bros. Crew 21	2490	17.87	3.31		D
	2494	17.36	2.91		D
	2499	18.09	8.35		D
	2503	18.13	10.56		D
	2507	17.61	12.37		C
	g 2509	18.78	15.21		C
	2513S	16.13	7.81		C

"g" indicates samples on which grain size measurements were conducted on the corresponding thin sections.

* indicates data reported by Marafa (1980).

TABLE 4 (continued)

Well Name		Sample Depth feet	Porosity percent	Permeability millidarcies	Effective Radius micrometers	Lithofacies
Jackson Bros. Crew 21		2513L	16.60	17.48		C
	g	2515	17.55	36.92	7.51	C
		2518	16.52	24.68		C
		2519	17.62	26.19		C
		2521.5	21.12	82.85		C
	g	2523.8	18.82	18.59		C
Phillips Lena 1		3053	12.30	1.01		D
	g	3061.3	15.95	13.52		C
		3066.5	14.22	2.04		C
Sinclair Weir 1		3413	14.64	0.37		E
	g	3418	13.42	0.12	.88	E
	g	3437	15.99	9.91	4.77	D

"g" indicates samples on which grain size measurements were conducted on the corresponding thin sections.

105

of porosity, permeability, and pore size made for this study. Figure 60 summarizes these data and grain size for each lithofacies. Careful attention must be paid to the number of samples from each lithofacies when making comparisons of lithofacies, because the range of values encountered appears to be partially dependent on the number of samples from that lithofacies.

POROSITY

Effective porosity is defined as the ratio of interconnected pore space to the bulk volume of the rock. This is in contrast to absolute, or total, porosity which is the ratio of the total void space, including pores that are not connected, to the bulk volume. Effective porosity is always less than or equal to absolute porosity. In highly cemented rocks, the difference in absolute and effective porosity can be great (Amyx et al., 1960; Scheidegger, 1960; Anderson, 1976).

Effective liquid porosity determinations were made on 149 samples using standard liquid saturation techniques and a 20,000 ppm NaCl brine solution. Brine was used rather than fresh water in the belief that it would better simulate reservoir fluids and in order to avoid damage to water-sensitive clays. The brine concentration was established by using Cherokee Group oil field brine data available at the Kansas Geological Survey. Oil-saturated samples were placed

106

LITHOFACIES	PROPERTY	NUMBER OF SAMPLES	RANGE	MEAN	STANDARD DEVIATION
A	POROSITY, %	12	13.43 TO 21.59	18.76	2.52
	PERMEABILITY, MD.	12	0.24 TO 233.24	11.52	7.51
	EFFECTIVE RADIUS, µM.	2	5.89 TO 17.13	——	——
	GRAIN SIZE, PHI UNITS	4	1.75 TO 2.98	2.48	0.52
B	POROSITY, %	2	15.37 TO 15.83	——	——
	PERMEABILITY, MD.	2	8.71 TO 32.97	——	——
	EFFECTIVE RADIUS, µM.	0	——	——	——
	GRAIN SIZE, PHI UNITS	1	3.01	——	——
C	POROSITY, %	83	6.46 TO 28.84	20.18	4.15
	PERMEABILITY, MD.	83	0.00 TO 412.32	31.63	7.48
	EFFECTIVE RADIUS, µM.	8	4.77 TO 16.86	8.39	1.52
	GRAIN SIZE, PHI UNITS	27	1.75 TO 3.37	2.49	0.40
D	POROSITY, %	48	5.35 TO 28.41	15.23	4.67
	PERMEABILITY, MD.	48	0.00 TO 127.89	2.28	10.32
	EFFECTIVE RADIUS, µM.	3	1.44 TO 3.54	2.27	1.57
	GRAIN SIZE, PHI UNITS	11	2.81 TO 3.52	3.21	0.30
E	POROSITY, %	14	10.34 TO 24.70	16.19	4.15
	PERMEABILITY, MD.	14	0.00 TO 427.04	1.19	58.46
	EFFECTIVE RADIUS, µM.	3	0.88 TO 5.77	2.95	2.85
	GRAIN SIZE, PHI UNITS	4	2.95 TO 3.48	2.96	0.49

Figure 60. Number of samples, range, mean, and standard deviation of porosity, permeability, effective radius (based on pore size distribution), and grain size of each lithofacies recognized in the sandstones in this study. The means for permeability and effective radius are geometric means. When comparing lithofacies, note the number of samples from each.

in a soxhlet extraction device and the petroleum was removed by using a commercial solvent.

Effective porosity values in Cherokee Group sandstones range from 5.4 to 28.5 percent (Table 4). The average porosity of all samples tested is 18.5 per cent.

PERMEABILITY

According to Amyx, Bass, and Whiting (1960), permeability is "the fluid capacity of a formation (rock)." API Code 27 (1952) defines permeability as "a property of the porous medium and a measure of the capacity of the medium to transmit fluids." The darcy is the standard unit of measurement for permeability and is defined by the American Petroleum Institute (1960) as follows:

> A porous medium has a permeability of 1.0 darcy when a single phase fluid of 1.0 centipoise viscosity that completely fills the (interconnected) voids of the medium will flow through it under conditions of viscous flow at a rate of one centimeter per second per square centimeter cross-sectional area under a pressure or equivalent hydraulic gradient of one atmosphere (76.0 centimeters of mercury per centimeter).

Determinations of liquid permeability were attempted on all 149 samples using the 20,000 ppm NaCl brine and measured with the Ruska permeameter available in the Tertiary Oil Recovery Project (TORP) laboratory. Nine of the samples were also tested using gas permeability techniques because of their immeasurably low permeabilities to the brine at the pressures used for testing. Of these nine samples, three were also impermeable to nitrogen gas. The range of

108

permeabilities measured is 0.0 to 427.0 millidarcies (Table 4). Notice that the variation in permeability is greater within an individual lithofacies than from lithofacies to lithofacies, although this is not always true.

PORE SIZE DISTRIBUTION

Determination of pore size distributions in 15 samples was conducted by Randall Ivey using the mercury porosimeter available in the TORP laboratory. The laboratory technique and calculations are described in Appendix A. From the calculations, the effective pore throat radius or pore throat radius at initial breakthrough is determined. Effective pore throat radius is inversely proportional to the pressure at which mercury passes through a large number of the pore throats and fills a significant amount of the pore volume. In a plot of pressure versus cumulative volume, this zone of breakthrough is a notable inflection point where most of the accessible pore volume is filled with the mercury. Pore throat radius directly influences permeability and is important in understanding fluid behavior. The calculations of so called "effective radius" are based on the assumption that the determined radius can be represented by the largest sphere that would fit in that pore throat. Although pore throats are generally not spherical in shape, this provides a standard of reference (Scheidegger, 1960). Values of effective radius range from 0.88 to 17.13 micrometers (Table 4). Comparison of porosity, permeability, and effective pore throat radius are included in the section comparing geologic and petrophysical properties. In places in this text, effective pore throat radius may be more simply referred to as effective radius.

POROSITY TYPES

From the geologic standpoint, several types of porosity exist in the sandstones studied. Nomenclature for such a classification is taken from Schmidt and MacDonald (1979) and Choquette and Pray (1970).

The dominant type of porosity in the sandstones studied is primary intergranular porosity (Figure 57), which is estimated to make up at least 75 per cent of the total porosity. This porosity has been reduced during diagenesis by the compaction of soft, argillaceous rock fragments into pore spaces; by crushing and fracturing of detrital grains such as micas and feldspars; and by kaolinite, silica, and carbonate cements filling pore spaces. Porosities were probably more than 50 per cent when the sandstones were deposited and have been reduced to the current range of 5 to 28 per cent. In thin sections, cementation and compaction of soft grains into pore spaces appear to be the most common causes of pore size reduction.

Secondary porosity is responsible for some of the porosity in the sandstones studied here. The types of secondary porosity noted are: 1) Partial dissolution of grains, particularly feldspars, resulting in intragranular porosity (Figures 24, 32, and 33); 2) Moldic porosity in which a detrital grain was dissolved, but the grain coatings were preserved (Figure 43); and 3) Solution of entire grains or clusters of grains resulting in oversized pores (Figures 34, 36, and 37). Grains that have been dissolved were

probably originally feldspars and, possibly, carbonate cements. This pore type and the moldic pores are probably of similar origin and represent end points of a continuum from grains with no coatings to those with complete grain coatings. In thin sections, secondary porosity appears to be a relatively minor constituent of the total porosity in the sandstones studied here.

Other types of porosity were noted. Corroded detrital grains, particularly in the presence of carbonate cements, are common (Figures 29 and 31). Intraparticle pores (microporosity of Pittman, 1979), particularly in kaolinite booklets, were recognized (Figures 34, 35, 36, and 37). Fractured grains, most commonly feldspars and micas, occur as a result of compaction (Figures 30 and 33). These are all forms of secondary porosity.

A plot of pore-filling constituents (the sum of kaolinite, siderite, dolomite-ankerite, mica, nonfoliated argillaceous rock fragments, and silty-shale clasts from Table 2) versus measured effective porosity (from Table 4) (Figure 61) generally indicates slightly higher porosities in samples with lesser percentages of pore-filling constituents. Interpretation of this plot must be tempered for at least three reasons. First, there are only fifteen points on the plot. More data might confirm or disprove the interpretation. Second, the data for pore-filling constituents was a mineralogic point count and does not include volumetrically important cements, especially silica

which has completely filled pores in the finer, dirtier sandstones of lithofacies D and E. In the future, point counts of only cements and pore space should be used. A method of determining volumetric amounts of pore-filling constituents would be best. Third, the presence of intraparticle secondary porosity in kaolinite and partially dissolved and fractured feldspars and micas means that the pore volume these constituents occludes is actually less than the point count measurement indicates.

A plot of the sum of pore-filling constituents and pore space from Table 2 versus measured effective porosity from Table 4 (Figure 62) again indicates slightly higher porosities in samples with lesser percentages of pore-filling constituents. The limitations discussed in the previous paragraph would also apply to this plot.
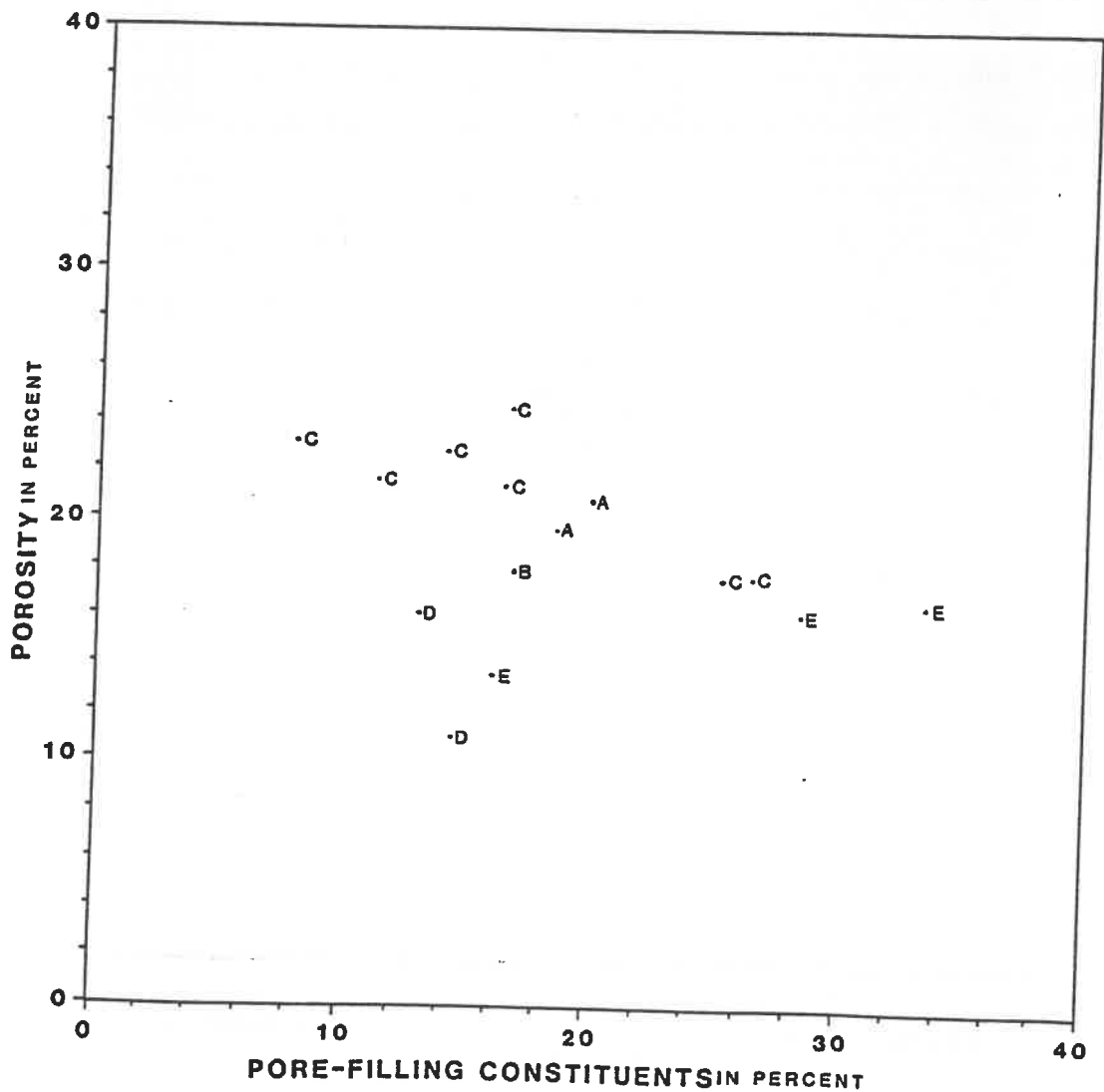
Figure 61. Plot of pore-filling constituents (the sum of kaolinite, siderite, dolomite-ankerite, mica, nonfoliated argillaceous rock fragments, and silty-shale clasts) from Table 2 versus measured effective porosity from Table 4. Porosity is generally higher in samples with fewer pore-filling constituents.

114
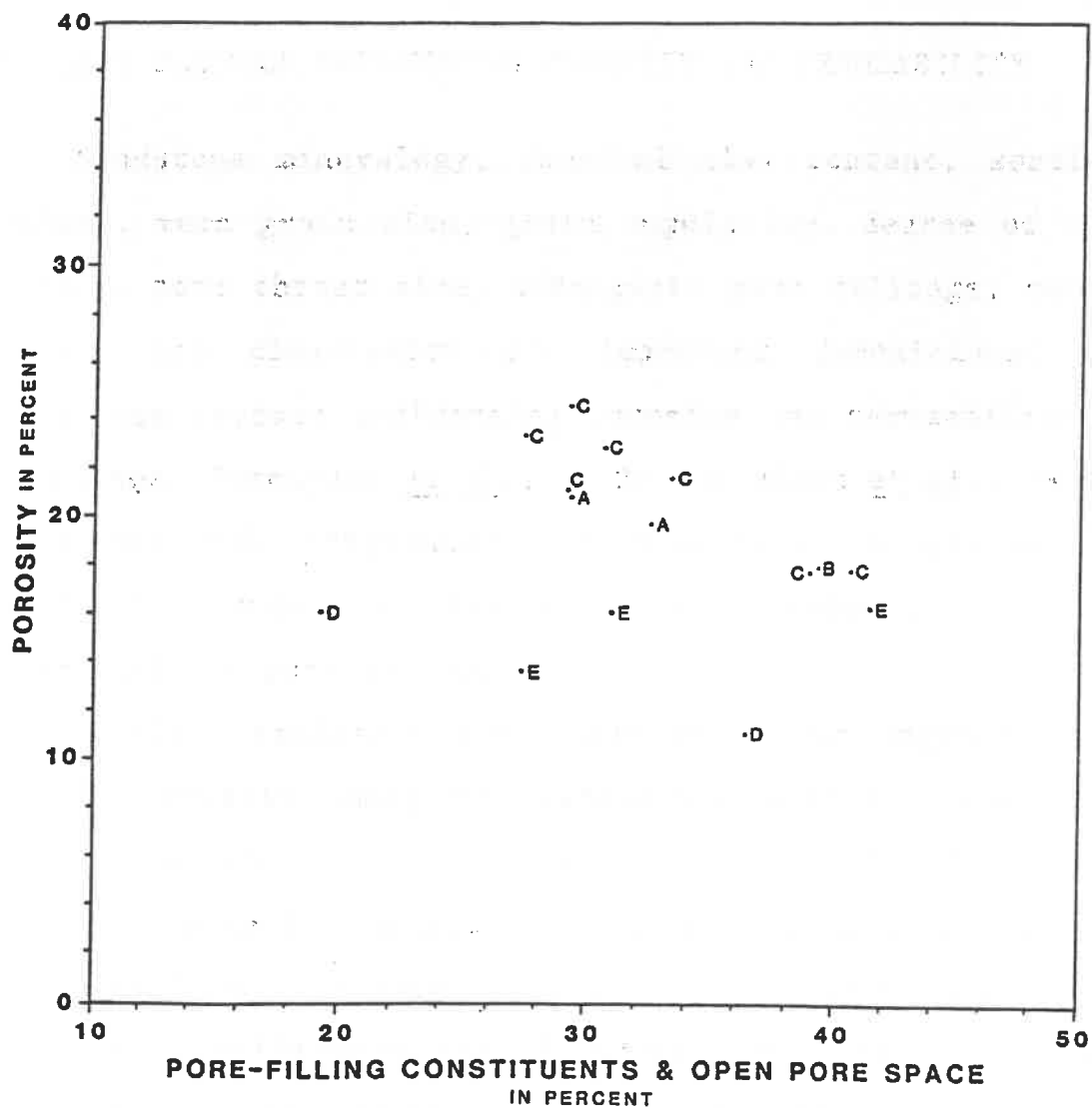
Figure 62. Plot of pore-filling constituents (the sum of kaolinite, siderite, dolomite-ankerite, mica, nonfoliated argillaceous rock fragments, and silty-shale clasts) plus open pore space from Table 2 versus measured effective porosity from Table 4. Porosity is generally higher in samples with fewer pore-filling constituents and open pore spaces.

RELATIONSHIPS BETWEEN GEOLOGICAL AND
PETROPHYSICAL PROPERTIES

POSSIBLE FACTORS INFLUENCING POROSITY AND PERMEABILITY

Sandstone mineralogy, detrital clay content, sorting, packing, mean grain size, grain angularity, degree of compaction, pore throat size, authigenic pore fillings, cementation, and dissolution are important depositional and diagenetic factors influencing porosity and permeability in sandstones (Pettijohn et al., 1972; and Blatt et al., 1980). These textural attributes and diagenetic processes are important because they represent the fundamental "building blocks" of the pore system.

Detrital sandstone mineralogy and grain angularity do not vary greatly among the sandstones used in this study and, therefore, these parameters were not studied as possible causes of variation in petrophysical properties of the sandstones. In thin sections, it has been established that soft argillaceous rock fragments are usually deformed around surrounding grains or into surrounding pore spaces, thus reducing porosity and permeability. These rock fragments are generally more common in the upper portion of sandstone sections probably due to local scour and rapidly decreasing current velocities during deposition.

The stability of the grain framework is influenced by the abundance of ductile grains, such as micas and soft rock fragments, and by grain-to-grain arrangements (packing).

116

The effect of changes in packing on porosity and permeability may be important, particularly with increasing amounts of ductile rock fragments (Pettijohn et al., 1972).

It is probable that variations in the amount of authigenic minerals cause variations in the porosity, permeability, and effective pore throat size. Concretions are rare, localized phenomena in sandstones, but, where present, fill all pore space. Chlorite coatings on grains have the opposite effect. Coatings inhibit subsequent silica cementation by decreasing the available locations for the cement to develop on grains and thereby preserve some of the original porosity. Ferroan carbonate cements and authigenic kaolinite aid in reduction of porosity and permeability primarily by decreasing the size of pores, but also by blocking off pore throats. In addition, kaolinite alters porosity from macroporosity of open pores to microporosity of tiny pores between kaolinite "booklets". Kaolinite and chlorite also create an increased polar surface area (Grim, 1968) in pores, a factor of potential economic importance when dealing with the expensive chemicals used in enhanced oil recovery techniques, because the concentrations of these chemicals may be altered by ion exchange or retained by the polar surfaces of the clays (Hower, 1974).

METHODS AND DISCUSSION

Eliminating sand mineralogy and grain angularity as possible variants, clay content, degree of compaction, amounts of authigenic minerals, grain size, and sorting are left as possible textural causes of variations in porosity, permeability, and pore throat size. Before discussing the relationships between geological and petrophysical properties, a discussion of the relationships betwen individual petrophysical properties studied here is presented.

Relationships of Petrophysical Properties

Hulse (1978) reported that Cherokee sandstones with large scale sedimentary structures had permeabilities greater than 10 millidarcies, but those with small scale sedimentary structures had permeabilities less than 10 millidarcies. He correctly classified about 80 percent of his samples using permeability values to predict type of sedimentary structures. The scale of sedimentary structures was established during core studies in the early part of this research. Lithofacies A, B, and C are dominated by large scale sedimentary structures including high- and low-angle ?trough? cross beds, horizontal bedding, and large-scale ripplemarks. Lithofacies D and E are dominated by small scale sedimentary structures including low angle ?trough? cross beds, small scale ripplemarks, small-scale

118

climbing ripples, and horizontal laminations. Table 4 contains porosity, permeability, and lithofacies data. In order to test Hulse's observation, a plot of porosity versus log permeability (permeability is lognormally distributed, Law, 1944) was constructed and each sample was marked as A, B, C, D, or E depending on the lithofacies where it occurred (Figure 63). This figure shows that Hulse's observation is generally true, with the large scale sedimentary structures having higher porosities and permeabilities than the small scale sedimentary structures, particularly for lithofacies C and D. However, careful observation of Figure 63 shows that 80 percent of the large scale sedimentary structures do not have permeabilities greater than 10 millidarcies. The problem is due, in part, to differences in permeabilities obtained by gas permeability techniques used to obtain Hulse's data and liquid permeability techniques used in this study. The liquid technique yields results lower in value than the gas technique. Another cause of the problem is that Hulse's data all came from one small area in 3 closely related sandstones while the data in this study represent a much broader area with numerous unrelated sandstones. Note that samples from lithofacies E cover the entire range of values. This result is not surprising. Lithofacies E was deposited episodically and at varying flow conditions.

Samples from lithofacies A, B, or C (large scale sedimentary structures) with low permeabilities and porosities are not surprising if cementation and compaction reduce

119
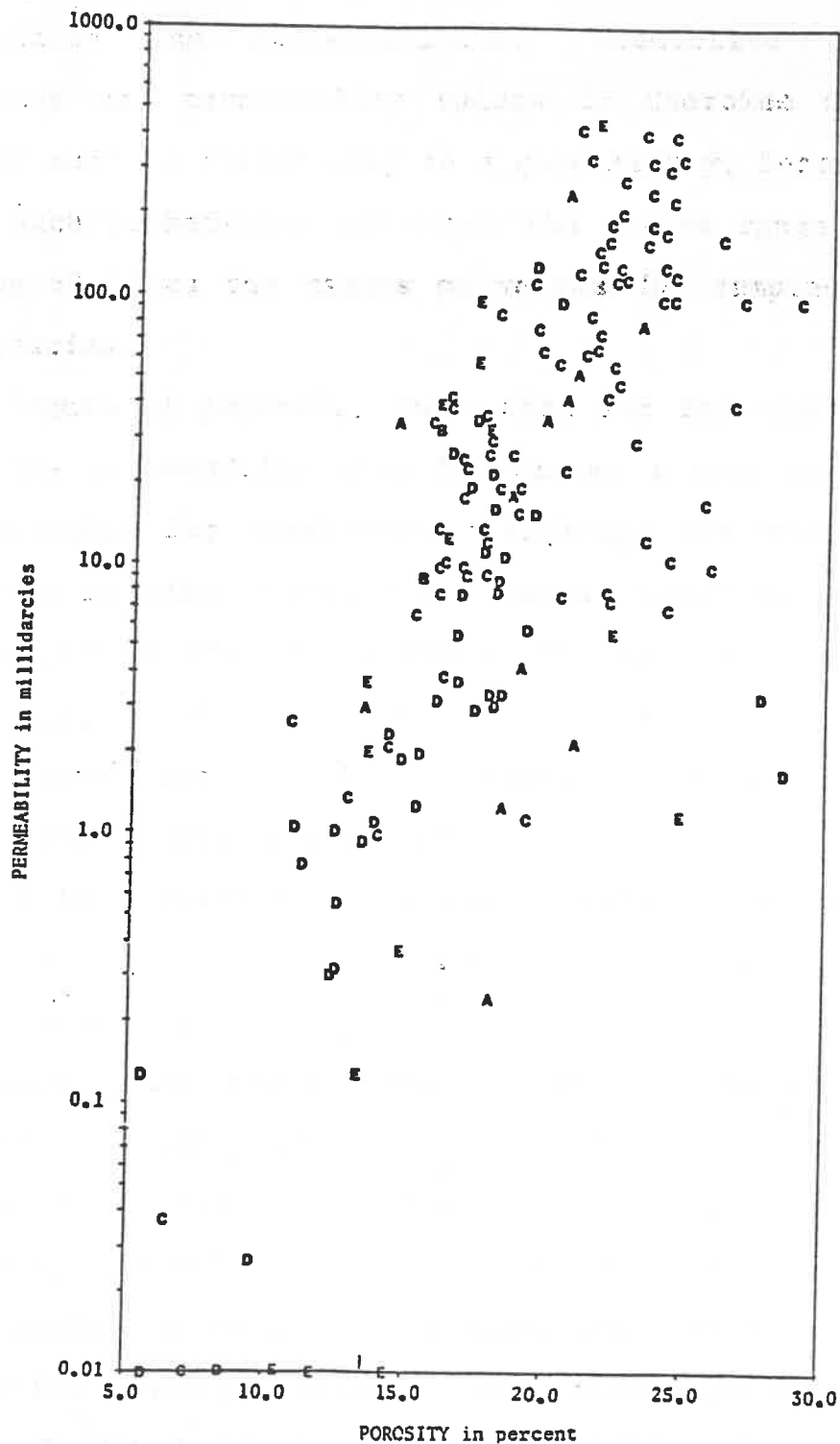
Figure 63. Plot of permeability versus porosity. Each letter indicates the lithofacies from which the samples were taken. Note the general increases in permeability with increases in porosity and that the coarse sandstones (lithofacies A, B, and C) generally have higher porosity and permeability than the fine sandstones (lithofacies D and E).

porosities and permeabilities. Predictive models for porosity and permeability values in Cherokee Group sandstones must be viewed only in a general way, because samples from each lithofacies may cover the entire range of values. Figure 60 lists the ranges of values for samples from each lithofacies.

Figure 63 generally shows that for increases in porosity, the permeability also increases, a well known general relationship for sandstones. Although the positive relationship between porosity and permeability is well established, it is one of the goals of this research to pursue the possible reasons for such a relationship, because depositional and diagenetic aspects of the sediment influence porosity and permeability.

Before investigating geologic effects, an analysis of the relations of effective pore throat radius to porosity and permeability was conducted. Figure 64 is a plot of effective pore throat radius, in micrometers, against percent porosity. Although there are only 16 points, the diagram indicates a positive relationship where porosity increases directly with effective pore throat radius. In other words, as porosity increases, the size of pore throats (effective radius) increases. Note that samples from lithofacies D and E (small scale sedimentary structures) have lower porosities and effective pore throat radii than samples from lithofacies A and C (large scale sedimentary structures). The effect of grain size on effective pore

Figure 64. Plot of effective pore throat radius versus porosity. Letters indicate the lithofacies from which the samples were taken. Note the general increase in effective pore throat radius with increasing porosity. Also note the coarse sandstones (lithofacies A and C) generally have higher effective pore throat radii and porosities compared to the fine sandstones (lithofacies D and E).

throat radius is discussed later in this section. Relatively high porosity with small effective pore throat radius, as in some samples from lithofacies C, might be an indicator of the effect of pore-throat blocking clays. Figure 65 is a plot of effective pore throat radius versus permeability which shows a strong positive relationship. This strong relationship is not surprising, because permeability is dominantly controlled by pore throat size (Blatt et al., 1980). Again, small scale structures (lithofacies D and E) have relatively low permeabilities and effective pore throat radii relative to large scale sedimentary structures (lithofacies A, B, and C).

Effect of Pore-Filling Cements and Rock Fragments on Petrophysical Properties

Using data from the mineralogic point count in Table 2, the sum of kaolinite, siderite, dolomite-ankerite, mica, nonfoliated argillaceous rock fragments, and silty-shale clasts was determined to represent pore-filling constituents. The pore-filling constituents do not include silica cement because this was not counted in the point count separately from quartz grains. A category for silica cements appears in Table 2, but this was determined for each quartz grain in the point count and not as a separate category. A point count specifically for cements would have included these silica cements, but was not used in this study. Because all plots involving pore-filling constituents have only 15 points, the interpretations of the plots

123

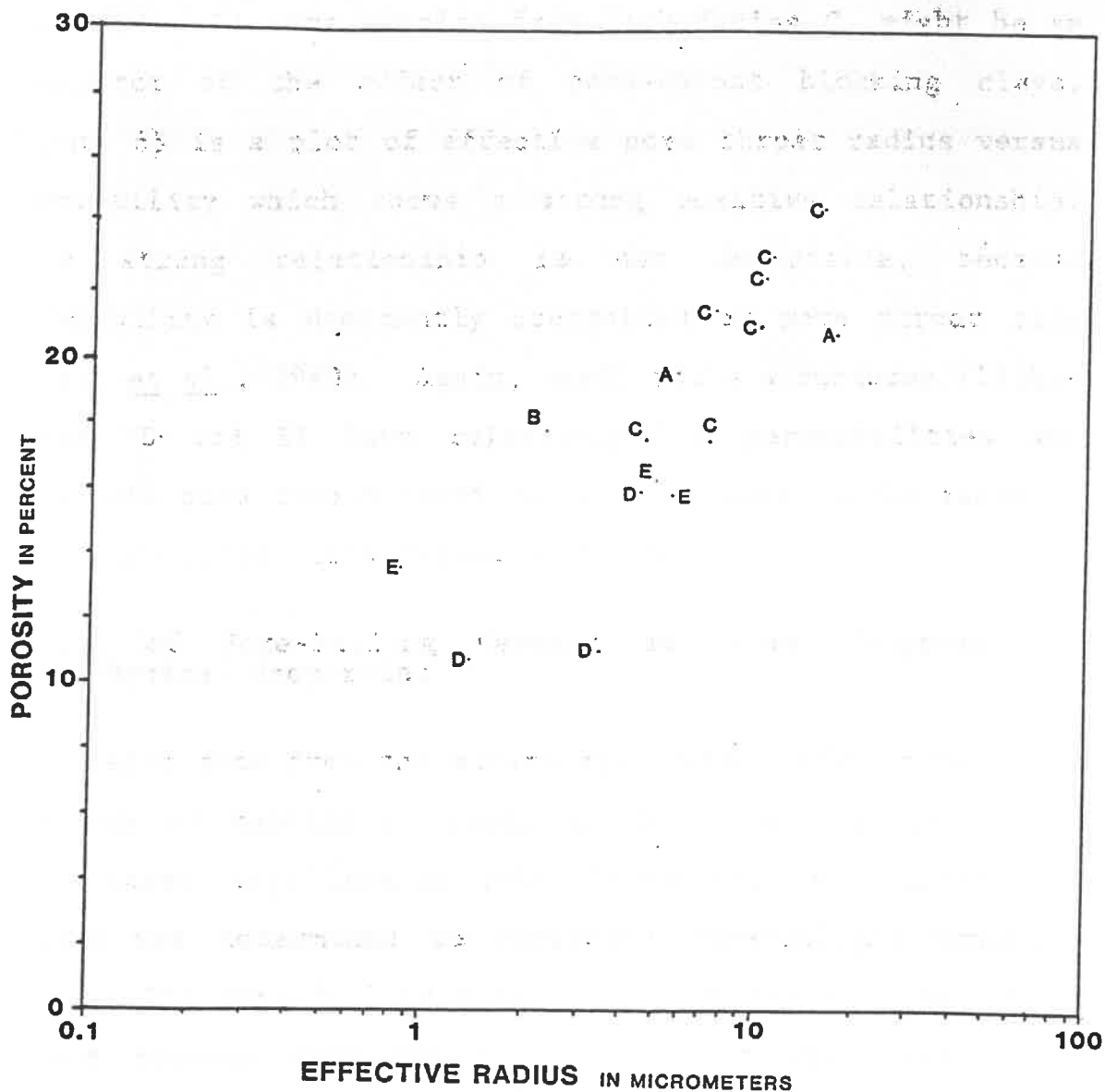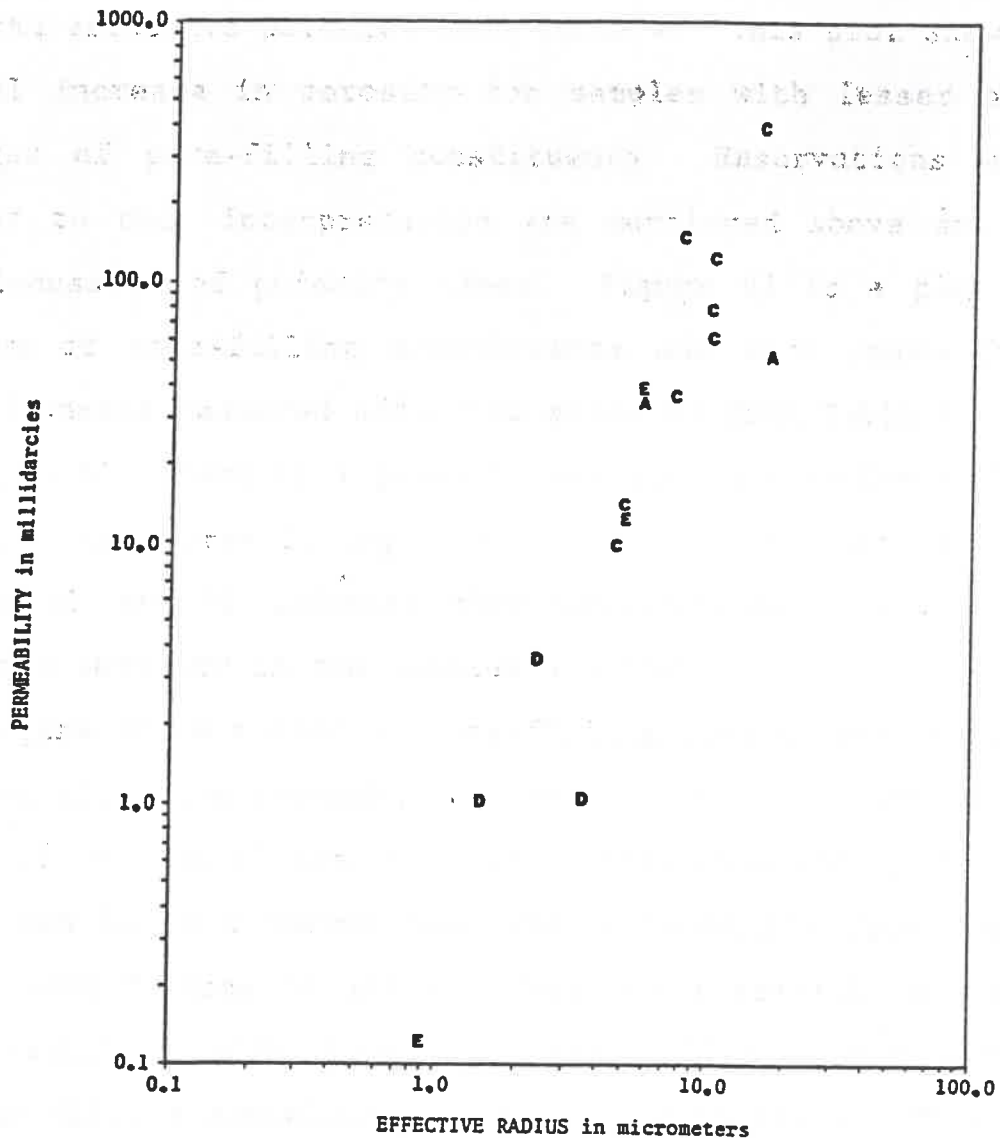Figure 65. Plot of permeability versus effective pore throat radius. Letters indicate the lithofacies from which the samples were taken. Note the general increase in permeability with increasing effective pore throat radius. Also note the coarse sandstones (lithofacies A and C) generally have higher permeabilities and effective pore throat radii compared to the fine sandstones (lithofacies D and E).

must be considered cautiously. More data may confirm or disprove the interpretations.

Figure 61 is a plot of pore-filling constituents versus measured effective porosity from Table 4. This plot shows a general increase in porosity for samples with lesser percentages of pore-filling constituents. Reservations with respect to this interpretation are mentioned above and in the discussion of porosity types. Figure 62 is a plot of the sum of pore-filling constituents and pore space from Table 2 versus measured effective porosity from Table 4. As in Figure 61, there is a general increase in porosity with a decrease in pore-filling constituents and open pores. Figures 61 and 62 indicate that pore-filling constituents influence porosity in the samples studied.

Figure 66 is a plot of pore-filling constituents versus measured effective permeability from Table 4. Figure 67 is a plot of the sum of pore-filling constituents and open pore space from Table 2 versus measured permeability from Table 4. In both Figures 66 and 67, there is a general increase in permeability with decreasing pore-filling constituents and pore-filling constituents plus open pore space. This is particularly notable for samples with permeabilities greater than 10 millidarcies. The relationship is more obvious in Figure 66. Based on only 15 samples, permeability appears to be affected by the amount of pore-filling constituents.

Figure 68 is a plot of pore-filling constituents versus effective pore throat radius. Figure 69 is a plot of the

125
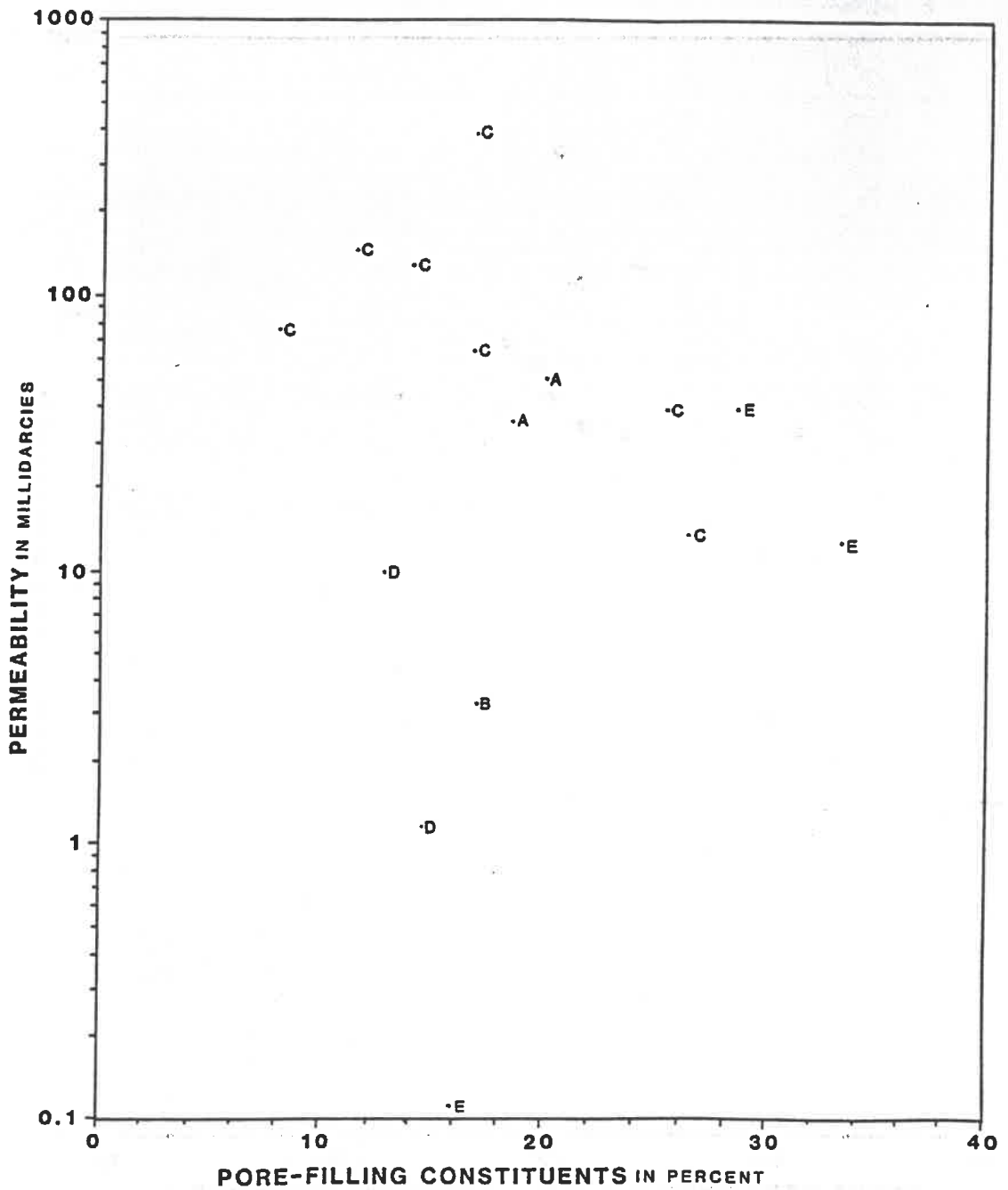
Figure 66. Plot of pore-filling constituents (the sum of kaolinite, siderite, dolomite-ankerite, mica, nonfoliated argillaceous rock fragments, and silty-shale clasts) from Table 2 versus liquid permeability from Table 4. In general, permeabilities are higher in samples with fewer pore-filling constituents.

126
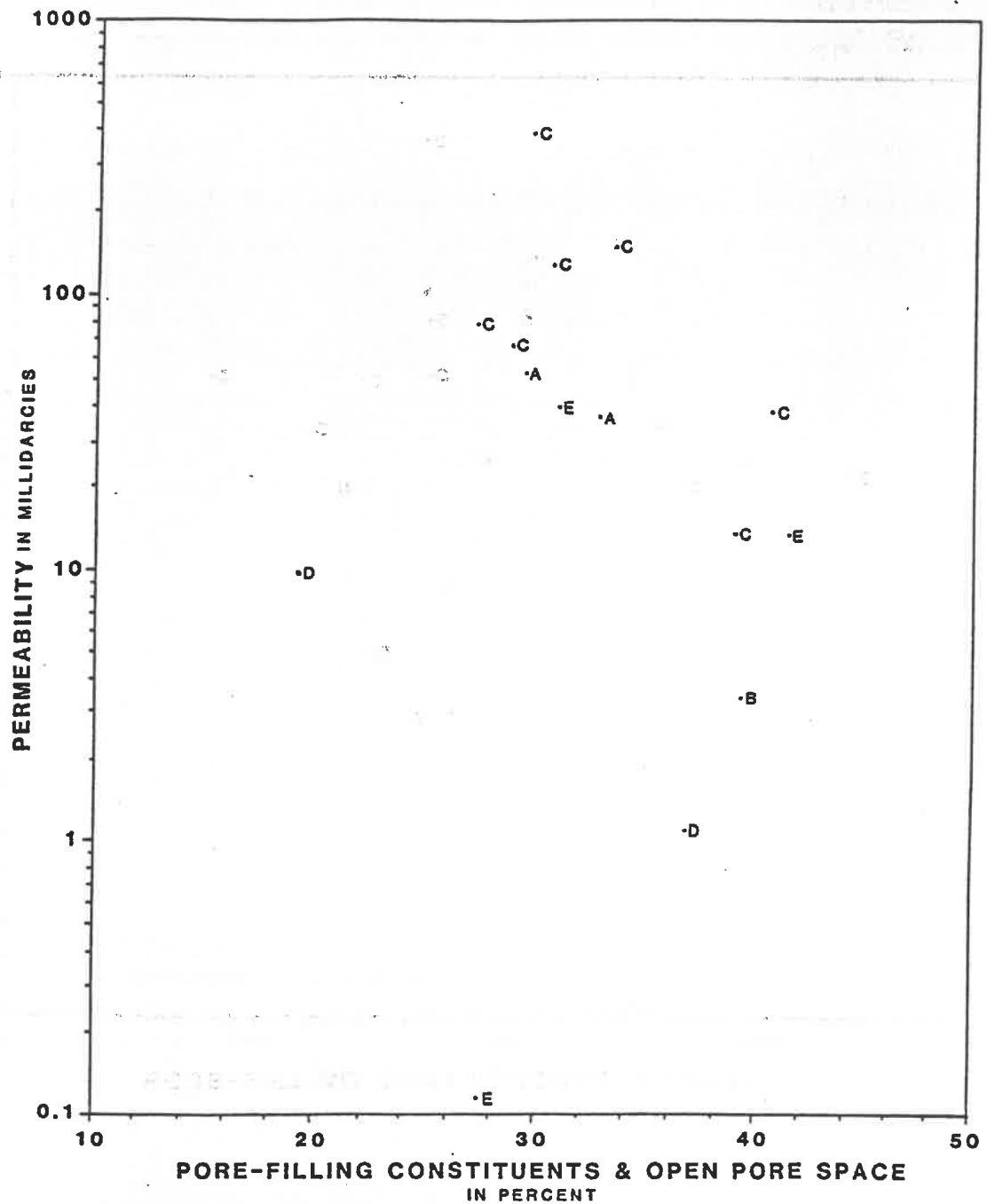
Figure 67. Plot of pore-filling constituents (the sum of kaolinite, siderite, dolomite-ankerite, mica, nonfoliated argillaceous rock fragments, and silty-shale clasts) plus open pore space from Table 2 versus liquid permeability from Table 4. In general, permeability is higher in samples with fewer pore-filling constituents and open pore space.
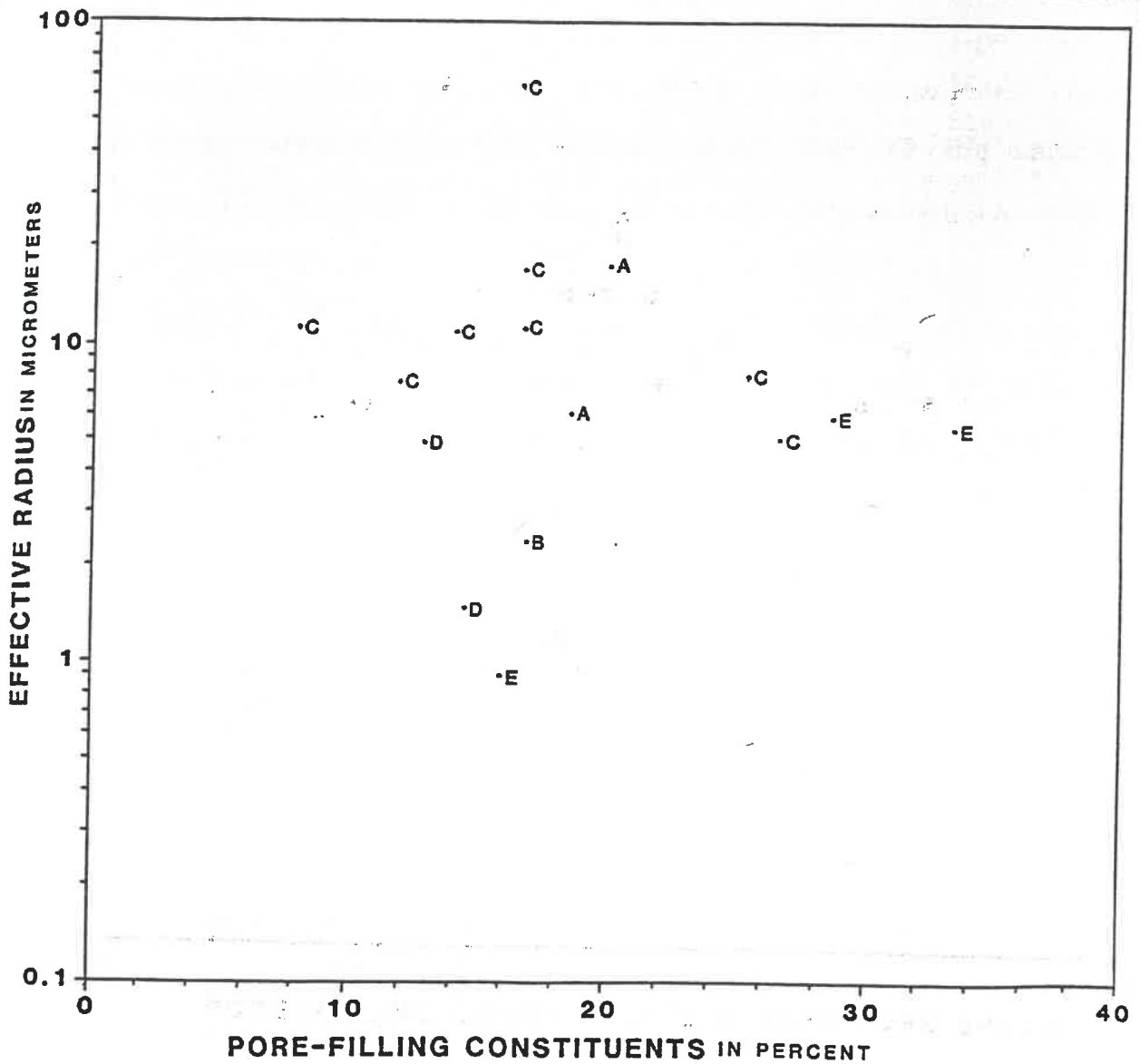
Figure 68. Plot of pore-filling constituents (the sum of kaolinite, siderite, dolomite-ankerite, mica, nonfoliated argillaceous rock fragments, and silty-shale clasts) from Table 2 versus effecitve pore throat radius from Table 4. Effective pore throat radius does not appear to be controlled by abundance of pore-filling constituents.
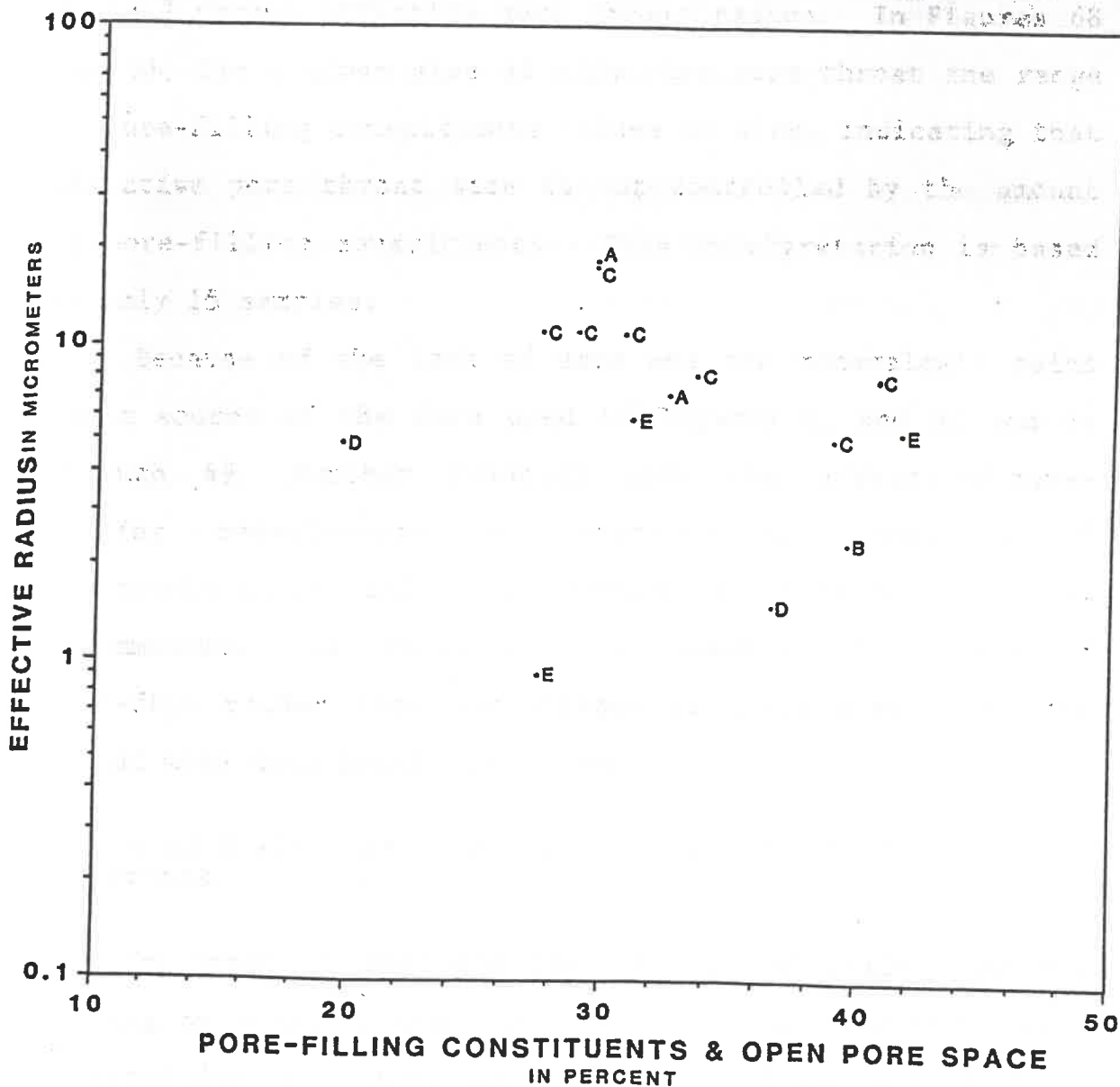
Figure 69. Plot of pore-filling constituents (the sum of kaolinite, siderite, dolomite-ankerite, mica, nonfoliated argillaceous rock fragments, and silty-shale clasts) plus open pore space from Table 2 versus effective pore throat radius from Table 4. Effective pore throat radius does not appear to be strongly influenced by the amount of pore-filling constituents and open pore space.

129

sum of pore-filling constituents and open pore space from Table 2 versus effective pore throat radius. In Figures 68 and 69, for a given size of effective pore throat the range of pore-filling constituents values is wide, indicating that effective pore throat size is not controlled by the amount of pore-filling constituents. This interpretation is based on only 15 samples.

Because of the lack of data and the mineralogic point count source of the data used in Figures 61 and 62 and 66 through 69, further research into the effects of pore-filling constituents on petrophysical properties of relatively dirty sandstones (compared to orthoquartzites) is recommended. In particular, a measure of volumes of pore-fill rather than percentages of constituents and the use of more data points are needed.

Effect of Grain Size, Sorting, and Packing on Petrophysical Properties

In order to evaluate the effects of grain size and sorting on porosity and permeability, 47 thin sections were selected for grain size determinations. These thin sections represent the sedimentary structures recognized, the range of porosities and permeabilities determined, and the various sandstone bodies encountered in this study as listed in Table 3. A rectangular grid pattern was established to cover each thin section so that the long axis of 100 mono-crystalline quartz grains could be measured (in millimeters)

130

with a calibrated ocular. The long axis of quartz grains, rather than the entire detrital fraction, was measured because the grain size of soft rock fragments and micas increased upward through the vertical section and the size of other detrital grains was assumed to be similar to quartz. The measured long axis of quartz grains is the grain size indicator referred to in the discussion of the relationships between grain size and petrophysical properties. Each set of 100 grain-lengths was converted to phi units using the relationship: phi = $-\log_2$ length (mm) (Krumbein, 1934) and averages and standard deviations of grain size for each sample of 100 were determined. Conversion to phi units changes the grain size distribution from the assumed lognormal distribution (length in mm) to a normal distribution (phi units) enabling the data to be plotted on arithmetic paper (Folk, 1974). It also simplifies calculation of statistical parameters such as standard deviation (Blatt et al., 1980). Standard deviation was determined as a close measure of the graphic standard deviation (Folk, 1974). Fifteen of the 47 samples used in the grain size determinations have been used in the compilation of Table 2 which contains data from 200 point counts for mineralogy. The core plugs for these 15 samples were also used to determine effective pore throat radius by mercury porosimetry techniques.

Figure 70 is a plot of an indicator of grain size versus porosity. The diagram shows that as the indicator of

GRAIN SIZE in millimeters
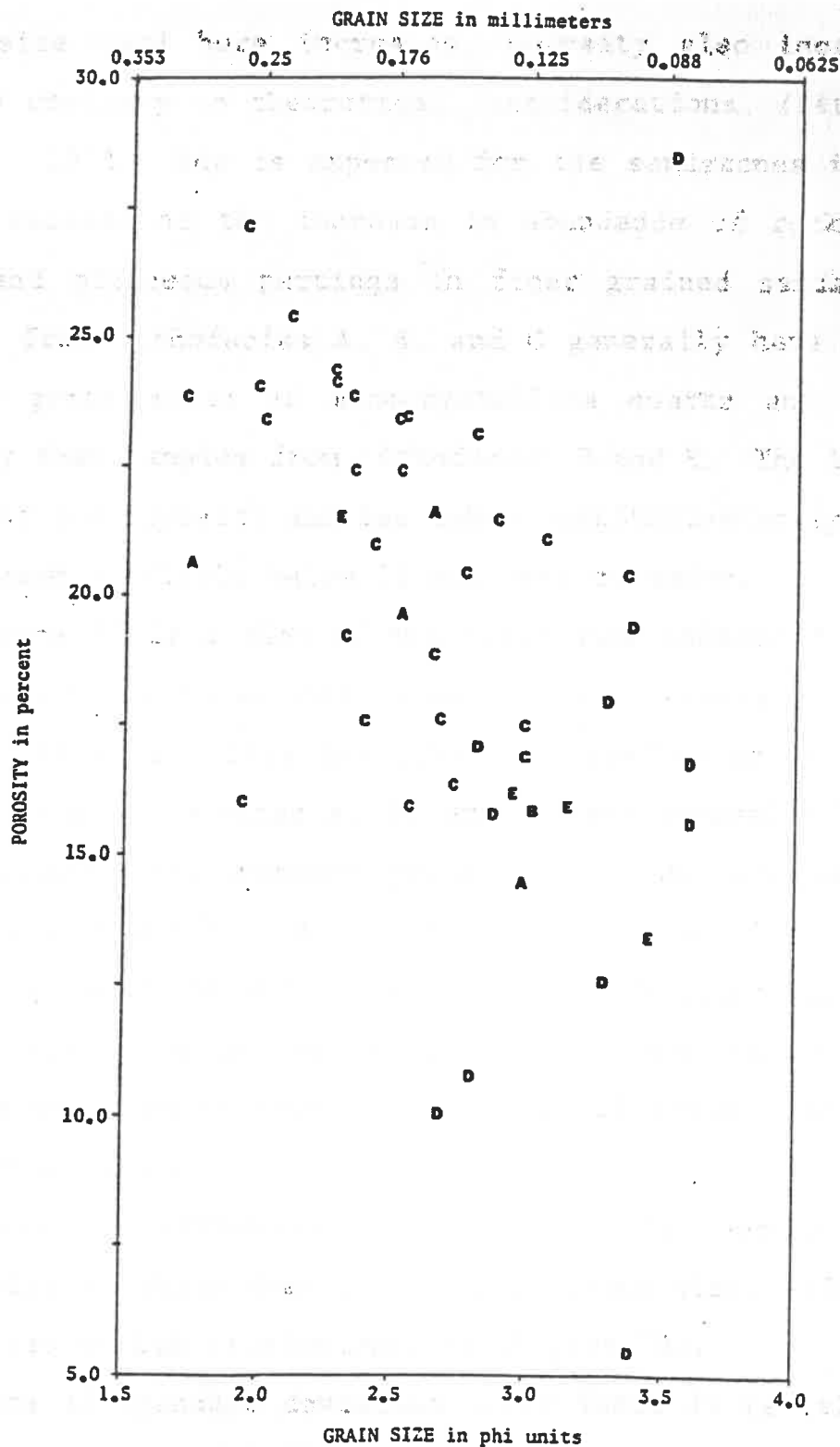
Figure 70. Plot of porosity versus grain size. Letters indicate the lithofacies from which the samples were taken. Note a general increase in porosity with coarsening grain size.

132

grain size used here increases, porosity also increases. This is contrary to theoretical considerations (Pettijohn et al., 1972) but is expected for the sandstones in this study, because of the increase in abundance of rock fragments and micaceous partings in finer grained sandstones. Samples from lithofacies A, B, and C generally have larger average grain sizes of monocrystalline quartz and higher porosity than samples from lithofacies D and E. The limited number of low porosity samples makes qualitative analysis of the diagram difficult below 15 per cent porosity.

Figure 71 is a plot of the grain size indicator versus permeability and shows that permeability is generally higher for coarser grain sizes and lower for smaller grain sizes. Samples from lithofacies A, B, and C have generally higher permeabilities and coarser grain sizes than samples from lithofacies D and E. In Figure 71 the spread of values of grain size indicator with a particular permeability is wide. If more samples with low permeabilities were tested, they would be expected to show a wide range of grain size for a given permeability.

A plot of effective pore throat radius versus grain size indicator shows that for smaller grain size, effective pore throat radius is also smaller (Figure 72).

Plots of standard deviation (from Table 3) (a reliable estimate of sorting according to Folk, 1974) versus porosity (Figure 73), permeability (Figure 74), and effective pore throat radius (Figure 75) were generated, but showed no

133
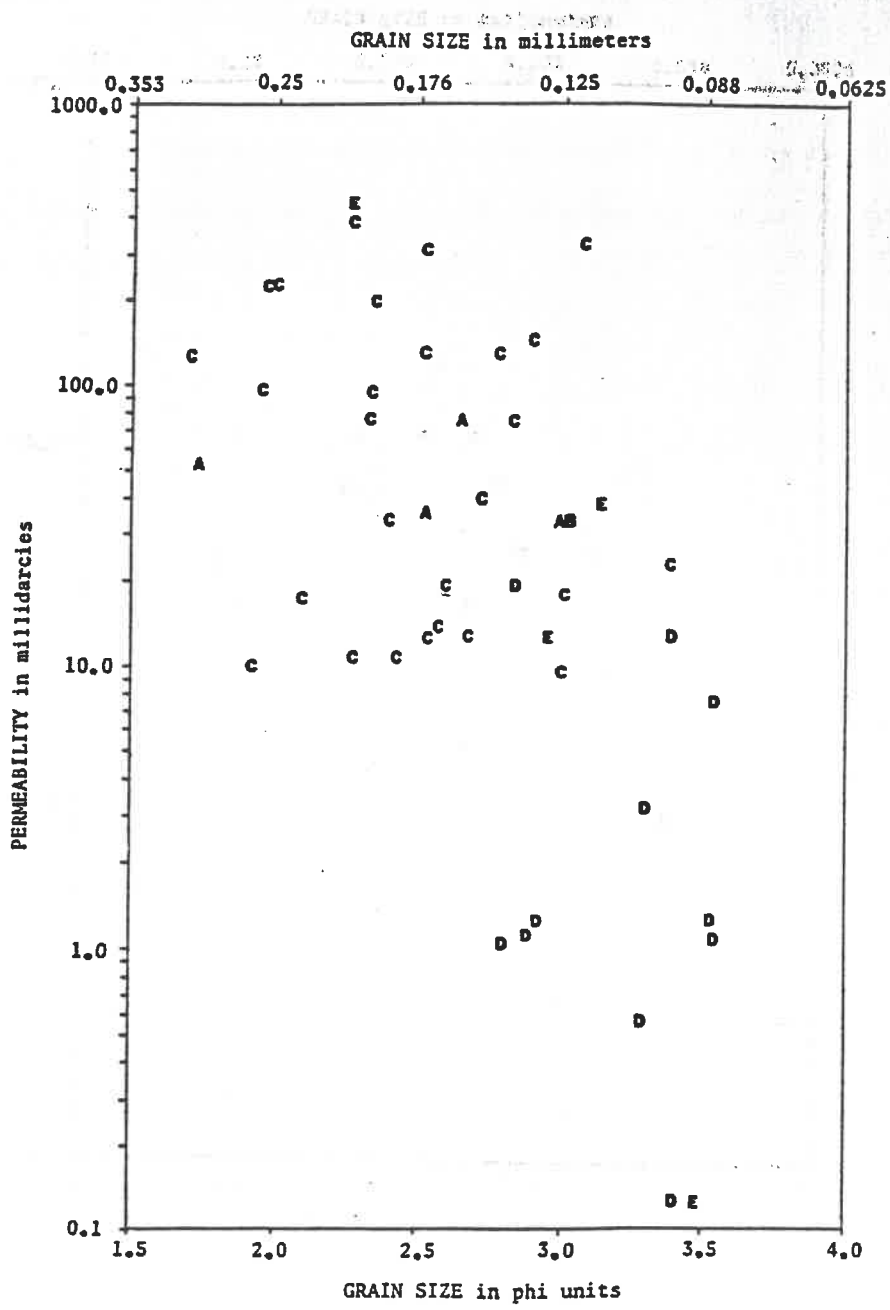
Figure 71. Plot of permeability versus grain size. Letters indicate the lithofacies from which the samples were taken. Note a general increase in permeability with coarsening grain size and that coarse sandstones (lithofacies A, B, and C) generally have coarser grain sizes and higher permeabilities compared to fine sandstones (lithofacies D and E).
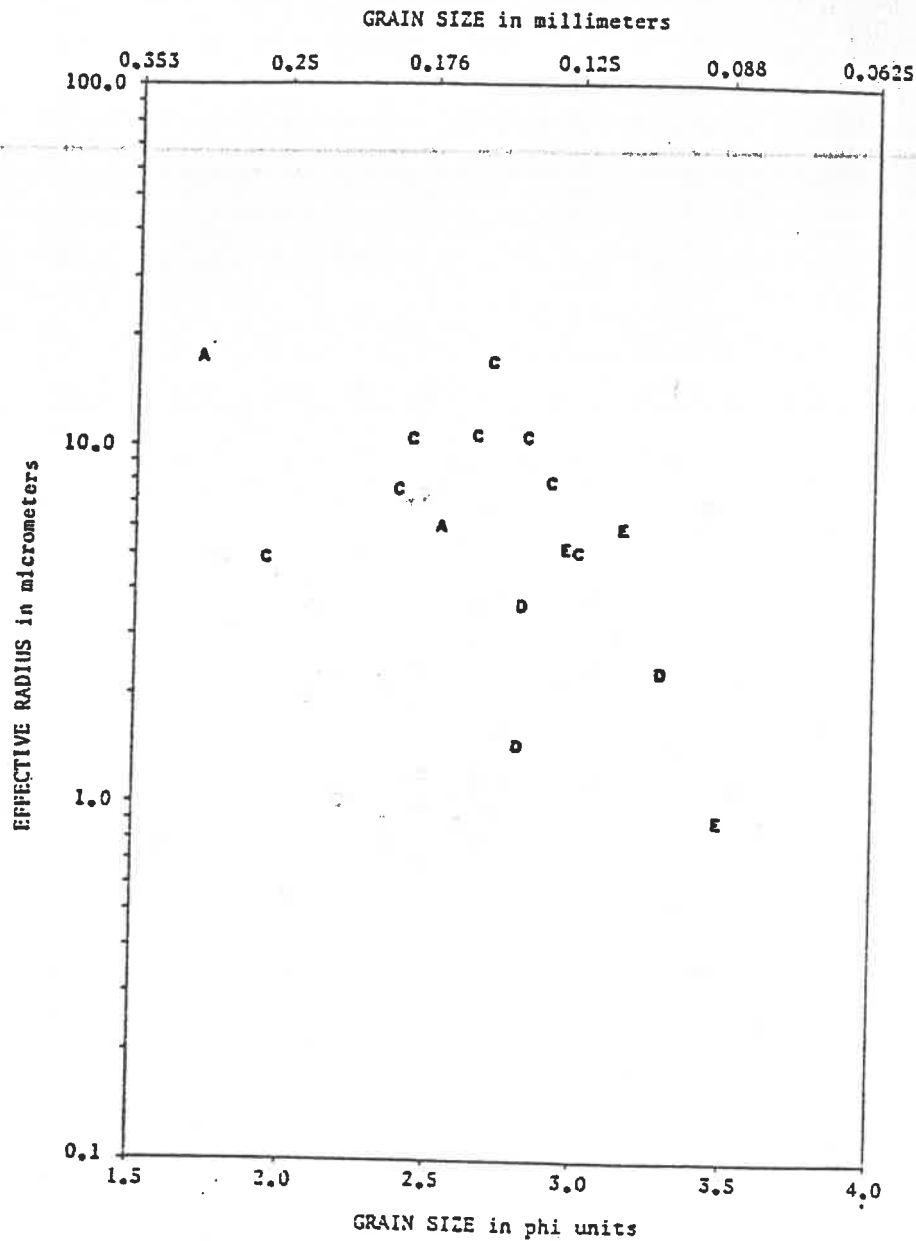
Figure 72. Plot of effective pore throat radius versus grain size. Letters indicate the lithofacies from which the samples were taken. Note the general increase in effective radius for coarser grain sizes. Also note the coarse sandstones (lithofacies A and C) have larger effective radii and coarser grain sizes compared to the fine sandstones (lithofacies D and E).
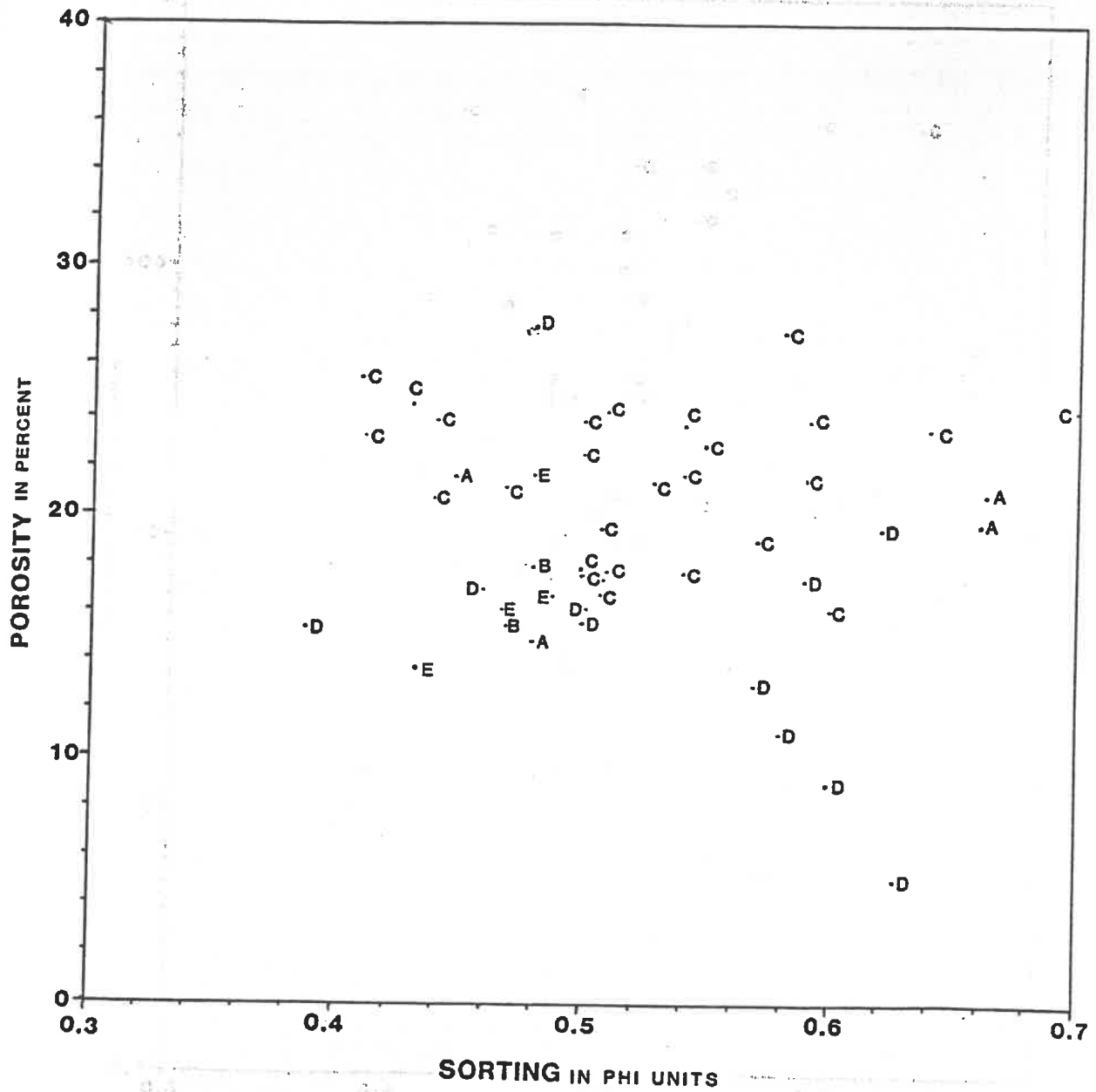
Figure 73. Plot of sorting (standard deviation) from Table 3 versus measured effective porosity from Table 4. Porosity is not affected by sorting according to this sorting indicator.

136
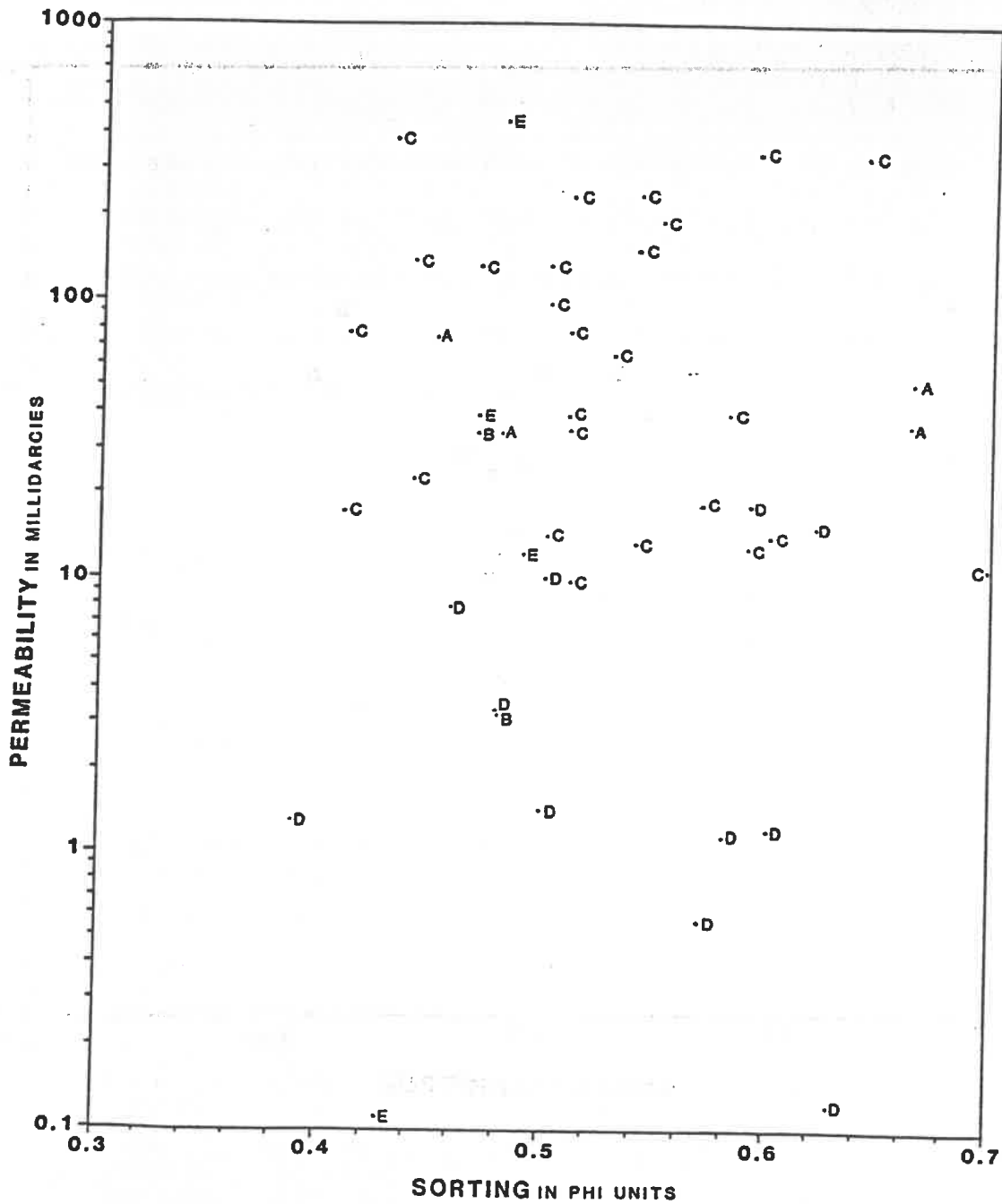
Figure 74. Plot of sorting (standard deviation) from Table 3 versus liquid permeability from Table 4. Permeability is not affected by sorting according to this sorting indicator.
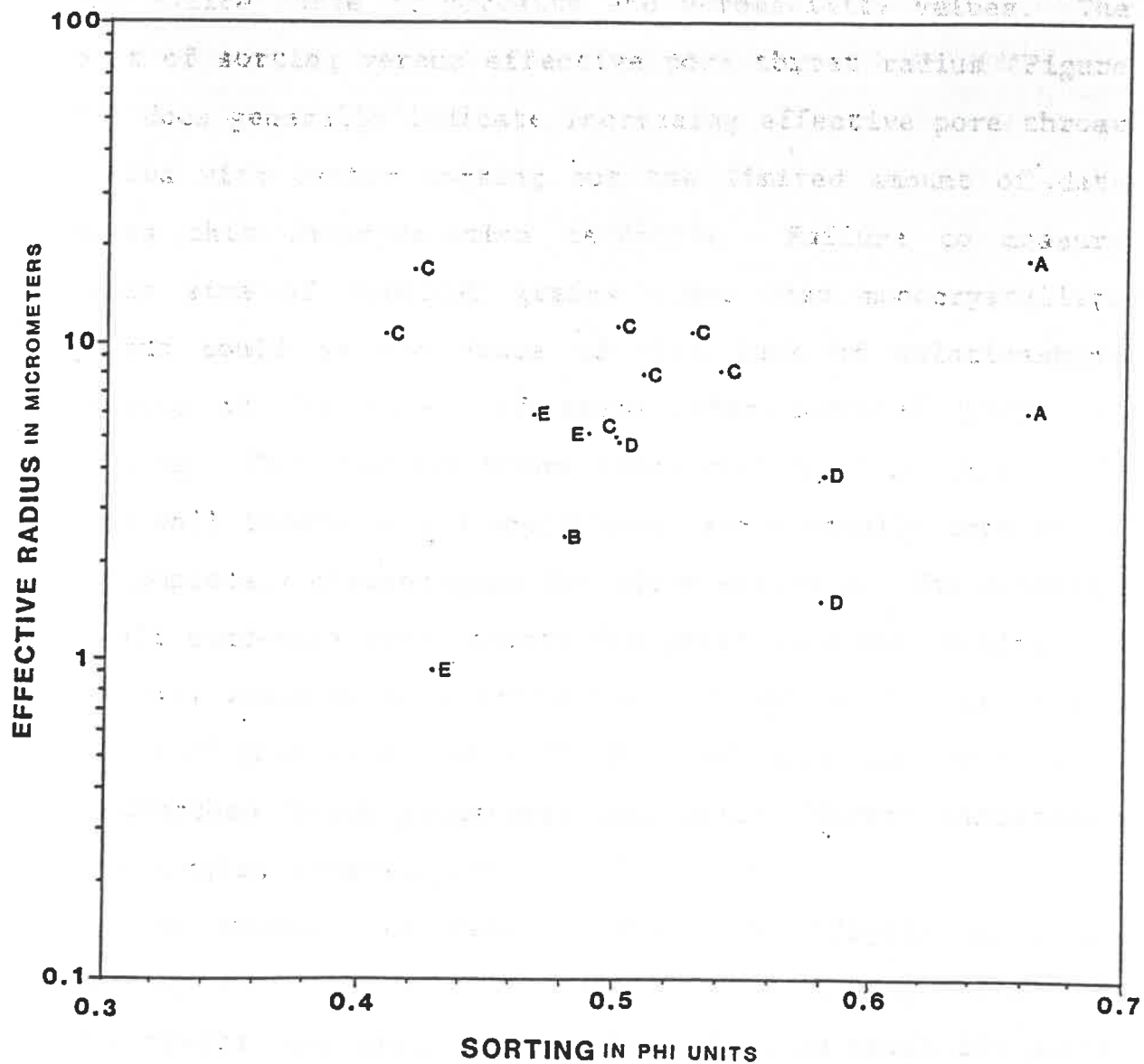
Figure 75. Plot of sorting (standard deviation) from Table 3 versus effective pore throat radius from Table 4. Based on the 15 samples tested, effective radius increases in samples with better sorting according to this sorting indicator.

definite relationships. In the plots of porosity versus sorting (Figure 73), and permeability versus sorting (Figure 74), a given value of sorting contains samples representing the entire range of porosity and permeability values. The plot of sorting versus effective pore throat radius (Figure 75) does generally indicate increasing effective pore throat radius with better sorting but the limited amount of data makes this interpretation tentative. Failure to measure grain size of detrital grains other than monocrystalline quartz could be the cause of this lack of relationships because of the effect of these other detrital grains on sorting. The Cherokee Group sandstones used in this study were well indurated and would have been virtually impossible to completely disaggregate for sieve analysis. The counting of all sand-size constituents for grain-size and sorting analysis would be more appropriate in future studies of the effect of grain-size and sorting on petrophysical properties of Cherokee Group sandstones and other "dirty" sandstones with complex mineralogies.

An attempt was made to study the effects of grain packing on petrophysical properties by measuring the number of contacts per grain in the 15 samples on which 200 point counts for mineralogy were made. Unfortunately, it was found that the technique was not reliable because of variations in the abundance of soft rock fragments and micas which tend to cover more of a grain than harder grains and

therefore reduce the number of contacts per grain although the percentage of grain-to-grain contacts is increased.

In "dirty" sandstones with complex mineralogies such as the Cherokee Group sandstones, future packing studies should study the total percentage of the periphery of an individual grain contacted by other grains rather than the number of grains contacting the grain. The application of the results of orthoquartzite (clean sandstone) packing studies to "dirty" sandstones with complex mineralogies is probably inappropriate since the overall nature of grain-to-grain contacts and the packing are probably entirely different for the two types of sandstones.

RESERVOIR MODEL

A general reservoir model for Cherokee Group sandstones reflects the associations of the various geologic and petrophysical properties (Figure 76). Particular emphasis has been placed on the sedimentary structures and their sequence (lithofacies); mineralogic variation, particularly argillaceous rock fragments; diagenetic variation, particularly chlorite coatings on grains and silica cements; diagenetic zonation, an interaction between grain size and carbonate cements; grain size; effective liquid porosity; liquid permeability; and effective pore throat radius.

Small scale sedimentary structures, which dominate the upper portions of sequences (lithofacies D and E), generally occur in finer grained sediments, with abundant argillaceous rock fragments and micaceous partings which, when compacted, block pores and pore throats. Cementation is more effective in reducing porosity and permeability in these finer grained rocks, because the pore throats are smaller initially. The finer grained rocks have lower porosity, permeability, and effective pore throat radius. It is predicted that moving fluid fronts associated with fluid production or injection in Cherokee Group sandstone reservoirs will move more slowly in these upper portions of sandstone bodies than in the coarser, lower parts of sandstone bodies.

Sediments with large scale sedimentary structures, dominant in the lower portion of sandstone bodies (lithofacies A, B, and C) in the Cherokee Group, are generally

141
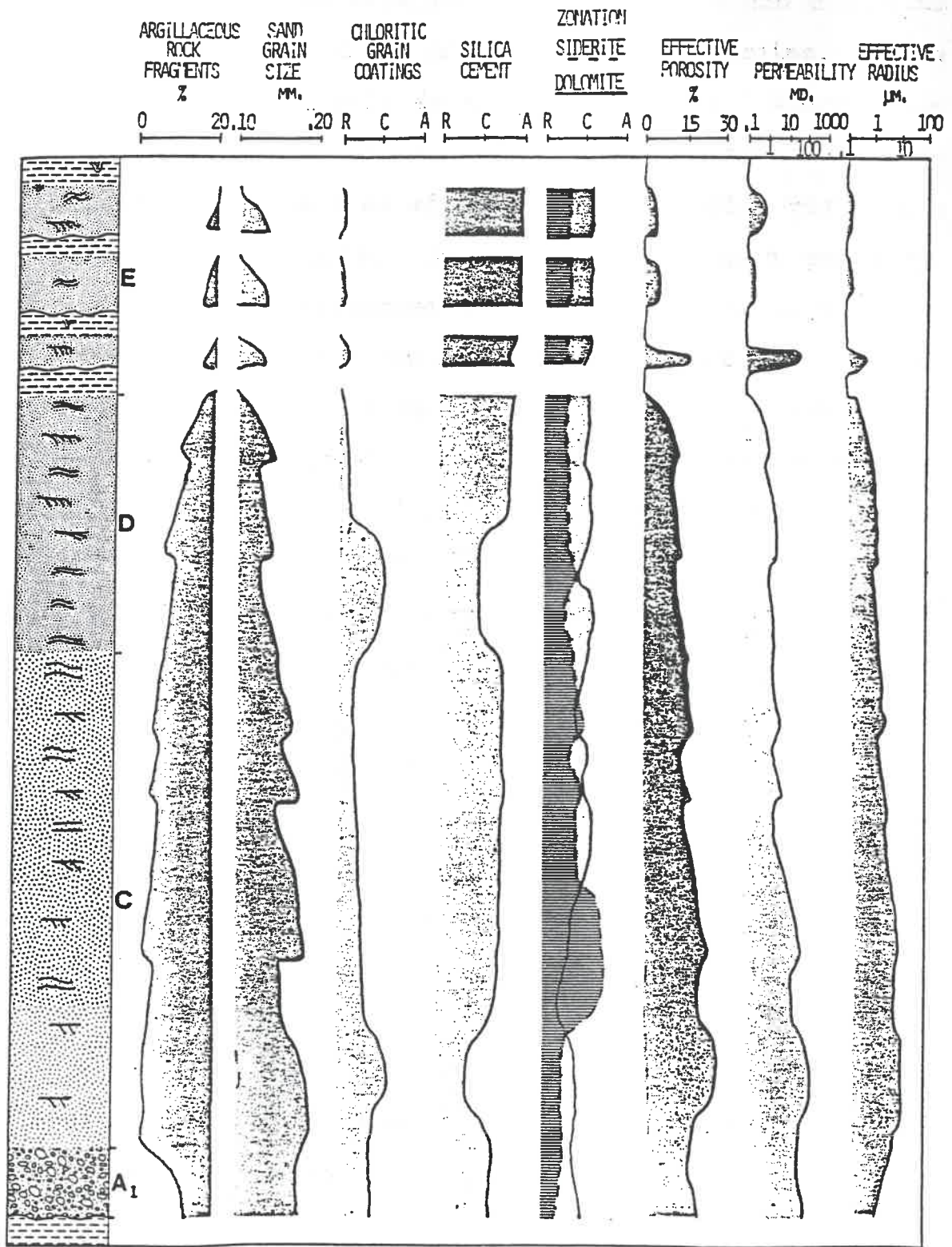
Figure 76. Idealized reservoir model for the Cherokee Group sandstones studied in this research.

coarser grained with rare soft rock fragments and micaceous partings. Because of chlorite coatings on grains, silica cements may not be well developed in places. Where these chlorite coatings occur, porosity, permeability, and effective radius will be less affected by diagenesis, yielding a high permeability zone. Another cause of high porosity, permeability, and effective pore throat radius is dissolution of feldspars, but this varies among sandstone bodies, rather than within individual ones. Minor variations in grain size in this lower portion favor the selective precipitation of siderite or dolomite-ankerite in the finer and coarser grained sandstones, respectively. Coarser grain size is always associated with larger effective pore throat radius in these sandstones and, consequently, with higher porosity and permeability. Kaolinite and carbonate cements are more common in the coarse sandstones, but, because of their patchy distribution and the initially larger pore throats of the coarse sandstones, the effect of these cements on porosity and permeability is not consistently great.

IMPLICATIONS for ENHANCED RECOVERY

The curves for porosity and permeability (Figure 76) are a generalized reflection of the uneven porosity and permeability profiles in a Cherokee Group sandstone reservoir. In general, a fluid will move more rapidly in the lower portion of the sequence and may form even faster

143

moving 'fingers' in thinner zones of relatively higher permeability. This will decrease the vertical sweep efficiency of reservoirs undergoing enhanced recovery processes, because the lower portion of the reservoir will be swept more thoroughly than the upper portion (Craig, 1971). Much of the oil remaining after water-flood may lie in the upper portion of Cherokee Group sandstone reservoirs. Because the upper portions of the reservoirs have lower porosities and permeabilities and have smaller pore throats than the lower portions of Cherokee Group sandstone reservoirs, an uneven sweep could result in injected fluids poorly, or even never, contacting the unrecovered oil in the upper part of the reservoir, while the lower part of the reservoir is more thoroughly swept (Craig, 1971). This problem may be compounded by the presence of several different fluids with differing viscosities, molecular sizes, shear strengths, and other mechanical properties because each fluid will behave differently in the rocks (Craig, 1971).

The ubiquitous presence of reduced iron in pyrite, siderite, ankerite, and chlorite in the sandstones may result in potentially damaging chemical reactions in the reservoir, unless the reduced iron and carbonate minerals in the reservoir are chemically stablized prior to and during injection of the acidic chemicals. For example, the precipitation of iron hydroxides ($Fe(OH)_3$) due to breakdown of reduced iron-rich minerals, particularly chlorite, may occur. The iron oxide precipitates could block pore throats

144

and halt or slow down fluid movement. According to Almon and Davies (1979, p. 390) the problem can be avoided if "an oxygen scavenger and an iron chelating agent are added to the acid, and care is taken to recover all the acid introduced into the well." Iron-rich calcite and dolomite-ankerite minerals in the reservoir may precipitate CaF_2 (fluorite) unless a chelating agent is used (Almon and Davies, 1979).

Another ubiquitous constituent in the sandstones is platy 'booklets' of kaolinite and, more locally, plate-like chlorite. Both of these clay minerals introduce very high surface areas on grains and in pores. Loss of expensive chemicals to adsorption on these clays may be a problem in the application of enhanced recovery techniques to Cherokee Group sandstones. This presents a paradox. Plate-like chlorite coatings on grains have inhibited subsequent quartz cementation and, therefore, have helped maintain higher porosities, permeabilities, and effective pore throat radii; but the loss of chemicals due to their contact with the great surface area in the chlorite could be counter-productive. In addition, changing the chemistry of the pore fluids or injecting fluids at high rates may cause these clays to become mobile. In a mobile state, the clays, especially kaolinite, could block pore throats and thereby exclude fluids from previously accessible pore volumes; and porosity, permeability, and pore throat radius could be reduced. These potentially mobile clays can be stabilized

by maintaining low flow rates in the reservoir or by using hydrolyzable metal salts as a clay stabilizer (Almon and Davies, 1978).

Another problem may exist with these clays. It was observed in thin sections that some oil was trapped in the micropores associated with kaolinite. This trapped oil is not recoverable without damaging the reservoir. Calculations of residual oil saturation may be too high because of this trapped oil. Similarly, water trapped in the micropores associated with kaolinite may affect calculations of water saturation especially in neutron density geophysical logs.

A generalized model of a Cherokee Group sandstone reservoir (Figure 76) has been presented as a result of this study, but caution must be emphasized in its application. The relatively complex mineralogy of Cherokee Group sandstones, and the resulting vertical heterogeneity recognized in the sandstones studied, means that one model for all producing fields or enhanced recovery candidates cannot represent all of the variations that may be encountered in different fields.

It is recommended that smaller scale studies of individual producing fields should be conducted to establish the potential problems in applying tertiary recovery processes to particular reservoirs with known residual petroleum. The observations resulting from this study should be a useful guide in conducting these more specific field studies.

by maintaining low flow rates in the reservoir or by using hydrolyzable metal salts as a clay stabilizer (Almon and Davies, 1978).

Another problem may exist with these clays. It was observed in thin sections that some oil was trapped in the micropores associated with kaolinite. This trapped oil is not recoverable without damaging the reservoir. Calculations of residual oil saturation may be too high because of this trapped oil. Similarly, water trapped in the micropores associated with kaolinite may affect calculations of water saturation especially in neutron density geophysical logs.

A generalized model of a Cherokee Group sandstone reservoir (Figure 76) has been presented as a result of this study, but caution must be emphasized in its application. The relatively complex mineralogy of Cherokee Group sandstones, and the resulting vertical heterogeneity recognized in the sandstones studied, means that one model for all producing fields or enhanced recovery candidates cannot represent all of the variations that may be encountered in different fields.

It is recommended that smaller scale studies of individual producing fields should be conducted to establish the potential problems in applying tertiary recovery processes to particular reservoirs with known residual petroleum. The observations resulting from this study should be a useful guide in conducting these more specific field studies.

CONCLUSIONS

1) Medium-to very fine-grained sandstones of the Cherokee Group in southeastern Kansas were deposited by unidirectional currents in continental channels resulting in sandstone deposits up to 35 meters (116 feet) thick. Five lithofacies have been established: A) conglomeratic sandstones subdivided into 1) thin basal and 2) thick sequence-capping conglomerates, B) stacked sandstones, C) crossbedded coarse sandstones, D) rippled fine sandstones, and E) interbedded sandstones, shales, and siltstones. Grain size of the sandstone sequences decreases upwards, accompanied by a decrease in scale of sedimentary structures and by increasing abundance of argillaceous rock fragments, micaceous partings, and silt.

2) Sandstone mineralogy does not vary significantly across the basin. Within an individual sandstone, however, the abundance of argillaceous rock fragments and micaceous partings increases upward. They are common in the interbedded sandstone-shale lithofacies.

3) The following diagenetic stages have been recognized:

Stage 1: Rare, localized precipitation of concretionary calcite and siderite cements in both sandstones and shales. Where these occur, porosity and permeability have been eliminated, resulting in no further diagenetic

147

alteration. These concretions were found in close association with thick shale interbeds in the sandstones.

Stage 2: Extensive chlorite coatings on grains and varying degrees of silica cementation. Chlorite coatings on grains have inhibited subsequent silica cementation and thereby preserved porosity and permeability. Silica cements in interbedded sandstone-shale sequences form an interlocking cement which, along with compaction of soft rock fragments and micas, reduce porosity and permeability. In coarse sandstone, silica cements occur as optically continuous, well developed subhedral to euhedral overgrowths on quartz and feldspar grains.

Stage 3: Patchy kaolinite, siderite, and dolomite-ankerite cements develop while feldspars, micas, and argillaceous rock fragments dissolve. It is likely that the dissolution of aluminosilicate grains and the alteration of smectitic to illitic clays during compaction of shales liberated the cations necessary for the precipitation of the cements.

4) The diagenetic sequence found in Cherokee Group sandstones in southeastern Kansas is similar to sequences found in sandstones of both similar and differing mineralogies deposited at about the same time in Oklahoma, north central Texas, England, and Poland.

5) Although the Cherokee Group sandstones in southeastern Kansas were deposited on a stable, shallow, cratonic plat-

148

form and buried up to depths of 1200 meters (4000 feet) where burial temperatures at the present geothermal gradient (1.75°C/100ft) could be expected to approach 70 degrees centigrade, the diagenetic sequence is very similar to those found in deeper (3500 meter), hotter (exceeding 150 degrees centigrade) Tertiary sandstones of the rapidly subsiding Gulf Coast. This suggests that either the influence of time and fluid composition was also important in the diagenesis of Cherokee Group sandstones or that the geothermal gradient was appreciably higher during the late Paleozoic Era (2.5-3.0°C/100ft).

6) Effective liquid porosities in Cherokee Group sandstones range from 5 to 28 percent. Liquid permeabilities range from 0 to 427 millidarcies. Effective pore throat radii range from 0.88 to 17 micrometers. Porosity and permeability increase with increasing effective pore radius.

7) Variations in porosity, permeability, and effective pore throat radius are related to grain size variations, sedimentary structures, abundance of soft rock fragments and micaceous partings, and assemblage and abundance of diagenetic minerals. Porosity, permeability, and effective radius increase with increasing grain size. Porosity, permeability, and effective radius are generally higher for large scale sedimentary structures than for small scale sedimentary structures. Porosity and permeability generally increase with decreasing amounts of pore-filling cements and

149

soft rock fragments. Effective pore throat radius does not appear to be affected by amounts of pore-filling cements and soft rock fragments.

8) A model is proposed for Cherokee Group sandstones which shows that coarser grain size, less cementation, and fewer argillaceous rock fragments are found in the coarse sandstone lithofacies in the lower portion of sandstone sequences and these are accompanied by higher porosity, permeability, and effective pore throat radius. This model should be helpful in evaluating these sandstones for enhanced recovery projects by providing both a method of study and a set of variables to investigate.

REFERENCES

Allen, J. R. L., and Banks, N. L., 1972, An interpretation and analysis of recumbent folded deformed cross-- bedding: Sedimentology, v. 19, p. 257-283.

Almon, W. R., and Davies, D. K., 1978, "Clay Technology and Well Stimulation", Gulf Coast Association of Geologists Society, Transactions, Vol. 28, pp. 1-6.

Almon, W. R., and Davies, D. K., 1979, Regional Diagenetic Trends in the Lower Cretaceous Muddy Sandstone, Powder River Basin, in Aspects of Diagenesis, SEPM Spec. Pub. No. 26, pp. 379-400.

Amyx, J. M., Bass, D. M., Jr., and Whiting, R. L., 1960, Petroleum Reservoir Engineering, Physical Properties: McGraw-Hill, New York, 610 p.

American Petroleum Institute RP 40, 1960, Recommended prac- tice for core analysis procedure.

American Petroleum Institute Code 27, 1952, Recommended practice for determining permeability of porous media.

Anderson, G., 1976, Coring and Core Analysis Handbook: Petroleum Publishing Co., Tulsa, 200 p.

Baker, D. R., 1962, Organic geochemistry of Cherokee Group in southeastern Kansas and northeastern Oklahoma: Am. Assoc. Petr. Geol. Bull., v. 46, p. 1621-1642.

Bass, N. W., 1936, Origin of the shoestring sands of Greenwood and Butler Counties, Kansas: Kansas Geol. Survey Bull. 23, 135 p.

Bennison, A. P., 1979, Mobile basin and shelf border area in northeast Oklahoma during Desmoinesian cyclic sedimen- tation, p. 283-294, in Hyne, N. J. (ed.), Pennsylvanian Sandstones of the Mid-Continent, Tulsa Geol. Soc. Spec. Pub. 1.

Berner, R. A., 1970, Sedimentary pyrite formation: Am. Jour. Sci., v. 268, p. 1-23.

Berner, R. A., 1980, Early Diagenesis, A Theoretical Approach, Princeton Univ. Press, Princeton, N.J., 241 p.

Berner, R. A., 1981, A new geochemical classification of sedimentary environments: Jour. Sed. Pet., v. 51, p. 359-365.

Berner, R. A., and Holdren, G. R., Jr., 1979, Mechanisms of feldspar weathering- II. Observations of feldspars from soils: Geochim. et Cosmochim. Acta, v. 43, p. 1173-1186.

Blatt, H., Middleton, G., and Murray, R., 1980, Origin of Sedimentary Rocks, 2nd ed.: Prentice-Hall, Inc., New Jersey, p. __??__ .

Boles, J. R., 1978, Active ankerite cementation in the sub- surface Eocene of southwest Texas: Contr. Min. and Petr., v. 68, p. 13-22.

Boles, J. R., and Franks, S. G., 1979, Clay diagenesis in Wilcox sandstones of southwest Texas: Implications of smectite diagenesis on sandstone cementation: J. Sed. Pet., v. 49, p. 55-70.

Brown, L. F., 1979, Deltaic sandstone facies of the Mid-Continent, p. 35-64 in Hyne, N. J. (ed.), Pennsylvanian Sandstones of the Mid-Continent, Tulsa Geol. Soc. Spec. Pub. 1.

Bucke, D. P., Jr., and Mankin, C. J., 1971, Clay-mineral diagenesis within interlaminated shales and sandstones: J. Sed. Pet., v. 41, p. 971-981.

Burggraf, D. R., Jr., White, H. J., and Lindsay, C. G., 1981, Part II: Facies and depositional Environments of the Cherokee Group in Webster County, Iowa, p. 23-49, in Lemish, J., Burggraf, D. R., Jr., and White, H. J. (eds.): Cherokee Sandstones and Related Facies of Central Iowa: An Examination of Tectonic Setting and Depositional Environments: Iowa Geol. Survey Guidebook Series 5.

Burst, J. F., 1969, Diagenesis of Gulf Coast clayey sedi- ments and its possible relation to petroleum migration: Am. Assoc. Petr. Geol. Bull., v. 53, p. 73-93.

Busch, D. A., 1959, Prospecting for stratigraphic traps: Am. Assoc. Petr. Geol. Bull., v. 43, p. 2829-2843.

Busenberg, R. A., and Clemency, C. V., 1976, The dissolution kinetics of feldspars at 25 C and 1 atm CO partial pressure: Geochim. et Cosmochim. Acta, v. 40, p. 41-50.

Cecil, C. B., and Heald, M. T., 1967, Experimental investi- gation of effects of coatings on quartz growths (abs.): Am. Assoc. Petr. Geol. Bull., v. 51, p. 457.

Charles, H. H., 1941, Bush City Oil Field, Anderson County, Kansas, p. 43-56, in Levorsen, A. I. (ed.), Stratigraphic Type Oil Fields: Am. Assoc. Petr. Geol., 902 p.

Chenoweth, P. A., 1979, Geological prospecting for Mid-Continent sandstones, p. 13-34: in Pennsylvanian Sandstones of the Mid-Continent, Tulsa Geol. Soc. Spec. Pub. 1.

Choquette, P. W., and Pray, L. C., 1970, Geologic nomenclature and classification of porosity in sedimentary carbonates: Am. Assoc. Petr. Geol., v. 54, p. 207-250.

Craig, F. F., Jr., 1971, The Reservoir Engineering Aspects of Waterflooding, SPE Monograph No. 3, 134 pp.

Crowell, J. C., 1978, Gondwanan glaciation, cyclothems, continental positioning, and climate change: Am. Jour. Sci., v. 278, p. 1345-1372.

Curtis, C. D., 1978, Possible links between sandstone diagenesis and depth-related geochemical reactions occurring in enclosing mudstones, Journal of the Geol. Soc. London, v. 135, p. 107-117.

Dapples, E. C., 1979, Diagenesis of sandstones, p. 31-98: in Larson, G., and Chilingar, G. V. (eds.), Diagenesis in sediments and sedimentary rocks, Developments in Sedimentology, v. 25A, Elsevier.

Dickson, J. A., 1966, Carbonate identification and genesis as revealed by staining: J. Sed. Pet., v. 36, p. 491-505.

Dillard, W. R., Oak, D. P., and Bass, N. W., 1941, Chanute Oil Pool, Neosho County, Kansas- a waterflooding operation, p. 57-77: in Levorsen, A. I., (ed.), Stratigraphic Type Oil Fields: Am. Assoc. Petr. Geol., 902 p.

Ebanks, W. J., Jr., 1975, Kansas Oil for Enhanced Recovery-A Resource Appraisal: Tertiary Oil Recovery Project Contribution 1, 31 p.

Ebanks, W. J., Jr., 1979, Correlation of Cherokee (Desmoinesian) sandstones of the Missouri-Kansas-Oklahoma Tri-State Area, p. 295-312: in Hyne, N. J. (ed.), Pennsylvanian Sandstones of the Mid-Continent, Tulsa Geol. Soc. Spec. Pub. 1.

153

Ebanks, W. J., Jr., and James, G. W., 1974, Heavy-crude oil bearing sandstones of the Cherokee Group (Desmoinesian) in southeastern Kansas: in Canadian Society of Petroleum Geol., Memoir 3, Oil Sands, Fuel of the Future, p. 19-34.

Ebanks, W. J., Jr, James, G. W., and Livingston, N. D., 1977, Evaluation of Heavy Oil and Tar Sands in Bourbon, Crawford, and Cherokee Counties, Kansas-Final Report: Bartlesville Energy Research Center, Report of Investigation 77/20, 110 p.

Folk, R. L., 1974, Petrology of Sedimentary Rocks: Hemphilli, Austin, Texas, 170 p.

Fothergill, C. A., 1955, The cementation of oil reservoir sands and its origin: in Proceedings of the 4th World Petroleum Congress, p. 300-312.

Garrels, R. M., and Christ, C. L., 1965, Solutions, Minerals, and Equilibria: Harper and Row, New York, 450 p.

Garrels, R. M., and Howard, P., 1957, Reactions of feldspar and mica with water at low temperature and pressure: Clays and Clay Mineralogy, v. 6, p. 68-88.

Gould, G. F., 1975, Maturation and alteration of crude oils in the Cherokee Group (Middle Pennsylvanian) of southeastern Kansas: unpub. M. S. thesis, Kansas Univ.

Green, J. C., 1977, Keweenawan plateau volcanism in the Lake Superior region: in Baragar, W. R. A., Coleman, L. C., and Hall, J. M. (eds.), Volcanic Regimes in Canada: Geol. Assoc. Can. Spec. Paper 16, p. 407-422.

Grim, R. E., 1968, Clay Mineralogy, McGraw-Hill, New York, 596 pp.

Ham, W. E., and Wilson, J. L., 1967, Paleozoic epeirogeny and orogeny in the central United States: Am. Jour. Sci., v. 256, p. 322-407.

Harms, J. C., Southard, J. B., Spearing, D. R., and Walker, R. G., 1975, Depositional environments as interpreted from primary sedimentary structures and stratification sequences: SEPM Short Course 2, 161 p.

Hawkins, P. J., 1978, Relationship between diagenesis, porosity reduction, and oil emplacement in Late Carboniferous sandstones reservoirs, Bothamsall Oilfield, E. Midlands: Jour. Geol. Soc. London, v. 135, p. 7-24.

Hayes, M. O., 1963, Petrology of Krebs Subgroup (Pennsylvanian, Desmoinesian) of western Missouri: Am. Assoc. Petr. Geol. Bull., v. 47, p. 1537-1551.

Heald, M. T., 1965, Lithification of sandstones in West Virginia: West Virginia Geological and Economic Survey Bull., v. 30, 28 p.

Heald, M. T., and Larese, R. E., 1973, The significance of the solution of feldspar in porosity development: Jour. Sed. Pet., v. 43, p. 458-460.

Heald, M. T., and Larese, R. E., 1974, Influence of coatings on quartz cementation: Jour. Sed. Pet., v. 44, p. 1269-1274.

Heckel, P. H., 1977, Origin of phosphatic black shale in Pennsylvanian cyclothems of mid-continent North America: Am. Assoc. Petr. Geol. Bull., v. 61, p. 1045-1068.

Helgeson, H. C., 1971, Kinetics of mass transfer among silicates an aqueous solutions: Geochim. et Cosmochim. Acta, v. 40, p. 41-50.

Howe, W. B., 1956, Stratigraphy of pre-Marmaton Desmoinesian (Cherokee) rocks in southeastern Kansas: Kansas Geol. Survey Bull., v. 123, 132 p.

Hower, W. F., 1974, Influence of Clays on the Production of Hydrocarbons, SPE 4785, 11 pp.

Hower, J., Eslinger, E. V., Hower, M. E., and Perry, E. A., 1976, Mechanism of burial metamorphism of argillaceous sediment: 1. Mineralogical and chemical evidence: Geol. Soc. Amer. Bull., v. 87, p. 727-737.

Hulse, W. J., 1978, A geologic study of the Sallyards Field area, Greenwood County, Kansas: unpub. M. S. thesis, Kansas University, 152 p.

Jewett, J. M., 1954, Oil and gas in eastern Kansas: Kansas Geol. Survey Bull., v. 104, 397 p.

Jewett, J. M., 1959, Graphic column and classification of rocks in Kansas: Kansas Geol. Survey, chart.

Johnson, C. T., 1973, Environment of deposition of the Pennsylvanian Bartlesville sandstone, Labette County, Kansas: unpub. M. S. thesis, Texas A and M University, 72 p.

Jordan, L., 1957, Subsurface stratigraphic names of Oklahoma: Okla. Geol. Survey Guide Book VI.

Keller, W. D., 1970, Environmental aspects of clay minerals: Jour. Sed. Pet., v. 40, p. 788-813.

Kluth, C. F., and Coney, P. J., 1981, Plate tectonics of the Ancestral Rocky Mountains: Geology, v. 9, p. 10-15.

Krumbein, W. C., 1934, Size frequency distribution of sediments: Jour. Sed. Pet., v. 4, p. 65-77.

Lagache, M., 1976, New data on the kinetics of the dissolution of alkali feldspars at 200 C in CO charged water: Geochim et Cosmochim. Acta, v. 40, p. 157-161.

Lahann, R. W., 1980, Smectite diagenesis and sandstone cement: the effect of reaction temperature: Jour. Sed. Pet., v. 50, p. 755-760.

Land, L. S., and Dutton, S. P., 1978, Cementation of a Pennsylvanian deltaic sandstone: isotopic data: Jour. Sed. Pet., v. 48, p. 1167-1176.

Land, L. S., and Milliken, K., 1981, Feldspar diagenesis in the Frio Formation, Brazoria County, Texas Gulf Coast: Geology, v. 9, p. 314-318.

Law, J., 1944, Statistical approach to the interstitial heterogeneity of sand reservoirs: Trans. Am. Instit. Metall. Engineers, v. 155, p. 202-222.

Levorsen, A. I., 1973, Geology of Petroleum, 2nd ed.: Freeman and Co., Sand Francisco, 724 p.

Loucks, R. G., Bebout, D. G., and Galloway, W. E., 1977, Relationships of porosity formation and preservation to sandstone consolidation history- Gulf Coast lower Tertiary Frio Formation: Texas Univ. Bur. Econ. Geology Geol. Circ. 77-5, 12 p.

Marafa, H. Y., 1980, A study of the relationships between porosity, permeability, dispersion, pore size distribution, and sedimentary structures for two sandstone bodies: unpub. M. S. thesis, Kansas University, 133 p.

McKee, E. D., and Oriel, S. S., 1967, Paleotectonic maps of the Permian System: U. S. Geological Survey Miscellaneous Geological Investigations Map I-450, 164 p.

McMillan, N. J., 1956, Petrology of the nodaway underclay (Pennsylvanian), Kansas: Kansas Geol. Survey Bull., v. 119, no. 6, p. 187-249.

McQuillan, M. W., 1968, Geology of the Davis-Bronson Pool, Allen and Bourbon Counties, Kansas: unpub. M. S. thesis, Kansas State Univ., 117 p.

Milliken, K. L., Land L. S., and Loucks, R. G., 1981, History of burial diagenesis determined from isotopic geochemistry, Frio Formation, Brazoria County, Texas: Am. Assoc. Petr. Geol. Bull., v. 65, p. 1397-1413.

Millot, G., 1970, Geology of Clays: Springer-Verlag, New York, 388 p.

Oros, M., 1979, 25 year update to Oil and Gas in Eastern Kansas by J. M. Jewett: Kansas Geol. Survey Bull. 104 Reprint.

Paces, T., 1973, Steady-state kinetics and equilibrium between groundwater and granitic rocks: Geochim. et Cosmochim. Acta, v. 37, p. 2641-2663.

Perry, E. A., Jr., and Hower, J., 1970, Burial diagenesis in Gulf Coast pelitic sediments: Clays and Clay Minerals, v. 18, p. 165-177.

Petrovic, R., 1976, Rate control in fledspar dissolution-II. The protective effect of precipitates: Geochim. et Cosmochim. Acta, v. 40, p. 1509-1522.

Pettijohn, F. J., Potter, P. E., and Siever, R., 1972, Sands and Sandstones: Springer-Verlag, Heidelberg, Germany, 618 p.

Pittman, E. D., 1971, Plagioclase feldspar as an indicator of provenance in sedimentary rocks: Jour. Sed. Pet., v. 40, p. 591-598.

Pittman, E. D., 1979, Porosity, diagenesis, and productive capability of sandstone reservoirs, p. 159-174: in Scholle, P. A., and Schluger, P. R. (eds.), Aspects of Diagenesis, Society of Economic Paleontologists and Mineralogists Special Publication no. 26.

Pittman, E. D., and Lumsden, D. N., 1968, Relationships between chlorite coatings on quartz grains and porosity, Spiro Sand, Oklahoma: Jour. Sed. Pet., v. 38, p. 668-670.

Potter, P. E., and Glass, H. D., 1958, Petrology and sedimentation of the Pennsylvanian sediments in southern Illinois, a vertical profile: Ill. State Geol. Survey Rept. Invest. 204, 60 p.

Reineck, H. E., and Singh, I. B., 1975, Depositional Sedimentary Environments: Springer-Verlag, New York, 439 p.

157

Rex, R. W., 1966, Authigenic kaolinite and mica as evidence for phase equilibria at low temperatures: Clays and Clay Minerals, v. 13, p. 95-105.

Rich, J. L., 1923, Shoestring sands of eastern Kansas: Am. Assoc. Petr. Geol. Bull., v. 7, p. 103-113.

Scheidegger, A. E., 1960, The Physics of Flow Through Porous Media: MacMillan Co., New York, 236 p.

Schmidt, V., and MacDonald, D. A., 1979, Secondary reservoir porosity in the course of sandstone diagenesis: AAPG Continuing Education Course Note Series 12, 125 p.

Shelton, J. W., 1964, Authigenic kaolinite in sandstone: Jour. Sed. Pet., v. 34, p. 102-111.

Taylor, J. M., 1950, Pore-space reduction in sandstones: Am. Assoc. Petr. Geol. Bull., v. 34, p. 701-716.

Teisseyre, A. K., 1973, Diagenetic carbonization due to kaolinization: A hypothesis (with examples from Sudetic Carboniferous Sandstones): Rocznik Polskiego Towarzystwa Geologicznego, v. 43, p. 453-487.

Van Dyke, R. J., 1975, Geology and depositional environments of the reservoir sandstone, Kincaid oil field, Anderson County, Kansas: unpub. M. S. thesis, Kansas University, 81 p.

van Eysinga, F. W. B. (compiler), 1978, Geologic Time Table, 3rd edition, Elsevier, Amsterdam.

Van Schmus, W. R., and Bickford, M. E., 1981, Proterozoic chronology and evolution of the mid-continent region, North America, p. 261-296 in Kroner, A. (ed.) Precambrian Plate Tectonics, Elsevier, Amsterdam.

Visher, G. S., Saitta, B. S., and Phares, R. S., 1971, Pennsylvanian delta patterns and petroleum occurrences in eastern Oklahoma: Am. Assoc. Petr. Geol. Bull., v. 55, p. 1206-1230.

Weirich, T.E., 1953, Shelf principle of oil origin, migration, and accumulation: Am. Assoc. Petr. Geol. Bull., v. 37, p. 2027-2045.

Wilson, M. D., and Pittman, E. D., 1977, Authigenic clays in sandstones: recognition and influence on reservoir properties and paleoenvironmental analysis: Jour. Sed. Pet., v. 47, p. 3-31.

Wollast, R. A., 1967, Kinetics of the alteration of K-feldspar in buffered solutions at low temperature: Geochim. et Cosmochim. Acta, v. 31, p. 635-648.

Zeller, D. E. (ed.), 1968, The Stratigraphic succession in Kansas: Kansas State Geol. Survey Bull. 189, 81 p.

Ziegler, A. M., Scotese, C. R., McKerrow, W. S., Johnson, M. E., and Bambach, R. K., 1979, Paleozoic paleogeography: Ann. Rev. Earth Planet. Sci., v. 7, p. 473-502.

Appendix A. Laboratory Methods

This appendix is a description of the laboratory procedures for determining effective liquid porosity, liquid and gas permeability, and pore size distribution as reported in this research. Samples of Cherokee Group sandstones with different sedimentary structures, grain sizes, and mineralogies were tested.

A. Plug Preparation

Plugs were cut from core samples using a tungsten carbide rotary cutter mounted on a drill press. The rough ends of the plugs were removed to form a right cylinder. A brine solution of 20,000 parts per million NaCl was used as a coolant. This brine solution was chosen to represent reservoir fluid as determined by Cherokee sandstone oil field brine data available at the Kansas Geological Survey. It is believed the use of simulated reservoir brines avoids damage to water-sensitive clays in the samples.

The samples were then placed in a soxhlet extraction device to remove hydrocarbons. The extraction device circulates a solvent, heated to approximately 95 degrees centigrade, over the samples by cyclically filling the device, soaking the samples, removing the solvent and extracted hydrocarbons, then refilling the device with clean solvent again. Each cycle lasts about 10 minutes and the samples are cleaned for approximately 24 hours. Because the

hydrocarbons in some of the samples were difficult to remove, those samples were left in the extraction device for several days. Standard laboratories use toluene as the extracting solvent, but because of the heavy oils in many of the sandstones studied, a more effective (but toxic) solvent, tetrahydronaphthalene, was employed. The extraction operation was always conducted under a fume hood.

Following extraction of the hydrocarbons, the samples were placed in an oven set at 100 degrees centigrade for 24 hours to dry the samples and remove any remaining solvent. After drying the samples, they were placed in a desiccator and allowed to cool.

Once the samples were cool, six measurements of the diameter of the plugs, three on each side spaced 120 degrees apart, and four measurements of the length spaced 90 degrees apart were made. The averages of these measurements were used to calculate the average length, average diameter, area, and bulk volume of each sample as show in equations 1, 2, 3, and 4 in figure A-1.

B. Determination of Effective Liquid Porosity

Porosity was determined using the liquid saturation technique which "consists of saturating a clean, dry sample with a fluid of known density and determining the pore volume from the gain in weight of the sample" (Amyx, Bass, and Whiting, 1960, p. 52). First the dry weight of each

$$\text{(1)} \qquad l_{ave} = \frac{\sum\limits_{i=1}^{4} l_i}{4} \qquad \text{(length, l, in cm)}$$

$$\text{(2)} \qquad d_{ave} = \frac{\sum\limits_{i=1}^{6} d_i}{6} \qquad \text{(diameter, d, in cm)}$$

$$\text{(3)} \qquad \text{area} = \frac{\pi}{4} \cdot (d_{ave})^2 \qquad (cm^2)$$

$$\text{(4)} \qquad \text{bulk volume (BV)} = \text{area} \cdot l_{ave} \qquad (cm^3)$$

$$\text{(5)} \qquad \text{fluid weight (gms)} = \text{saturated sample weight} - \text{dry sample weight}$$

$$\text{(6)} \qquad \text{void volume } (cm^3) = \frac{\text{fluid weight}}{\text{fluid density}} \quad \frac{\text{(gm)}}{(gm/cm^3)}$$

$$\text{(7)} \qquad \text{porosity } (\%) = \frac{\text{void volume}}{\text{bulk volume}}$$

Figure A-1.   Calculation of effective liquid porosity.

plug was measured. Then the plugs were placed in an Erlenmeyer flask which was sealed with a rubber stopper that had two glass tubes connecting the flask to a brine reservoir and a vacuum pump. The brine filled reservoir was connected to the tube by a leak-proof valve which was initially closed to the flask. The dry samples in the flask were evacuated by a vacuum pump overnight and allowed to achieve a minimum vacuum of 200 Torr. (0.26 atm.). The vacuum line was then closed to the flask containing the samples by a valve and the vacuum pump was turned off. The flask containing the plugs, which was now under a vacuum, was then opened to the brine reservoir and brine was allowed to cover the samples completely but the system was not allowed to contact atmospheric pressure. The samples, still under a vacuum, were then saturated with the brine. The flask and samples were kept closed under the vacuum for at least 15 minutes following the initial saturation. The samples were then kept immersed in the brine and the saturated weight of each sample was determined taking care to remove all free moisture from the surface of each sample. The difference in the saturated sample weight and dry sample weight was determined and represents the weight of fluid in the saturated sample (equation 5 of figure A-1). Division of the fluid weight by the known density of the brine yields the void volume (equation 6 of figure A-1). Effective liquid porosity was determined by dividing the void volume by the bulk volume (equation 7 of figure A-1).

C. Determination of Permeability

   1. Liquid Permeability

   Liquid permeabilities were determined for samples using
the Ruska liquid permeameter available in the Tertiary Oil
Recovery Project Laboratory and shown schematically in
figure A-2. The procedure was as follows: The saturated
plug was placed in a tight fitting rubber sleeve which was
then fitted in a stainless steel coreholder and mounted on
the permeameter as shown in figure A-2. Next the burette
was filled with the 20,000 ppm brine from a reservoir to a
point above the upper timing mark. This also floods the
coreholder. The valve connecting the reservoir to the
permeameter was then closed to prevent the flow of fluid
back into the reservoir. The pressure gauge was then set to
1.5 atmospheres (the net difference in pressure). The pres-
sure was provided by a pressured air source in the labora-
tory and regulated by the permeameter to maintain constant
pressure. The pressured air is then allowed to enter the
top of the burette and the time necessary for the liquid to
pass through the core plug was measured between two index
marks ten cubic centimeters apart. This procedure was
followed three times for each plug yielding three time
values, which were averaged. The calculation of permeabil-
ity is shown in figure A-3. The time necessary to flow 10
cc of brine through a plug ranged from a few seconds for
very permeable samples to hours for samples with low perme-
abilities.

FILLING   OPERATION
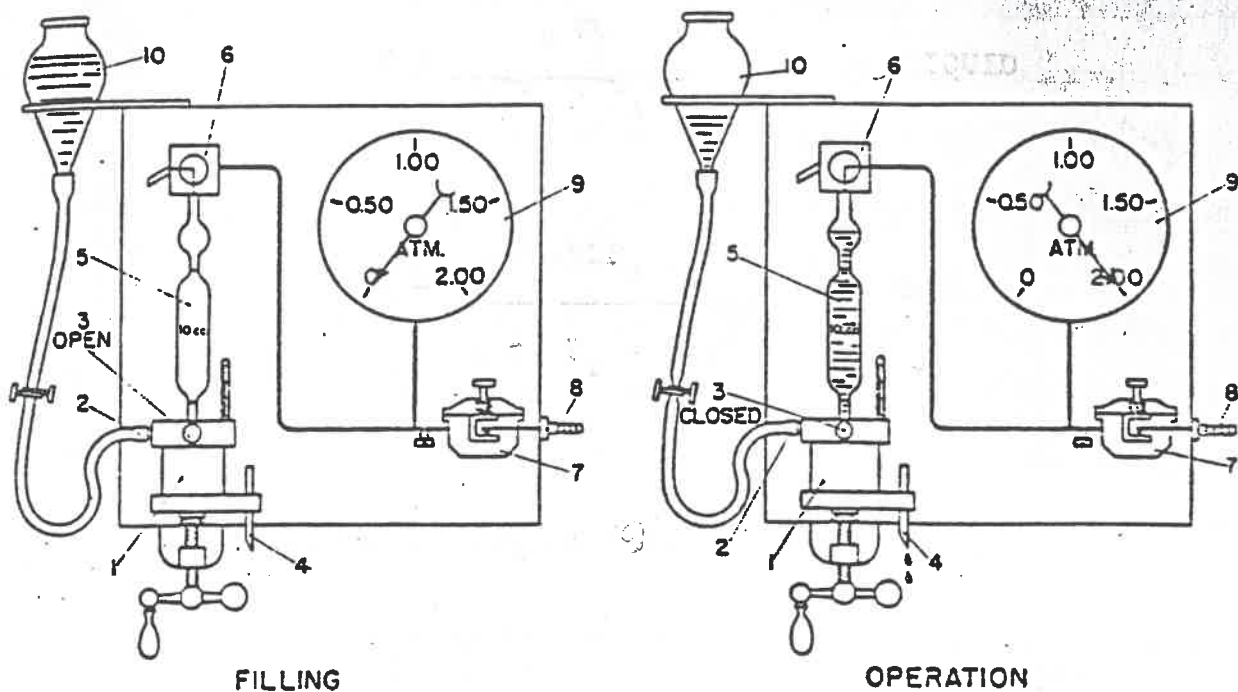
Figure 13:   Liquid Permeameter.

1.   Coreholder with built-in thermometer
2.   Fill connection
3.   Cut-off valve
4.   Flow tube
5.   Burette
6.   Discharge-fill valve
7.   Pressure regulator and gas line connector
8.   Pressure tube
9.   Pressure gauge
10.   Brine reservoir

Figure A-2.   Schematic diagram of the Ruska permeameter used in permeability determinations.

$$K = \frac{\mu VL}{A(P_i - P_o)t} \qquad \text{LIQUID}$$

$$K = \frac{2 \mu VLP_o}{A t (P_i - P_o)^2} \qquad \text{GAS}$$

K is permeability in millidarcies

μ is the viscosity of the fluid
(1.0 cp for brine; 0.017 cp for nitrogen gas)

V is the volume of fluid flowed through the sample
(in cc)

A is the area of the plug (in cm^2)

t is the average time (if three) to flow volume (V)
of fluid through the plug

P_i entry pressure of the fluid (in atm)

P_o exit pressure of the fluid (in atm)

L is the average length of the plug (in cm)

Figure A-3. Liquid and gas permeability calculations.

2. Gas Permeability

Nine of the samples chosen for permeability measurements were impermeable to the brine at the permeameter flow pressures. These samples were removed from the brine solution and dried for 24 hours in a 100 degree centigrade oven and then cooled in a desiccator.

A procedure similar to the liquid permeability determination was followed with the major difference being that nitrogen gas, rather than brine, was the fluid used for the measurement. Because the fluid used in the gas permeability technique was a gas rather than a liquid, Boyle's Law applies and the formula is slightly different as shown in figure A-3. Gas permeabilities were corrected for the Klinkenberg effect using the chart on page 95 in Amyx, Bass, and Whiting (1960). This correction accounts for gas slippage effects in the pores of the samples.

D. Pore Size Distribution

Pore size distributions were determined for 16 Cherokee Group sandstone samples using the mercury porosimeter available in the Tertiary Oil Recovery Project Laboratory at the University of Kansas. Following the measurement of liquid permeabilities, the plugs were dried in a 100 degree centigrade oven for 24 hours and placed in a desiccator to cool. Marafa (1980, p. 38-41) described the equipment used to measure the pore size distribution.

Briefly, the technique involves taking a series of measurements of the change in volume of mercury in a sample at increasing pressures from 0 to 2000 psi absolute. Changes in volume are measured from a vernier scale attached to a piston displacement device. The calculations for determining pore size distribution are as follows (also see figure A-4): The change in volume at a new pressure is determined by subtracting the initial volume from the new volume. This change in volume is divided by the total volume. Total volume is obtained by subtracting the initial volume from the final volume. This procedure is followed at each increment in pressure recorded. Above atmospheric pressure a correction factor, obtained by calibration of the porosimeter and the known compressibility of nitrogen gas, is included to account for the compressibility of nitrogen gas used to force mercury into the sample. A plot is made of the logarithm of the pressure versus the saturation of the wetting phase, air. Saturation of the wetting phase is one minus mercury saturation. Mercury saturation is determined by dividing the change in volume at a given pressure by the total volume. An interpolated curve is drawn between the points on the plot. In all but one sample, this curve had a distinct point at which the slope flattened. The pressure at this point represents the breakthrough pressure at which mercury passes through most of the pore throats and into the adjoining pores. From this pressure the pore throat radius at initial breakthrough, mean controlling

Total Volume, V_t = Final Chamber Volume - Initial Chamber Volume

Apparent Change in Volume, V_a = Chamber Volume - Initial Chamber Volume

Real or Actual Change in Volume, $V_r = V_a$ - Nitrogen Compressibility Correction, V_c

Saturation of Non-Wetting Phase, Mercury, $S_{Hg} = \dfrac{V_r}{V_t}$

Saturation of Wetting Phase, $S_w = 1.0 - S_{Hg}$

Plot log P vs. S_w

Effective Pore Throat Radius, $r_e = \dfrac{2\sigma \cos \theta}{P}$

σ is the interfacial tension of mercury (480 dynes/cm)

θ is the contact angle of mercury against the solid (140°)

P   is the pressure at breakthrough

Figure A-4. Pore size distribution calculations.

radius, or effective pore radius can be calculated using the capillary curve equation from Purcell (1949) (figure A-4). This is the effective pore radius discussed in this text.

APPENDIX B
CORE DESCRIPTIONS

EXPLANATION of SYMBOLS USED in CORE DESCRIPTIONS

■ porosity datum

● permeability datum

▲ effective pore throat radius datum

○ horizontal burrows

ᴜ vertical burrows

∾ contorted bedding

C   coal

CB   clay balls

CC   calcite cement

CF   coal fragments

CL   clasts

DC   dolomite cement

EC   erosional contact

F   fossils

KC   kaolinite cement

OS   oil stained

PC   pyrite cement

PF   plant fragments

RM   root mottled

SC   siderite cement

TS   thin section

SEDIMENTARY STRUCTURES

Large Scale Crossbeds

H∠   high angle

L∠   low angle

HNP   horizontal nonplanar

HP   horizontal planar

R   ripples

Small Scale Crossbeds

L∠   low angle

R   ripples

CR   climbing ripples

L   laminar

WELL NAME: **Conoco J. Ord 47**

COUNTY: **Labette**   LOCATION: **35-32S-17E**

GRAIN SIZE — coarse to fine

SEDIMENTARY STRUCTURES

LITHO-FACIES

OTHER

DEPTH

EFFECTIVE LIQUID POROSITY %

LIQUID PERMEABILITY, md
EFFECTIVE PORE THROAT RADIUS, µm

SCALES
LARGE / SMALL
SAND vc c m f vf

DEPTH:
top 670
680
690
700
710
720
730
bottom

Litho-facies: D, B, D, B, D, B, A, E

Other: SC, TS, EC, EC, CL EC, TS, DC CB SC, TS, CL DC, CL, CL DC, CL EC, TS

WELL NAME: **Conoco J. Ord 34**   LOCATION: **26-32S-17E**

COUNTY: **Labette**

GRAIN SIZE — SEDIMENTARY STRUCTURES coarse to fine — LITHO-FACIES — OTHER — DEPTH — EFFECTIVE LIQUID POROSITY % — LIQUID PERMEABILITY, md — EFFECTIVE PORE THROAT RADIUS, μm

SCALES — LARGE — SMALL — SAND — vc c m f vf

Depth: 120, 130, 140, 150, 160, 170, 180, bottom

Porosity scale: 0 10 20 30 40
Permeability/pore throat scale: 0.1 0.5 1.0 5.0 10 50 100 500 1000

Other column labels: EC, SC, ∨, SC, ∨, SC, ∨, EC, OS, TS, OS, OS, ?clast?, OS, TS, EC, CV, ∨, ∨

Lithofacies: E, A, E

WELL NAME: Tenneco Bradley 8   LOCATION: 11-35S-21E

COUNTY: Labette

WELL NAME: **Tenneco Bradley 8**

COUNTY: **Labette**   LOCATION: **11-35S-21E**

WELL NAME: __K.G.S. Tar Sands N__

COUNTY: __Crawford__   LOCATION: __34-29S-24E__

GRAIN SIZE
SEDIMENTARY STRUCTURES coarse to fine.
LITHO-FACIES
OTHER
DEPTH
EFFECTIVE LIQUID POROSITY %
EFFECTIVE PORE THROAT RADIUS, μm
LIQUID PERMEABILITY, md

WELL NAME: **K.G.S. Tar Sands C**

COUNTY: **Bourbon**   LOCATION: **10-26S-25E**

WELL NAME: M.C. Colt 14AO Johnson   LOCATION: **33-24S-21E**

COUNTY: **Allen**

WELL NAME: **Tesoro W-35 Baker**

COUNTY: **Neosho**   LOCATION: **26-28S-19E**

GRAIN SIZE

SEDIMENTARY STRUCTURES
coarse to fine

LITHO-FACIES

OTHER

DEPTH

EFFECTIVE LIQUID POROSITY %

LIQUID PERMEABILITY, md
EFFECTIVE PORE THROAT RADIUS, µm

SCALES

SAND
vc c m f vf

LARGE
SMALL

1000
500
100
50
10
5.0
1.0
0.5
0.1

0 10 20 30 40

top
840
bottom 850
top
910
920
930
940
950
960
970
continued on next page

TS
TS
EC?
TS
TS
TS
TS
TS

CC
OS
CF
PC
V
V
V
SC
SC
PF
OS
CF
CF
CF
CF
CF

E

E

WELL NAME: **M.C. Colt 18AO Keown**

COUNTY: ___Allen___   LOCATION: ___22-23S-18E___

Based on open-file core description at the Kansas Geological Survey

WELL NAME: **M.C. Colt 18AO Keown**

COUNTY: **Allen**   LOCATION: **22-23S-18E**

\# Based on open-file core description at the Kansas Geological Survey

WELL NAME: M.C. Colt 18AO Keown

COUNTY: Allen   LOCATION: 22-23S-18E

\# Based on open-file core description at the Kansas Geological Survey

WELL NAME: **Brazos 0-5 Pierpoint**

COUNTY: **Wilson**   LOCATION: **9-28S-15E**

WELL NAME: M.C. Colt 22AO Lauber   LOCATION: 23-26S-14E

COUNTY: Woodson

WELL NAME: **Phillips Demalorie 30AW**

COUNTY: **Greenwood**   LOCATION: **32-22S-11E**

WELL NAME: **Phillips Demalorie 33AW**

COUNTY: **Greenwood**   LOCATION: **32-22S-11E**

EFFECTIVE LIQUID POROSITY %

LIQUID PERMEABILITY, md

EFFECTIVE PORE THROAT RADIUS, μm

GRAIN SIZE · coarse to fine

SEDIMENTARY STRUCTURES

LITHO-FACIES

OTHER

DEPTH

1000
500
100
50 10
5.0
1.0
0.5
0.1

0 10 20 30 40

top 1950

1960 bottom

CF
SC
CF

E

D

SCALES

SAND
vc c m f vf

LARGE
SMALL

WELL NAME: **Phillips Demalorie 13AW**

COUNTY: **Greenwood**   LOCATION: **32-22S-11E**

WELL NAME: **Jackson Bros. Barrier 36**

COUNTY: **Greenwood**   LOCATION: **3-26S-8E**

Porosity and permeability data from Marafa (1979)
Core also described by Hulse (1978)

GRAIN SIZE coarse to fine | SEDIMENTARY STRUCTURES | LITHO-FACIES | OTHER | DEPTH | EFFECTIVE LIQUID POROSITY % | LIQUID PERMEABILITY, md — EFFECTIVE PORE THROAT RADIUS, μm

Porosity scale: 0 10 20 30 40

Permeability / pore throat radius scale: 0.1 0.5 1.0 5.0 10 50 100 500 1000

Depth markers: top — 3050 — 3060 — bottom

Lithofacies column:
- D sc TS-
- D sc cf TS-
- C TS-
- C dc TS
- C dc cf TS-

WELL NAME: **Phillips Lena 1**   LOCATION: **17-32S-5E**

COUNTY: **Cowley**

GRAIN SIZE — coarse to fine

SEDIMENTARY STRUCTURES

LITHO-FACIES

OTHER

DEPTH

EFFECTIVE LIQUID POROSITY %

LIQUID PERMEABILITY, md

EFFECTIVE PORE THROAT RADIUS, μm

SCALES
LARGE | SMALL

SAND
vc c m f vf

Porosity axis: 0 10 20 30 40
Permeability / pore throat axis: 0.1 0.5 1.0 5 10 50 100 500 1000

Depth markers:
top
3420
3430
3440
bottom

Lithofacies:
E
D

Other column labels:
TS
SC
PF
SC
TS
missing core
SC
PF
TS
TS
PF
DC
TS

WELL NAME: Sinclair Weir 1

COUNTY: Cowley   LOCATION: 30-34S-3E

WELL NAME: **Jackson Bros. Crew 21**

COUNTY: **Greenwood**   LOCATION: **3-26S-8E**

Core also described by Hulse (1978)

WELL NAME: **Phillips Lena 1**   LOCATION: **17-32S-5E**

COUNTY: **Cowley**

LIQUID PERMEABILITY, md
EFFECTIVE PORE THROAT RADIUS, μm

1000
500
100
50
10
5.0
1.0
0.5
0.1

EFFECTIVE LIQUID POROSITY %
0 10 20 30 40

DEPTH

top
3420
3430
3440
bottom

OTHER

TS-
TS-
TS-
TS-
TS-

SC
PF
SC
missing core
SC
PF
PF
DC

SEDIMENTARY STRUCTURES

LITHO-FACIES
E
D
D

GRAIN SIZE
coarse to fine

SCALES
LARGE SMALL

SAND
vc, c, m, f, vf

WELL NAME: **Sinclair Weir 1**

COUNTY: **Cowley**   LOCATION: **30-34S-3E**

GRAIN SIZE | SEDIMENTARY STRUCTURES coarse to fine | LITHO-FACIES | OTHER | DEPTH | EFFECTIVE LIQUID POROSITY % | LIQUID PERMEABILITY, md / EFFECTIVE PORE THROAT RADIUS, μm

WELL NAME: **Jackson Bros. Crew 21**

COUNTY: **Greenwood**   LOCATION: **3-26S-8E**

Core also described by Hulse (1978)

WELL NAME: Jackson Bros. Barrier 36

COUNTY: Greenwood   LOCATION: 3-26S-8E

Porosity and permeability data from Marafa (1979)
Core also described by Hulse (1978)

WELL NAME: **Phillips Demalorie 13AW**

COUNTY: **Greenwood**   LOCATION: **32-22S-11E**

WELL NAME: **Phillips Demalorie 33AW**
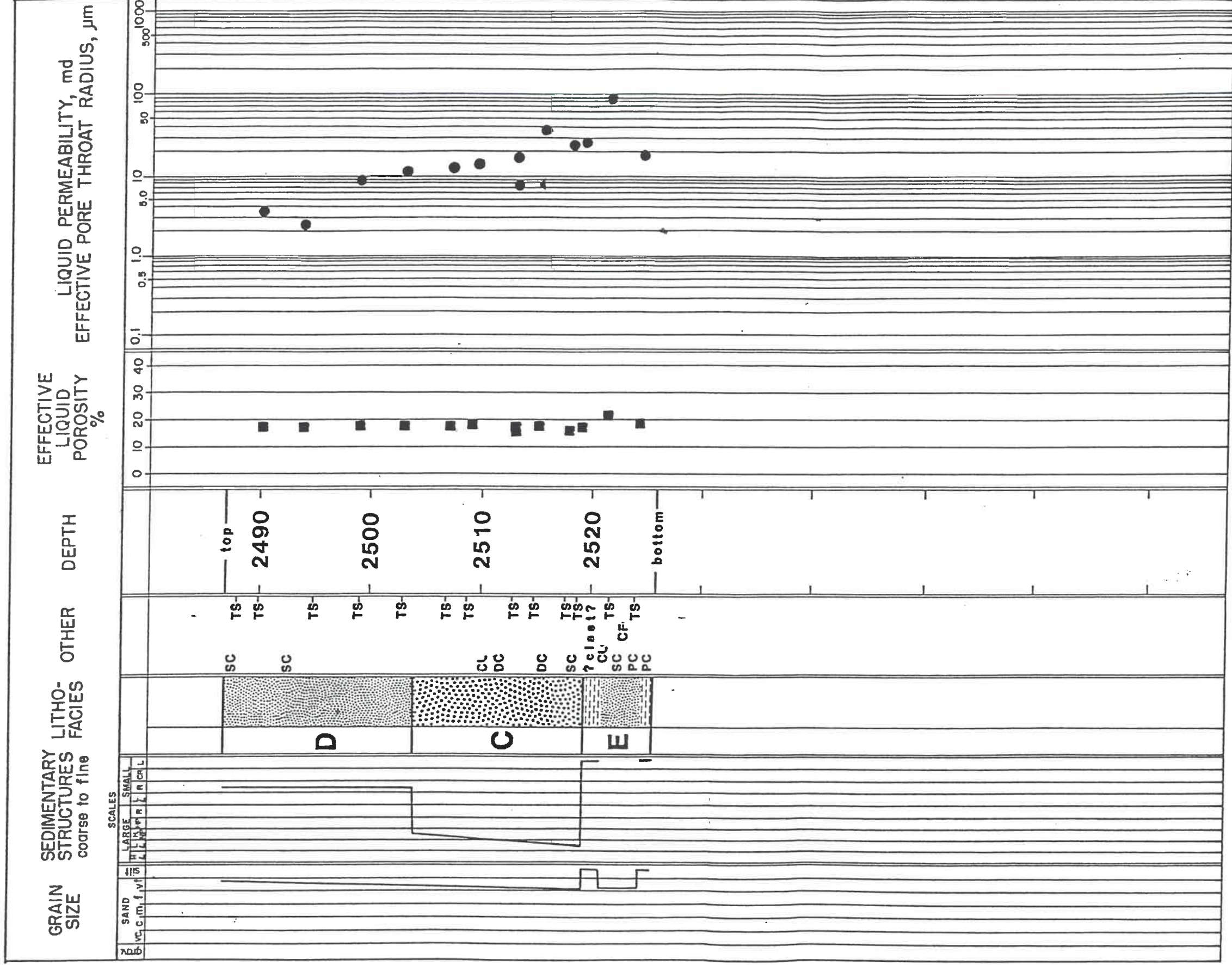
COUNTY: **Greenwood** LOCATION: **32-22S-11E**

WELL NAME: **Phillips Demalorie 30AW**

COUNTY: **Greenwood**   LOCATION: **32-22S-11E**

WELL NAME: M.C. Colt 22AO Lauber   LOCATION: 23-26S-14E

COUNTY: Woodson

GRAIN SIZE — SEDIMENTARY STRUCTURES — LITHO-FACIES — OTHER — DEPTH — EFFECTIVE LIQUID POROSITY % — LIQUID PERMEABILITY, md — EFFECTIVE PORE THROAT RADIUS, μm

WELL NAME: **Conoco J. Ord 47**   LOCATION: **35-32S-17E**
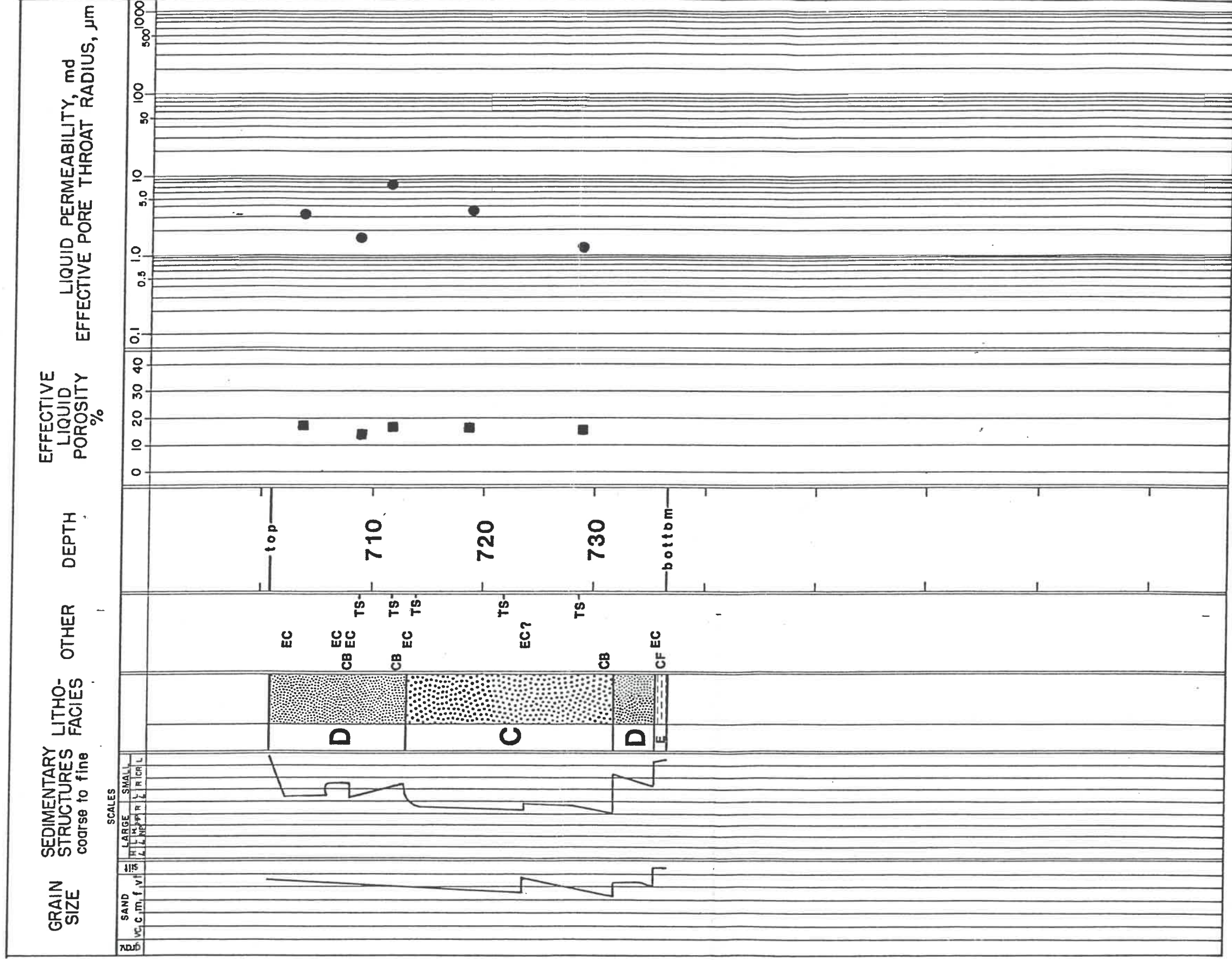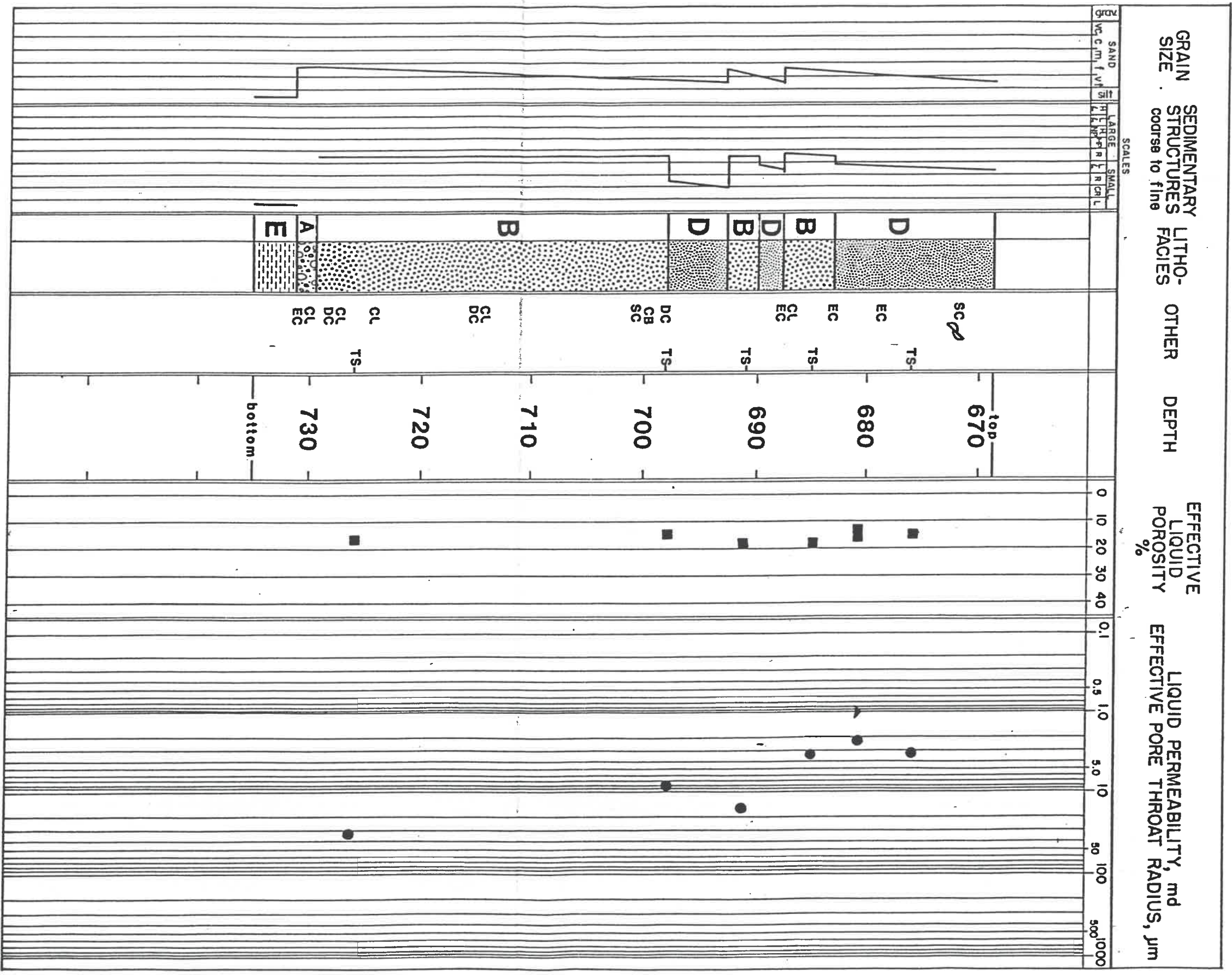
COUNTY: **Labette**

WELL NAME: **Conoco J. Ord 34**

COUNTY: **Labette**   LOCATION: **26-32S-17E**

GRAIN SIZE
coarse to fine

SEDIMENTARY STRUCTURES

LITHO-FACIES

OTHER

DEPTH

EFFECTIVE LIQUID POROSITY %

LIQUID PERMEABILITY, md
EFFECTIVE PORE THROAT RADIUS, μm

SAND — SCALES
grv | vc c m f vf | silt
LARGE | SMALL

Litho-facies columns (top to bottom): D, B, D, B, D, B, A, E

Other: SC, EC, EC, CL EC, DC SC, CL DC, CL, CL DC, CL EC CL EC

TS-, TS-, TS-, TS-, TS-

Depth: top 670, 680, 690, 700, 710, 720, 730, bottom

Porosity scale: 0 10 20 30 40

Permeability/pore throat scale: 0.1 0.5 1.0 5.0 10 50 100 500 1000
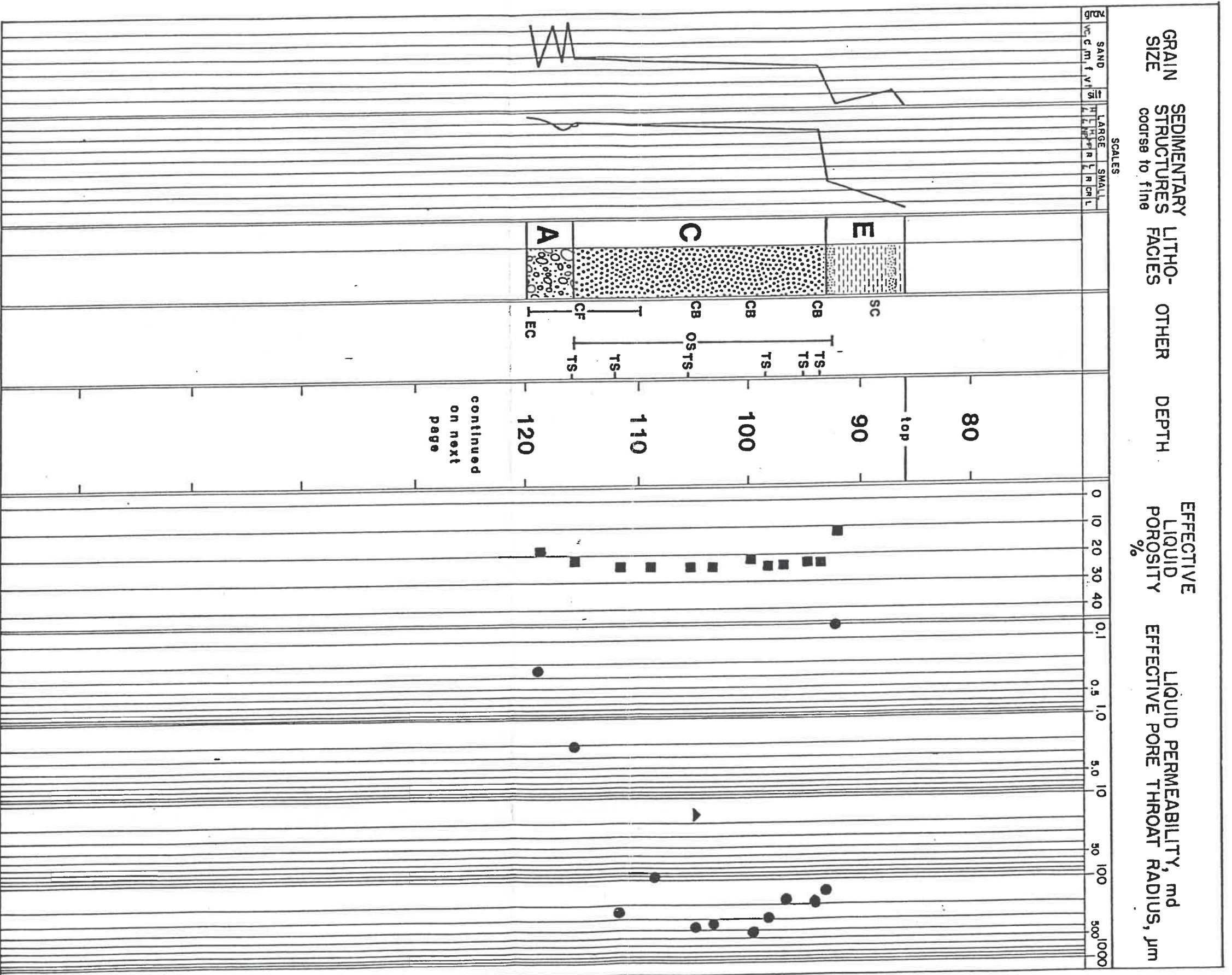
WELL NAME: __Tenneco Bradley 8__

COUNTY: __Labette__   LOCATION: __11-35S-21E__

GRAIN SIZE

SEDIMENTARY STRUCTURES

LITHO-FACIES

OTHER

DEPTH

EFFECTIVE LIQUID POROSITY %

LIQUID PERMEABILITY, md EFFECTIVE PORE THROAT RADIUS, μm

SAND vc c m f vf silt gry.

coarse to fine

SCALES LARGE SMALL

A   C   E

CF   CB   CB   CB   SC

EC

TS   TS   OS TS   TS   TS

80

top

90

100

110

120

0 10 20 30 40

0.1 0.5 1.0 5.0 10 50 100 500 1000

WELL NAME: K.G.S. Tar Sands N

COUNTY: Crawford   LOCATION: 34-29S-24E

WELL NAME: K.G.S. Tar Sands C

COUNTY: Bourbon   LOCATION: 10-26S-25E

GRAIN SIZE

grav.

SAND
vc c m f vf | silt

SCALES
LARGE | SMALL
M L TL T R | L M T R CH L

coarse to fine

SEDIMENTARY STRUCTURES

LITHO-FACIES

OTHER

DEPTH

EFFECTIVE LIQUID POROSITY %

LIQUID PERMEABILITY, md
EFFECTIVE PORE THROAT RADIUS, μm

C

D

D

E

SC L

PC
DC
SC

OS

TS-

TS-
TS-

TS-
TS-

TS-
TS-

TS-
TS-

OS

TS-
TS-

C
TDC
OS
I

PPc
F
CC

c
d
v

PPc
e

TS-
TS-

TS-

bottom

260

250

top 240

bottom 200

190

top

0 10 20 30 40   0.1   0.5 1.0   5.0 10   50 100   500 1000

GRAIN SIZE

SEDIMENTARY STRUCTURES

LITHO-FACIES

OTHER

DEPTH

EFFECTIVE LIQUID POROSITY %

LIQUID PERMEABILITY, md

EFFECTIVE PORE THROAT RADIUS, μm

coarse to fine

grav.

SAND
vc, c, m, f, vf | silt

LARGE
H | L | R | R
L | N | R | R

SMALL
L | R
L | R | CR | L

SCALES

D

E

DC

EC

OS

TS

TS

TS

TS

top
30

40
bottom

0   10   20   30   40

0.1   0.5   1.0   5.0   10   50   100   500 1000

WELL NAME: **M.C. Colt 14AO Johnson**

COUNTY: **Allen**   LOCATION: **33-24S-21E**

GRAIN SIZE

grav | SAND vc c m f vf | silt

SEDIMENTARY STRUCTURES
coarse to fine

SCALES — LARGE — SMALL

LITHO-FACIES

OTHER

DEPTH

EFFECTIVE LIQUID POROSITY %

LIQUID PERMEABILITY, md

EFFECTIVE PORE THROAT RADIUS, μm

C   E

CF   DC   SC   OS   EC   PC   CF   C   TS-

top 710   720   730   740   750   bottom

0 10 20 30 40

0.1 0.5 1.0 5.0 10 50 100 500 1000

WELL NAME: __Tesoro W-35 Baker__

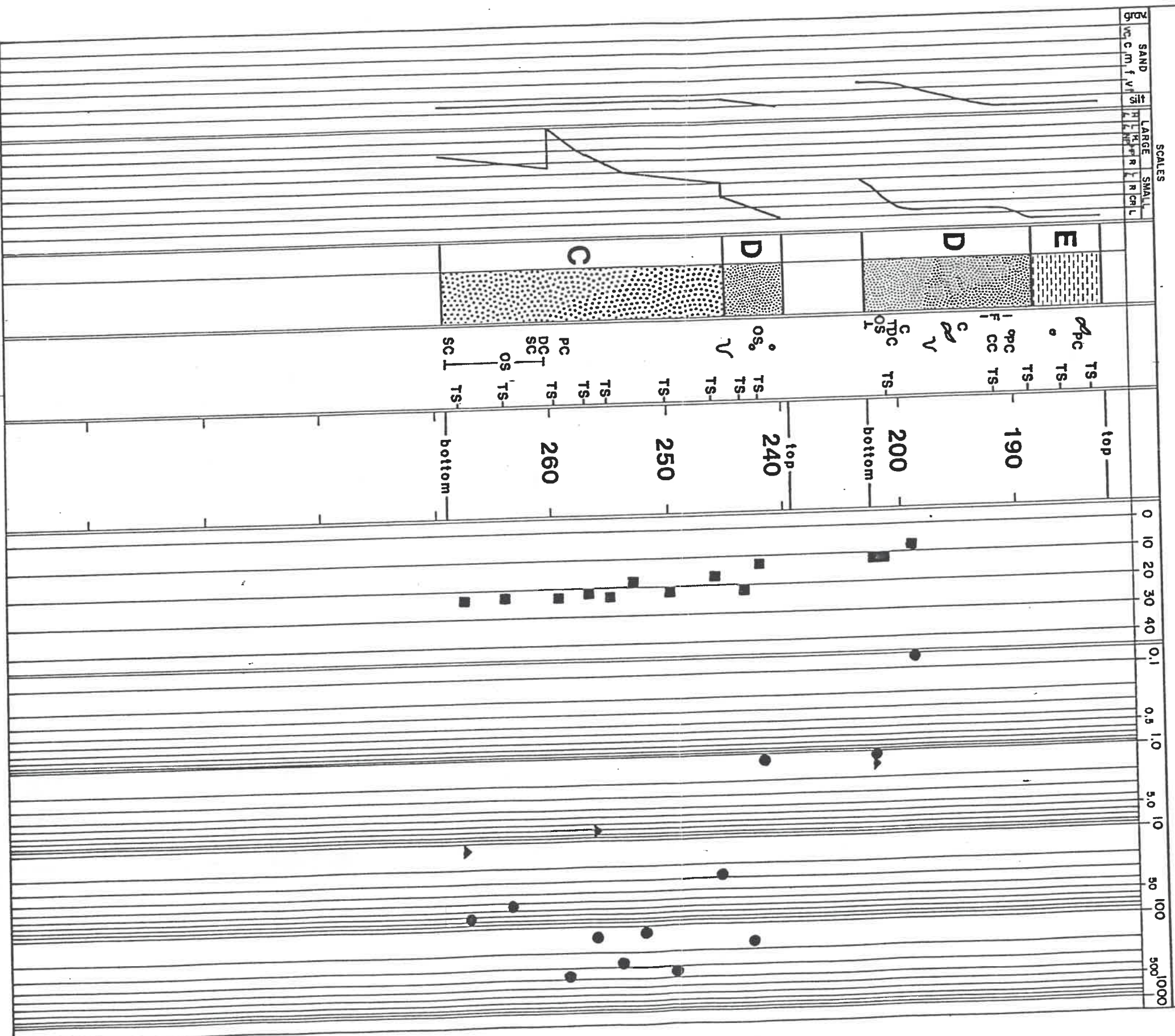COUNTY: __Neosho__   LOCATION: __26-28S-19E__

GRAIN SIZE

SEDIMENTARY STRUCTURES

LITHO-FACIES

OTHER

DEPTH

EFFECTIVE LIQUID POROSITY %
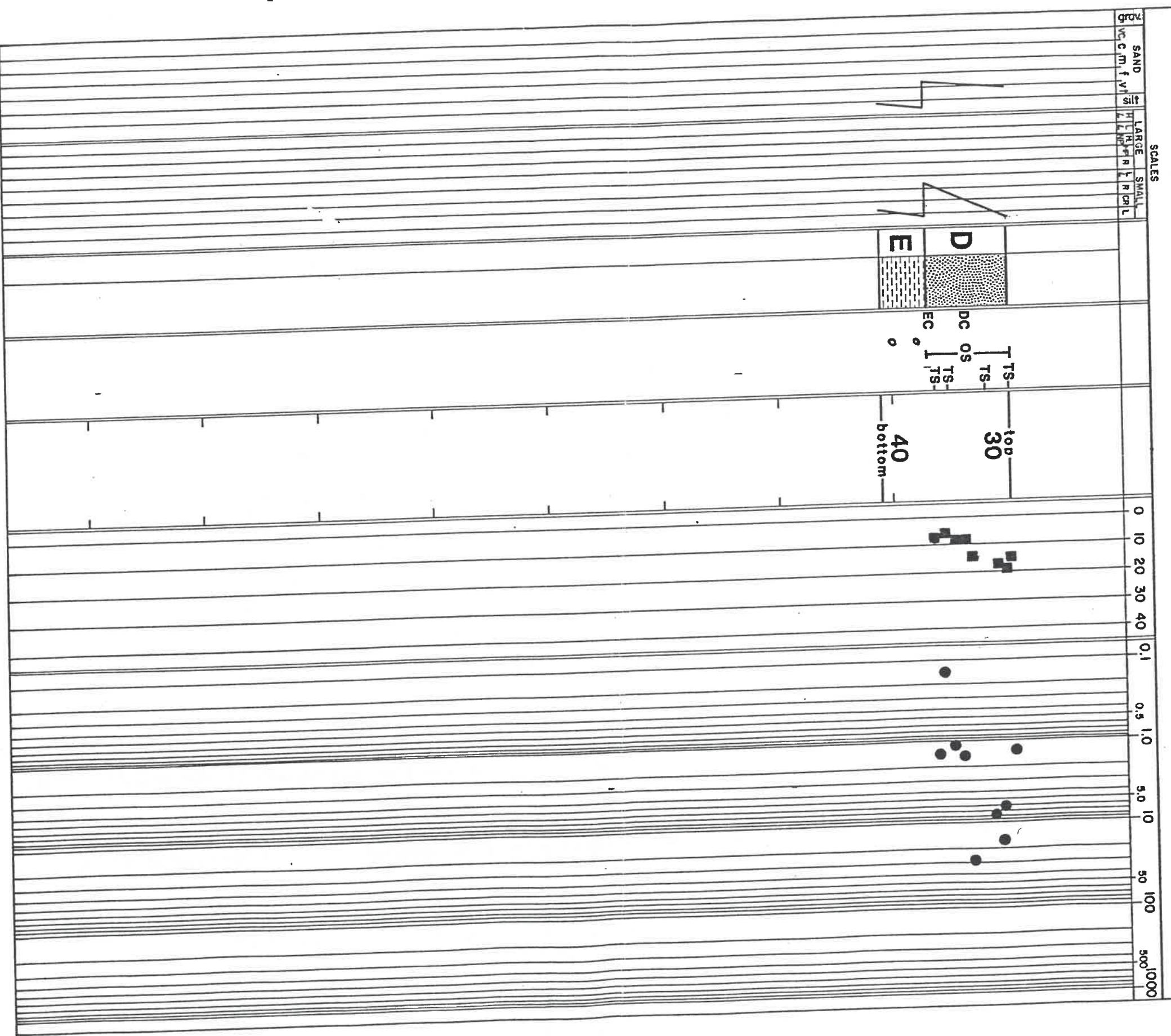
LIQUID PERMEABILITY, md
EFFECTIVE PORE THROAT RADIUS, μm

SCALES

coarse to fine

SAND
grv. vc. c. m. f. vf. silt
LARGE   SMALL

WELL NAME: **M.C. Colt 18AO Keown**

COUNTY: **Allen**　　LOCATION: **22-23S-18E**

\# Based on open-file core description at the Kansas Geological Survey

GRAIN SIZE
coarse to fine

SEDIMENTARY STRUCTURES

LITHO-FACIES

OTHER

DEPTH

EFFECTIVE LIQUID POROSITY %

LIQUID PERMEABILITY, md

EFFECTIVE PORE THROAT RADIUS, μm

SAND — gr | vc c m f vf sil

SCALES — LARGE | SMALL — M L P R | R CM L

Depth scale: 840, 850 (top / bottom), 910 (top), 920, 930, 940, 950, 960, 970 continued on next page

Porosity scale: 0 10 20 30 40

Permeability / pore throat scale: 0.1 0.5 1.0 5.0 10 50 100 500 1000

Lithofacies labels: E, E

Other column labels: CC, CF, PC, EC?, OS, TS, SC, PF, V

WELL NAME: **M.C. Colt 18AO Keown**

COUNTY: **Allen**   LOCATION: **22-23S-18E**

GRAIN SIZE #

SEDIMENTARY STRUCTURES #

LITHO-FACIES #

OTHER

DEPTH

EFFECTIVE LIQUID POROSITY %

LIQUID PERMEABILITY, md
EFFECTIVE PORE THROAT RADIUS, μm

coarse to fine

SAND
gr vc c m f vf silt

SCALES
LARGE / SMALL

E | A | C | E

PF
CF
CB
PF
PCCB
EC

DC PF
CF
PF

PF
PF

PF

TS
CL
TS
TS

TS
TS
TS
OS
TS
TS
TS

bottom
1020
1010
1000
990
980

0 10 20 30 40

0.1 0.5 1.0 5.0 10 50 100 500 1000

WELL NAME: **M.C. Colt 18AO Keown**

COUNTY: **Allen**   LOCATION: **22-23S-18E**

\# Based on open-file core description at the Kansas Geological Survey
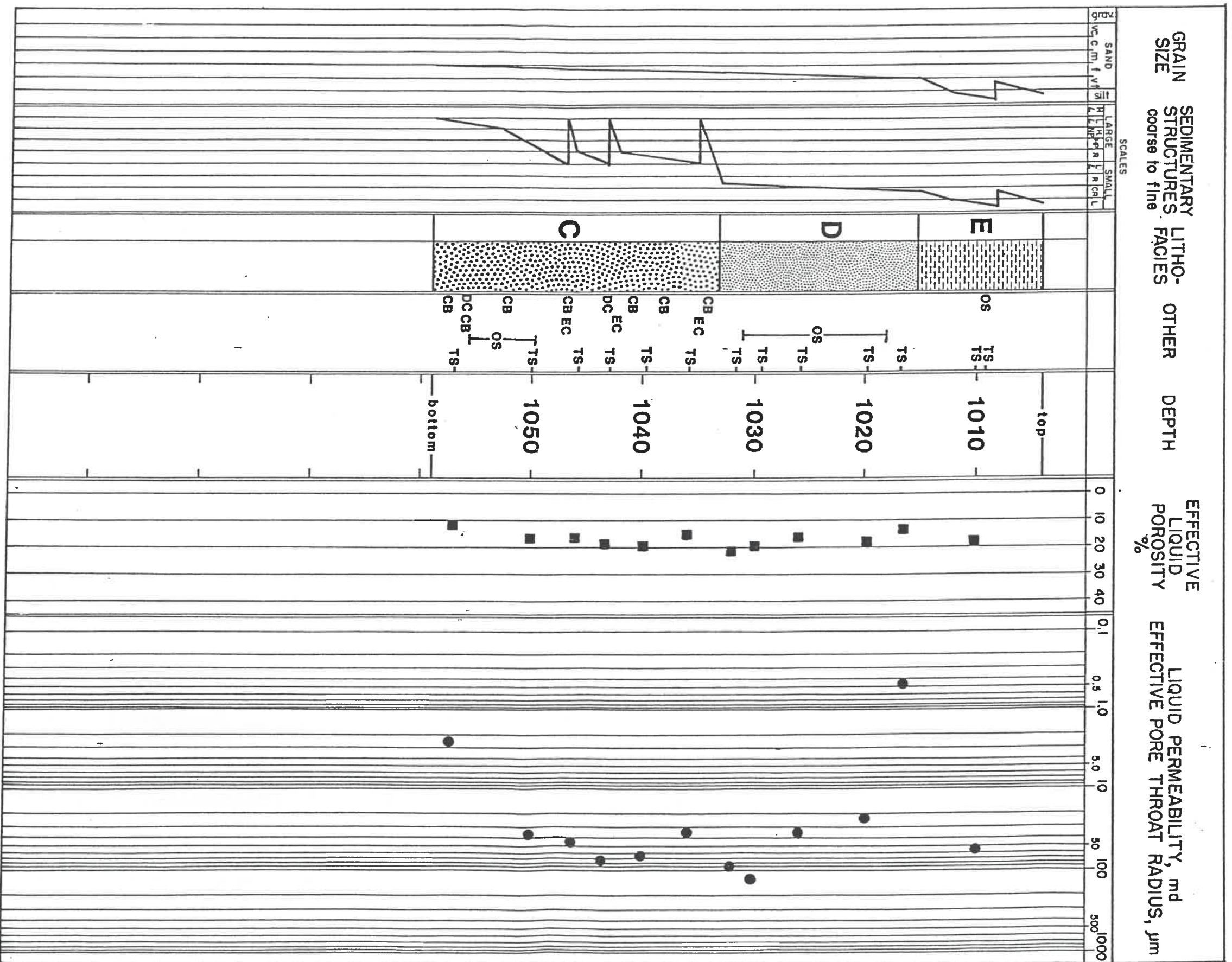
GRAIN SIZE

SEDIMENTARY STRUCTURES coarse to fine #

LITHO-FACIES #

OTHER

DEPTH

EFFECTIVE LIQUID POROSITY %

LIQUID PERMEABILITY, md   EFFECTIVE PORE THROAT RADIUS, µm

SAND: vc, c, m, f, vf | silt

SCALES — LARGE / SMALL

Facies: C E A C A C E

Depth markings: top, 1130, 1140, 1150, 1160, 1170, 1180 bottom

Porosity scale: 0 10 20 30 40

Permeability/radius scale: 0.1 0.5 1.0 5.0 10 50 100 500 1000

Labels: TS, PF, CB, CL, CF, EC, SC?

WELL NAME: **Brazos 0-5 Pierpoint**

COUNTY: __Wilson__   LOCATION: __9-28S-15E__

GRAIN SIZE
coarse to fine

SEDIMENTARY STRUCTURES

LITHO-FACIES

OTHER

DEPTH

EFFECTIVE LIQUID POROSITY %

LIQUID PERMEABILITY, md
EFFECTIVE PORE THROAT RADIUS, μm